Nonlinear Fiber Optics for Bio-Imaging

by

Roque Gagliano Molla

Ingeniero Electricista

Universidad de la República, Montevideo, Uruguay, 2001

Submitted to the Department of Electrical Engineering and Computer Science and the faculty of the Graduate School of the University of Kansas in partial fulfillment of the requirements for the degree of Master of Science.

Chair: Dr. Rongqing Hui

Dr. Victor Frost

Dr. Kenneth Demarest

Date of Thesis Defense: May 20th, 2005

Acknowledgements

I would like to show my appreciation and gratitude to my advisor Dr. Rongqing Hui. This has been an amusing and rewarding learning experience that we started by putting some living cells in a Pyrex back in January 2004. I would like to thank him not only for his advice and financial support but also for being an endless source of optimism and an example of self-motivation.

I would also like to thank the rest of my committee, Dr. Victor Frost and Dr. Kenneth Demarest.

Special thanks to Jay Unruh and the rest of the group at Dr. Carey Johnson's laboratory of the Chemistry Department at the University of Kansas where all the experiments of this work were performed.

Also, I would like to acknowledge the Fulbright Program, the OAS-LASPAU Program, the Barca Family and the KU International Program for their support.

Finally I would like to thank my family and friend for helping me removing all the obstacles in order to make my dream of a graduate education possible.

Table of Contents

Acknowledgements ii
Table of Contents iii
List of Figures vi
Abstract viii
Chapter 1: Introduction 1
1.1 Motivation 1
1.2 Two-photon microscopy and wavelength-tunable pulsed laser sources 1
1.3 Organization 4
Chapter 2: Nonlinear Effects of Optical Fibers 5
2.1 General Analysis 5
2.2 Nonlinear Pulse Propagation 7
2.3 Chromatic Dispersion 10
2.4 Nonlinear effects 11
2.4.1 Self Phase Modulation (SPM) 11
2.4.2 Cross Phase Modulation (XPM) 12
2.4.3 Four Wave Mixing (FWM) 12
2.4.4 Stimulated Raman Scattering (SRS) 13
2.4.5 Stimulated Brillouin Scattering (SBS) 15
2.5 Split Step Fourier Method 15
Chapter 3: Optical Solitons 17
3.1 Solitons in Physics 17
3.2 Fiber Solitons 18
3.3 Fundamental Soliton 20
3.4 Higher Order Solitons 20
3.5 Soliton Interaction 20
3.6 Loss-Managed Solitons 21
3.7 Dispersion Management Solitons (Average Solitons) 22
Chapter 4: Short Pulsed Fiber Lasers 24

4.1 Short Pulsed Cavity Lasers 24
4.2 Mode-locking 25
4.2.1 Active Mode-locking 26
4.2.2 Passive Mode Locking 26
4.3 Solid State Laser 27
4.4 Fiber Lasers 29
4.4.1 Ring Cavity Fiber Lasers 30
4.4.2 Fabry-Perot or Linear cavities 32
4.5 High Power Pulsed Fiber Lasers 33
Chapter 5: Photonic Crystal Fibers 35
5.1 Fundamentals of photonic crystal waveguiding 35
5.2 Classification of PCF 36
5.3 Modelling of microstructured fibers 37
5.4 Fabrication of photonic crystal fibers 39
5.5 Applications 40
Chapter 6: Experimental and Numerical Analysis of Soliton Self-Frequency Shift 42
6.1 Experimental Results 42
6.2 Generalized Non-Linear Schrödinger Equation 45
6.3 Numerical Analysis 49
Chapter 7: Analytical Analysis of Soliton Self-Frequency Shift 60
7.1 Analytical Model 61
7.2 Limitations of the previous analytical model 66
7.3 A semi-analytical method for soliton self frequency shift in an optical fiber. 67
7.3.1 Semi-Analytic Method Formulation 68
7.3.2 Results and Discussion. 72
Chapter 8: Short Pulsed Lasers Applications for Two Photons Microscopy 79
8.1 One-Photon Confocal Microscopy 80
8.2 Two Photons Microscopy 82
8.3 Experimental Acquisition of Two-Photon Microscopy 84

8.4 Other applications 89
CONCLUSIONS 90
FUTURE WORK 92
GLOSSARY 93
REFERENCES 95
APPENDIX A: Optical Fibers Characteristics 99
APPENDIX B: VPI Models and Numerical Parameters 104
APPENDIX B: MATLAB CODE 116
APPENDIX D: Submitted Publication 118

List of Figures

Figure 2.1: Stimulated Raman Scattering. 14
Figure 4.1: Ti:Sapphire laser setup with Argon CW pump and self-mode-locking. 28
Figure 4.2 All-fiber ring-laser. 31
Figure 4.3 Pulses Shortening in a Ring Fiber Laser [Nel97]. 31
Figure 4.4: Schematic of a fiber laser 33
Figure 4.5: MM fiber oscillator side-pumped 34
Figure 5.1: Classification of PCF [Bja03]. 36
Figure 5.2: Geometrical characteristics of PCF. 37
Figure 6.1: Experimental Setup for a Wavelength-Tunable Pulsed Laser Source. 43
Figure 6.2: Experimental spectrums for a wavelength shifter 44
Figure 6.3: Raman Response Function [Agr01]. 46
Figure 6.3: Normalized Raman Gain for a SiO2 fiber. 47
Figure 6.5: Soliton formation from the original pump pulse. 50
Figure 6.6: Time domain Characteristics of the output from a 7m HNL-PCF. 51
Figure 6.7: Wavelength Shift for different Input Average Power in a 7m HNL-PCF. ... 52
Figure 6.8: Wavelength Shift and Input Average Power for 3m and 7m HNL-PCF. 54
Figure 6.9: Supercontinuum generation after applying 5mW pulses to 7m of PCF. 55
Figure 6.10: Time domain characteristics for different HNL-PCF lengths 56
Figure 6.11: Wavelength Shift and Fiber length for a HNL-PCF. 57
Figure 6.12: Soliton Pulse width and Fiber Length for a HNL-PCF. 58
Figure 6.13: Soliton order N ans fiber length. 59
Figure 6.14: Numerical and Experimental Results Wavelength Shifts 59
Figure 7.1: Semi-analytical method for SSFS in an optical fiber. 68
Figure 7.2: Block diagram for the semi-analytical method. 72
Figure 7.3: Frequency shift versus pulse width for a 100m PMF. 74
Figure 7.4: SSFS for a HNL-PCF with different fiber lengths in log scale. 75
Figure 7.5: Frequency shift and pulse width for a 10m HNL-PCF. 76

Figure 7.6: Wavelength shift and fiber length for a PCF. 77
Figure 8.1: A Scanning Laser Confocal Microscope Setup. 80
Figure 8.2: Absorption and emission spectrum of the Alexa-series dyes. 82
Figure 8.3: Experimental setup for acquiring a two-photon image. 86
Figure 8.4: Two-photon image of a fluosphere using a 780nm pump laser. 87
Figure 8.5: Radial intensity profile for a fluosphere using a pump laser at 780nm. 87
Figure 8.6: Two-photon image of a fluosphere using a shifted pump laser to 920nm. .. 88
Figure 8.7: Radial intensity profile for the fluosphere at the center of figure 8.6. 88
Figure A.1: Crystal Fibre NL-18-710 axial profile (http://www.crystal-fibre.com) 99
Figure A.2: Attenuation Parameter (α) for Crystal Fibre NL-18-710. 101
Figure A.3: Nonlinear Coefficient (γ) for a Crystal Fibre NL-18-710. 101
Figure A.4: Dispersion Coefficient (D) for a Crystal Fibre NL-18-710. 102
Figure B.1: VPI Model used for simulations. 104

Abstract

Two-photon excitation (TPE) is a modern technology with applications in microscopy and spectroscopy that has gained a great amount of attention in recent years. This technique is the best suitable to analyze thick tissues and live animals as it works in the near-infrared (NIR) region.

In this work we implement and evaluate a two-photon setup that allows the shifting of the working wavelength over a wide range using the soliton self-frequency shift (SSFS) effect. The shifter is implemented using a pulsed fiber laser and a photonic crystal fiber (PCF). We also include a numerical evaluation of the dependency of the fiber shift on the input average power and the fiber length.

A semi-analytical model is proposed to investigate the characteristics of the SSFS in optical fibers. SSFS in two different types of fibers were evaluated and the results agree very well with those of numerical simulations. We show that when the frequency shift is small enough, it is inversely proportional to the fourth power of the initial soliton pulse width. However, with large frequency shift, this fourth power rule needs to be modified.

We finally show the first two-photon images obtained at the University of Kansas.

Chapter 1: Introduction

1.1 Motivation

Every day one is bombarded with press releases covering new discoveries in areas such as DNA analysis and molecular analysis. Many of these new technological breakthroughs are achieved thanks to the use of powerful microscopy instruments that rely heavily on lasers [Sch01]. In this work we investigate innovative technologies that open the doors for the improvement of existing instruments as well as of our understanding of these phenomena.

1.2 Two-photon microscopy and wavelength-tunable pulsed laser sources

When using florescence microscopy, the pump's photons are absorbed by the target substance which then emits a photon in a longer wavelength. Different species are labeled with different fluorescent dyes that emit in different wavelengths. Recognizing a dye is equivalent to recognizing the targeted molecule.

A particular technique that has growing interest in the scientific community is the two-photon laser scanning microscopy (TPLSM), where two photons from the pump are absorbed simultaneously to generate one signal photon. This techniques allows higher penetration lengths (you can see deeper into the object) and higher resolution

(you can see smaller objects) than conventional confocal microscopy instruments [Den90].

A classical fluorescence microscopy instrument includes a solid state pulsed laser. These devices are not only expensive, but also difficult to manipulate and not suitable for field operation. In recent years, all-fiber pulsed laser based in fiber amplifiers have become commercially available. These lasers are compact, easy to operate and easy to translate. Their output power has consistently increased during the past two years [Nel97].

In a photonic crystal fiber (PCF), air-holes are located around the core [Bja03]. These air structures have several designs for different applications. A very common implementation is characterized by its very high nonlinear index. Thanks to this high non-linear parameter and due to the stimulated Raman scattering (SRS), as high-power short pulses propagate along the fiber, an optical soliton is formed. The soliton's central frequency is then shifted to lower values [Nor02].

Fundamental optical solitons are pulses that do not change their shape while propagating along an optical fiber [Agr03]. Raman solitons are formed from the breaking of a high power pulse and have the characteristic of shifting their frequency as a function of their pulse width [Bea87]. The soliton self-frequency shift (SSFS) was first discovered by Mitschke et al in 1986 [Mit86]. At the same time, Gordon

[Gor86] formulated how the frequency shift inversely depends on the fourth power of its width. However, this formulation does not take into account the fiber losses and the frequency dependency of the fiber parameters. As the pulse changes its central wavelength, the fiber group-delay dispersion, nonlinear parameter, effective area and attenuation can vary considerably, modifying the fourth power rule [Gor86].

In this work we introduce a simple semi-analytic method to model SSFS in optical fibers. By taking into account the fiber wavelength dependent attenuation, dispersion and nonlinearity, we show that the SSFS becomes less sensitive to the input pulse width when this width is narrow enough and the fourth power rule needs to be modified for many practical applications. The results of semi-analytic calculations are found to be in good agreement with numerical simulations using the split-step Fourier method. Our results also indicate that the fourth-power rule predicted in [Gor86] is accurate when the wavelength shift is small and the fiber loss is negligible.

Thanks to the SSFS, we were able to implement a highly wavelength-tunable pulsed fiber laser that delivers femtosecond pulses to a two-photon microscope. The wavelength tunable capability was achieved by introducing a PCF in the light path. The two-photon images shown in this work were the first ones performed at the University of Kansas [Nor02].

1.3 Organization

This Thesis is organized as follows: Chapters 2 to 5 introduce concepts such as nonlinear effects in optical fibers, optical solitons, short pulses fiber lasers and photonic crystal fibers. This work also includes extensive references for further study of these topics.

In Chapter 6 we study the propagation of a short pulse in an optical fiber, particularly in a PCF. We show numerical results for different input powers and fiber lengths and contrast some of these simulations with experimental data.

A detailed analysis of the SSFS phenomenon is done in Chapter 7, where the semi-analytical method is introduced. The results are also contrasted with numerical data and with the analytical model in [Gor86].

In the last chapter we briefly describe a two-photon microscopy system and we show the recorded images. These experiments were performed at Dr. Carey Johnson's laboratory at the Department of Chemistry of the University of Kansas.

Finally we present our conclusions and describe possible future works.

Chapter 2: Nonlinear Effects of Optical Fibers

2.1 General Analysis

The propagation of an electromagnetic field along an optical fiber is generically described by Maxwell´s Equations [Agr01] from which we deduce the wave equation:

$$\nabla \times \nabla \times \vec{E}(\vec{r},t) = -\frac{1}{c}\frac{\partial^2 \vec{E}(\vec{r},t)}{\partial t^2} - \mu_0 \frac{\partial^2 \vec{P}(\vec{r},t)}{\partial t^2} \qquad (2.1.1)$$

Where $\vec{E}$ is the electrical field, $\vec{P}$ the induced polarization, ε_0 is the vacuum permittivity, μ_0 the vacuum permeability and $c = \sqrt{\frac{1}{\mu_0 \varepsilon_0}}$ is the speed of the light in vacuum. Although the relationship between $\vec{E}$ and $\vec{P}$ will normally require a quantum-mechanical study, many times a phenomenological relationship can be applied:

$$\vec{P} = \varepsilon_0 \left(\chi^{(1)} \vec{E} + \chi^{(2)} : \vec{E}\vec{E} + \chi^{(3)} \vdots \vec{E}\vec{E}\vec{E} + \ldots \right) \qquad (2.1.2)$$

Where $\chi^{(j)}$ is the j^{th} order susceptibility, generally a tensor of rank j+1. The term j=1 represents the linear relationship; it affects the refractive index and the attenuation coefficient of the fiber. The second order susceptibility, responsible for second order harmonic generation, is negligible for SiO_2 and thus is not present in optical fibers. The third order susceptibility, $\chi^{(3)}$, is responsible for phenomena such as third order

harmonic generation, four-wave mixing and nonlinear refraction (Kerr effect). In this last effect, the intensity dependency of the refractive index is reflected as:

$$\tilde{n}\left(\omega,\left|\vec{E}\right|^2\right)=n(\omega)+n_2\left|\vec{E}\right|^2 \tag{2.1.3}$$

Where n(ω) represent the linear contribution and n_2 is the nonlinear-index, related to $\chi^{(3)}$.

If we include the nonlinear effects, the induced polarization is obtained by adding two terms: the linear contribution $\left(\vec{P}_L(\vec{r},t)\right)$ and the nonlinear contribution $\left(\vec{P}_{NL}(\vec{r},t)\right)$:

$$\vec{P}(\vec{r},t)=\vec{P}_L(\vec{r},t)+\vec{P}_{NL}(\vec{r},t) \tag{2.1.4}$$

The linear and nonlinear contributions are related to the electrical field by:

$$\vec{P}_L(\vec{r},t)=\varepsilon_0\int_{-\infty}^{\infty}\chi^{(1)}(t-t')\vec{E}(\vec{r},t')dt' \tag{2.1.5}$$

$$\vec{P}_{NL}(\vec{r},t)=\varepsilon_0\int\int\int_{-\infty}^{\infty}\chi^{(3)}(t-t_1,t-t_2,t-t_3)\vdots\vec{E}(\vec{r},t_1)\vec{E}(\vec{r},t_2)\vec{E}(\vec{r},t_3)dt_1dt_2dt_3 \tag{2.1.6}$$

A simplified analysis consists of considering the nonlinear term as a small perturbation to the total polarization. In that sense, we should first find the solution for the electrical field in a linear medium.

Following the analysis in [Agr01], we consider only the wave equation for the field in the propagation axis (z):

$$\tilde{E}_z(\vec{r},\omega)=A(\omega)F(\rho)e^{\pm im\phi}e^{i\beta z} \tag{2.1.7}$$

Where $\widetilde{E}_z$ is the z component of the Fourier transform of the electrical field, A is a normalization constant, β is the propagation constant and m an integer. The solution for the field dependency on ρ is well known and given by Bessel functions [Agr01].

2.2 Nonlinear Pulse Propagation

Nonlinear effects in optical fibers are particularly important when considering the propagation of short pulses (from 10ns to 10fs). While these pulses travel through the fiber their shape and spectrum are affected not only by nonlinearities, but also by group-delay dispersion.

Considering (2.1.1) and (2.1.4) we build the wave equation that considers both linear and nonlinear effects:

$$\nabla^2 \vec{E} - \frac{1}{c}\frac{\partial^2 \vec{E}}{\partial t^2} = \mu_0 \frac{\partial^2 \vec{P}_L}{\partial t^2} + \mu_0 \frac{\partial^2 \vec{P}_{NL}}{\partial t^2} \qquad (2.2.1)$$

In order to solve this equation, we will make several simplifications. Firstly, we will consider that the nonlinear effect is a small perturbation of the linear solution. Secondly, we will assume that the optical field maintains its polarization along the fiber length; consequently, we can use scalar magnitudes. Thirdly, we will consider that the optical field is quasi-monochromatic, which means that $\frac{\Delta\omega}{\omega_0} << 1$. Finally, we will take a slowly varying envelope approximation for the field and we will find a solution using the variable separation method:

$$\widetilde{E}_z(\vec{r},\omega-\omega_0)=F(x,y)\widetilde{A}(z,\omega-\omega_0)e^{i\beta_0 z} \tag{2.2.2}$$

Where $\widetilde{A}(z,\omega)$ is the slowly varying of z pulse envelope and β_0 is the wave number to be determinate by solving the eigenvalues equation.

Equation (2.2.1) can be transformed to the Helmholtz equation,

$$\nabla^2\widetilde{E}+\varepsilon(\omega)k_0^2\widetilde{E}=0 \tag{2.2.3}$$

Here we generalize the definition for the field permittivity as

$$\varepsilon(\omega)=1+\widetilde{\chi}^{(1)}_{xx}(\omega)+\varepsilon_{NL} \tag{2.2.4}$$

Where ε_{NL} summarizes the nonlinear contribution to the dielectric constant:

$$\vec{P}_{NL}(\vec{r},t)\approx\varepsilon_0\varepsilon_{NL}\vec{E}(\vec{r},t) \tag{2.2.5}$$

$$\varepsilon_{NL}=\tfrac{3}{4}\chi^{(3)}_{xxxx}\left|\vec{E}(\vec{r},t)\right|^2 \tag{2.2.6}$$

The dielectric constant and the diffraction index are related by:

$$\varepsilon(\omega)=\left(\tilde{n}(\omega)+\frac{i\tilde{\alpha}(\omega)}{2k_0}\right)^2 \tag{2.2.7}$$

Where $\tilde{\alpha}(\omega)$ has a similar definition as $\tilde{n}(\omega)$ in (2.1.3). All the material parameters are normally complex magnitudes. It is important to observe that we are considering the induced polarization as an instantaneous event, and so we are neglecting the contribution of delayed effects such as molecular vibrations (especially the Raman Effect).

The dielectric constant can now be approximated by considering the nonlinear contribution as a small perturbation of the linear effect:

$$\varepsilon(\omega) = \left(n + n_2 |E|^2 + \frac{i\tilde{\alpha}(\omega)}{2k_0} \right)^2 = (n + \Delta n)^2 \approx n^2 + 2n\Delta n \tag{2.2.8}$$

Using (2.2.2) for solving the Helmholtz equation (2.2.3) when a permittivity like (2.2.8) is considered, we get the following equation for the slowly varying envelope A(z,t):

$$\frac{\partial A}{\partial z} + \beta_1 \frac{\partial A}{\partial t} + \frac{i\beta_2}{2} \frac{\partial^2 A}{\partial t^2} + \frac{\alpha}{2} A = i\gamma |A|^2 A \tag{2.2.9}$$

This equation is known as the nonlinear Schrödinger (NLS) equation. The fiber parameters in this equation are related to the perturbation of the diffraction index introduced in (2.2.8). The term $1/\beta_1$ represent the Group Velocity, β_2 the Group-Velocity Dispersion (GVD) and the nonlinear parameter γ is defined as:

$$\gamma = \frac{n_2 \omega_0}{c A_{eff}} \tag{2.2.10}$$

Where the parameter A_{eff} is known as the effective core area and is defined as:

$$A_{eff} = \frac{\left(\int\int_{-\infty}^{\infty} |F(x,y)|^2 \, dxdy \right)^2}{\int\int_{-\infty}^{\infty} |F(x,y)|^4 \, dxdy} \tag{2.2.11}$$

In order to evaluate it, we need to consider the modal distribution for the fundamental fiber mode. If we approximate F(x,y) by a Gaussian distribution, we can express: $A_{eff} = \pi w^2$, the width parameter w is a half of the Modal Diameter Field (MDF).

2.3 Chromatic Dispersion

The main source of group-delay dispersion for short pulse propagation along an optical fiber is the chromatic dispersion which represents the wavelength dependency of the diffraction index, n(ω). Mathematically, the effects can be understood by expanding the mode-propagating constant β in a Taylor series:

$$\beta(\omega) = n(\omega)\frac{\omega}{c} = \beta_0 + \beta_1(\omega - \omega_0) + \frac{1}{2}\beta_2(\omega - \omega_0)^2 + \ldots \qquad (2.3.1)$$

Where:

$$\beta_m = \left(\frac{d^m \beta}{d\omega^m}\right)_{\omega=\omega_0} \quad (m = 0,1,2,\ldots) \qquad (2.3.2)$$

The dispersion parameter D is defined as:

$$D = \frac{d\beta_1}{d\lambda} = -\frac{2\pi c}{\lambda^2}\beta_2 \approx \frac{\lambda}{c}\frac{d^2 n}{d\lambda^2} \qquad (2.3.3)$$

Dispersion is normal when D<0 and anomalous when D>0. An important parameter is the zero-dispersion wavelength, where D=0.

As a pulse propagates along the fiber, chromatic dispersion causes different wavelength to travel at different speeds. The effect at the output is a broadening of the initial pulse, without changing the amplitude spectrum.

The second order dispersion (β_3) is related to the slope of the D(λ) function. A short optical pulse will have a broad optical bandwidth and the second order dispersion should normally not be neglected.

Other sources of dispersion are waveguide dispersion, multimodal dispersion and polarization mode dispersion (PMD) [Agr01].

2.4 Nonlinear effects

The effects of the instantaneous nonlinear response of an optical fiber are summarized on the right hand side of the NLS equation (2.2.9). In this section we are going to give a short description of them, where the first three phenomena (SPM, XPM and FWM) are elastic processes, as no energy is exchanged between the fields and the medium. The last two effects (SRS and SBS) are inelastic, in which the optical field transfers part of its energy to the nonlinear medium. The NLS equation will be modified in Chapter 6 in order to include SRS.

2.4.1 Self Phase Modulation (SPM)

Self Phase modulation (SPM) refers to the self-induced phase shift experienced by an optical field during its propagation in optical fibers [Agr01].

The intensity-dependent nonlinear phase shift (ϕ_{NL}) can be described by:

$$\phi_{NL} = \frac{2\pi}{\lambda} n_2 L \left|\vec{E}\right|^2 \tag{2.4.1}$$

Where L is the fiber length and $\left|\vec{E}\right|$ the module of the electrical field at the working wavelength.

Generally SPM brings a broadening of the amplitude spectrum and thus a stretching of the pulse in time domain. The final result depends on the frequency chirp of the original pulse as detailed in [Agr01].

2.4.2 Cross Phase Modulation (XPM)

Cross Phase Modulation (XPM) refers to the nonlinear phase shift induced by other fields, having a different wavelength, direction, or polarization state:

$$\phi_{NL} = n_2 \frac{2\pi}{\lambda} L\left(\left|E_1\right|^2 + 2\left|E_2\right|^2\right) \tag{2.4.2}$$

In this case the term depending on $\left|\vec{E}_1\right|$ is the SPM as in (2.4.1) and $\left|\vec{E}_2\right|$ represent the external field.

XPM is responsible for asymmetric spectral broadening of co-propagating optical pulses.

2.4.3 Four Wave Mixing (FWM)

When several optical signals at different frequencies propagate along the fiber, the total electrical field is equal to the vectorial addition of each individual field. The resulting optical intensity will have new components as a result of the cross products in the module calculation.

For example if three optical frequencies (f_1, f_2 and f_3) interact in a nonlinear medium, they will give rise to a fourth frequency (f_4), where:

$$f_4 = f_1 + f_2 - f_3 \tag{2.4.2}$$

FWM is responsible for inter-channel crosstalk in a WDM communication system.

2.4.4 Stimulated Raman Scattering (SRS)

Raman Scattering is an inelastic process where a photon of the incident field (called pump) is absorbed and reemitted again, via an intermediate electron state, in a lower frequency. The excess energy and impulse is dissipated as a phonon (vibrational energy) into the material. This process can be combined with stimulated emission where the new photon has the same frequency and momentum as an incident signal photon. Consequently, through SRS, pump photons are progressively destroyed while new photons, called Stokes photons, are created at a down-shifted frequency that correspond to the signal photon. Figure 2.1 shows the scheme of the process.

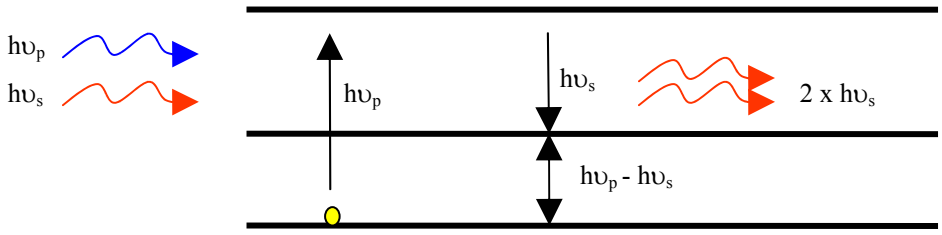

Figure 2.1: Stimulated Raman Scattering, two incident photons, one representing the signal (υ_s) and the other representing the pump (υ_p). At the output the signal is amplified, the energy loss is $h(\upsilon_p - \upsilon_s)$.

A less probable phenomenon is the emission of an anti-Stoke photon which has higher energy that the incoming pump. In this study, we will mainly focus in the generation of Stokes photons through SRS.

SRS has applications in amplification of optical communication signals and spectroscopy. As a vibrational contribution, the SRS has a delayed response characteristic for each material.

The relationship between the pump and the signal power (I_p and I_s) can be described as:

$$\frac{dI_s}{dz} = g_R I_p I_s \qquad (2.4.3)$$

Where g_R is the Raman gain that can be measured experimentally. The Raman gain bandwidth is very wide (around 13THz) and thus the effect is particularly important for large bandwidth signal (very narrow pulses in time domain).

SRS is only visible when the pump power exceeds a certain threshold level (typically $P_p^{th} \approx 1W$).

Spontaneous Raman Scattering occurs when a Raman photon is generated from a pump photon but without any relationship with the signal. This effect is normally considered as noise.

2.4.5 Stimulated Brillouin Scattering (SBS)

This effect is very similar to the previous one, but in this case an acoustic phonon is generated only in the backward direction. SBS has higher but narrower gain (less than 100MHz) then SRS. In optical communication systems, SBS will limit the total amount of power in the fiber. Because it only propagates in the backward direction and due to its very narrow gain, we will not consider SBS in this work.

2.5 Split Step Fourier Method

Equation (2.2.7) can only be solved numerically. The preferred method is the "Split Step Fourier Method", where dispersion and nonlinear effects are solved separately in time domain the first one and in frequency domain the last one [Agr01].

The fiber is chirped in small sections, where the dispersion is considered along each segment, while the nonlinear operator is only applied at each segment's middle point.

This method is implemented by the simulation software VPItransmissionMaker in which the numerical results of this work are based [VPI05].

Chapter 3: Optical Solitons

In this chapter we will give an overview of optical solitons, describing its historical origins and some fundamental properties. We will also cover some soliton categories of particular interest for this work.

3.1 Solitons in Physics

Solitons, also known as “solitary waves”, have been the subject of intense studies in many different fields, including hydrodynamics, nonlinear optics, plasma physics and biology [Agr03].

The first observation of a solitary wave was in 1834. John Scott Russell, a Scottish naval engineer, was riding a pair of horses along a narrow channel when he observed a wave that would continue its course without apparent change of form or speed.

When working in nonlinear optics, solitons are classified as temporal or spatial depending if they maintain their shape while propagating or if they are confined to the transverse plane (orthogonal to the propagation direction). In this work we will only consider temporal solitons which are formed thanks to compensation of the group-delay dispersion by the self phase modulation (SPM).

3.2 Fiber Solitons

Temporal Solitons in optical fibers were first predicted in 1973 [Agr03], and have several applications in the field of optical communications.

The goal is to find a solution for the NLS equation (that we will call soliton solution), in which the input pulse maintains its shape as it propagates: $|A(z,t)| = |A(0,t)| \ \ \forall z.$

We can re-write equation (2.2.8), without considering fiber losses, using the soliton variables:

$$\tau = \frac{t - \beta_1 z}{T_0} \tag{3.2.1}$$

$$Z = \frac{z}{L_D} \tag{3.2.2}$$

$$u = \sqrt{|\gamma| L_D}\, A \tag{3.2.3}$$

Where T_0 is a temporal scaling parameter (normally the input 1/e intensity pulse width) and $L_D = T_0^2 / |\beta_2|$ is the dispersion length. The time variable (τ) travels at the group velocity. The resulting equation for silica fibers is:

$$-i \frac{\partial u}{\partial Z} = \frac{sign(\beta_2)}{2} \frac{\partial^2 u}{\partial \tau^2} + |u|^2 u \tag{3.2.4}$$

The sign of the dispersion parameter plays an important role in determining the soliton solution. For normal dispersion (β_2>0), optical fibers can support dark solitons

where the pulse has zero amplitude at its center. Consequently, in order to support bright solitons, the GVD needs to be anomalous ($\beta_2<0$).

Using the inverse scattering method we can find a soliton solution for (3.2.4) which has the following expression for its initial pulse envelope:

$$u(0,\tau) = N \sec h(\tau) \tag{3.2.5}$$

Where the parameter N is the soliton's order and is related to the input pulse and the fiber parameters as:

$$N^2 = \gamma P_0 L_D = \frac{\gamma P_0 T_0^2}{|\beta_2|} = \frac{2\pi c}{\lambda^2}\frac{\gamma P_0 T_0^2}{D} \tag{3.2.6}$$

In a hyperbolic-secant pulse as in (3.2.5) we can relate its 1/e intensity pulse width (T_0) and its Full Width Half Width pulse width (T_{FWHW}) as:

$$T_{FWHW} = 2\ln\left(1+\sqrt{2}\right)T_0 \approx 1.763\,T_0 \tag{3.2.7}$$

For a Fourier-Transform (FT)-limited pulse the product of frequency uncertainty and temporal uncertainty is minimized. For these pulses all the information is located on its amplitude. The Frequency and time width are related as:

$$\Delta\omega\Delta t = \frac{1}{2} \tag{3.2.8}$$

Which for a sech^2 pulse it can be re-written as:

$$\Delta\upsilon \;\; T_{FWHW} = 0.315 \tag{3.2.9}$$

Normally, standard solitons are unchirped in the absence of Stimulated Raman Scattering (IRS) and consequently they are transform-limited. However, the chirp-free nature is not ensured when their spectrum shifts because of IRS [Agr03].

3.3 Fundamental Soliton

The fundamental order or first order temporal soliton correspond to the N=1 case. It is the only solution that maintains its shape in every moment. The pulse shape is given by:

$$u(Z,\tau) = \sec h(\tau) e^{iZ/2} \tag{3.3.1}$$

The fundamental soliton condition can also be understood as the solution where the nonlinearity (particularly the SPM) compensates the fiber dispersion in every point along the fiber. Thus, the dispersion length (L_D) and the nonlinear length ($L_{NL} = (\gamma P_0)^{-1}$) are always equal.

3.4 Higher Order Solitons

When N>1 in (3.2.5), we have a higher order soliton. Instead of maintaining its shape over the entire fiber, higher order solitons have a periodical behavior in the z direction with period [Agr03]:

$$z_0 = \frac{\pi}{2} L_D = \frac{\pi}{2} \frac{T_0^2}{|\beta_2|} \approx \frac{T_{FWHW}^2}{2|\beta_2|} \tag{3.4.1}$$

3.5 Soliton Interaction

The presence of other pulses in the neighboring perturbs a temporal soliton simply because the combining optical field is not a soliton solution of the NLS equation. This

phenomenon is called soliton interaction and can cause the pulses to come closer or move apart in time domain.

Soliton interaction is critical for high speed soliton communication systems. In our case, it occurs between the fundamental and the high order solitons in the fiber.

3.6 Loss-Managed Solitons

In section 3.2 we found a soliton solution for the NLS when the fiber had no loss. In more general case, while propagating a soliton will lose part of its energy. Consequently, the pulse will broaden as the SPM is weakened and can no longer counteract the GVD.

Optical Amplifiers can be used for compensating fiber losses. Two techniques have been proposed: the Lumped Amplification, where optical amplifiers (generally EDFA) are placed periodically along the fiber, causing a sort of average compensation effect; and Distributed Amplification which provides nearly lossless fibers by compensating losses locally at every point. This objective is achieved by using Raman Amplifiers [Mol85]. In both solutions the location and gain of the amplifiers are key design parameters.

3.7 Dispersion Management Solitons (Average Solitons)

Dispersion management is widely used in WDM systems by employing specially designed fibers. Optical solitons benefit from this technique as power losses can be overcome by modifying the dispersion parameter in order to satisfy (3.2.6).

Fundamental solitons can be maintained in a lossy fiber if its GVD decreases exponentially as:

$$|\beta_2(z)| = |\beta_2(0)|e^{-\alpha z} \tag{3.7.1}$$

Fibers with such a GVD have been fabricated and are called Dispersion-Decreasing Fibers (DDF). Their main characteristic is the reduction of the core diameter along the fiber length. A disadvantage of DDF is that the average dispersion along the fiber links is normally large.

Another solution for compensating the fiber losses by dispersion management consists of using a dispersion map. In this case, a map period is formed by a concatenation of a positive dispersion fiber and a negative dispersion fiber. Even though the local dispersion does not agree with (3.7.1), the average dispersion over a map period does.

At first sight, normal dispersion fibers (D<0) do not support bright solitons and this solution should not work. Nevertheless, it has been shown that when the map period

is a fraction of the nonlinear length, nonlinear effects are relatively small and the pulse evolves in a linear fashion over one map period. In this case the SPM is compensated by the average dispersion. As a result the solitons' peak power, width and shape will oscillate periodically [Agr03].

Long distance transmission of an average soliton has been demonstrated by [Gri00]. In that experiment a 10-GHz pulse train propagated along a 28000 km re-circulating loop with near zero average dispersion. The dispersion map consisted of 100km of dispersion-shifted fiber (D= -1.2ps/nm/km) and 7km of standard fiber (D= 16.7 ps/nm/km). Amplifiers were placed every 25km.

Chapter 4: Short Pulsed Fiber Lasers

Fiber lasers have been available since 1961 [Agr201] as an alternative for solid state short-pulses lasers. As in any laser, we can identify three main components: an optical cavity, a pump and a gain medium (that performs the population investment).

Since 1989, Er^{+3} doped fiber-lasers have kept most of the attention as they can be used on the 1550nm telecommunication windows. Other rare earth materials, such as Yb^{+3} or Nd^{+3}, are used for high power lasers.

The first fiber lasers were continuous-wave (CW), but since the late 80s pulsed lasers have been built using a mode locking technique.

This chapter will give a quick review to some basic laser concepts and to solid state lasers. We will then show some typical configurations for fiber lasers.

4.1 Short Pulsed Cavity Lasers

It could look contradictory, a priori, to generate ultrashort pulses with a laser source, because of the frequency selection imposed by the optical cavity. Normally, these cavities will allow oscillations in a few very narrow frequency domains around the discrete resonance frequency: $\upsilon_q = qc/2L$ (q is an integer, c the speed of light and L

the optical length of the laser cavity) [Rul03]. Consequently, it can not deliver ultrashort pulses while working in its usual regime.

In order to obtain a pulsed laser, the cavity needs to work on the multimode regime, where all the longitudinal modes of the laser (where the unsaturated gain is greater than the cavity losses) exist simultaneously. The time distribution of the laser output depends essentially on the phase relationship between the different modes.

4.2 Mode-locking

While operating in a multimode regime, there is usually a competition between modes to be amplified by stimulated emission from the same atoms, molecules or ions. This contest brings fluctuation on the output instantaneous intensity, where the worst scenario is a totally random noisy signal.

By organizing the mode competition, the mode-locking technique tries to obtain periodic pulses at the output of the laser source; in frequency domain, the problem could be formulated as finding constant relative phases between modes.

Mode-locking will normally be achieved by inserting a nonlinear material in the cavity. In time domain, as the wave travels back and forward into the cavity, each time it goes through the nonlinear material, the stronger fields will be considerable

more amplified than the weaker fields. If the conditions are well chosen, the situation can arise to have all the energy concentrated in one single pulse.

There are two major classifications of mode-locking: passive and active. However, in some occasions a self-locking process is possible, if the following conditions are fulfilled:

- The pulse regime is favored over the CW regime.
- The overall system possessing the property of shortening the pulses (normally by Kerr effect).
- Some mechanism initiating the self-locking process (for example knocking the table or randomly moving some element in the cavity).

4.2.1 Active Mode-locking

Active mode-locking consist of modulating the amplitude of each longitudinal mode by changing the cavity losses or the gain of the amplifying medium through an active element introduced inside the fiber cavity. The first effect can be achieved by using an acoustic-optical crystal and the second by pumping the medium with another mode-locked laser.

4.2.2 Passive Mode Locking

If an absorbing medium with a saturable absorption coefficient (normally a liquid dye solution) is placed inside the cavity, the combination of this material and the saturable amplifying medium leads to the natural mode-locking of the laser. This process is called passive mode locking which has no external monitoring or feedback circuit.

The pulse reaches its final shape when it becomes self-consistent in the cavity, which means, when it keeps the same shape after a round trip.

The main problems with passive mode locking are: first, there are many compatible pairs of saturable absorbing and amplifying media with the right properties. Secondly, the output pulses are not very powerful and their wavelength is not easily tunable.

The hybrid method tries to take the best from the two previous ones in order to obtain a wider choice of wavelengths and powers. In this case, the saturable absorber is introduced inside a cavity with an external modulator, making it easier to obtain sub-picoseconds pulses than the classical active mode-locking.

4.3 Solid State Laser

A Solid State Laser uses a solid crystalline material as the gain medium and is usually optically pumped. They should not be confused with semiconductor or diode lasers which are also ‘solid state’ but are almost always electrically pumped.

In recent years, most of the work in the field of ultrashort light pulse generation have been based on the development of titanium-doped aluminum oxide ($Ti:Al_2O_3$, Ti:sapphire) as a gain medium. The emission band of these lasers is centered in the red region (~750nm) and can be tuned as much as 200nm [Rul03].

Even though active or passive mode-locking can be implemented, self-mode-locking has shown to be the best choice. Normally a Kerr lens acts as the nonlinear medium in order to achieve the locking property. The laser may need an additional external cavity to improve its stability. Figure 4.1 shows a typical setup for a Ti:sapphire laser.

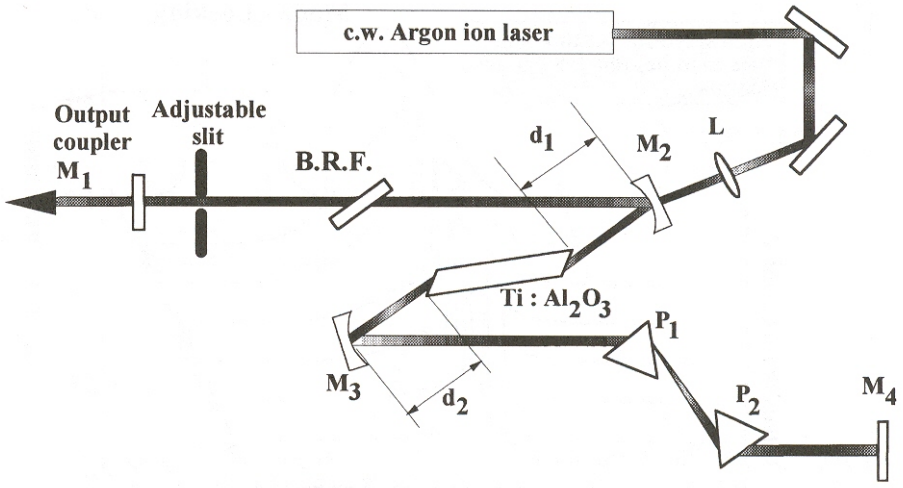

Figure 4.1: Ti:Sapphire laser setup with Argon CW pump and self-mode-locking. Fig 3-23 [Rul03].

The pump source can be an argon-ion CW laser (normally of about 10W of CW) or a diode pumped green emitting laser. The length of the crystal is in the order of 1cm. These kinds of lasers can generate 10fsec pulses at repetition rates of around 80Mhz.

4.4 Fiber Lasers

A quick overlook to figure 4.1 shows that Solid State lasers have several mechanically adjustable optical elements that make it difficult for a commercial implementation outside the optical table.

A fiber amplifier can be converted into a laser by placing it inside a cavity designed to provide optical feedback. In this case the cavity is formed by optical fibers, couplers and mirrors, the doped fiber acts as the gain medium, and a CW diode laser as pump.

The selection of the pumping laser for a fiber laser will depend on the dopant and the laser threshold for the system. Pumping schemes can be classified as three-level, four-level or up-conversion lasers [Agr201].

Fiber lasers have the following advantages:

- Simple doping procedure.
- Low loss and high efficiencies.
- Pumping by compact and efficient diodes.
- An all-fiber device minimizing the need of mechanical alignments.
- Mode-locking, simplified thanks to the long interaction length.
- Lower cost

Erbium doped fiber lasers work in the 1550nm region, which is ideal for long distances transmission. However, and thanks to the use of Periodically Poled Lithium Niobate (PPLN) waveguides, efficient 780nm lasers are feasible through frequency doubling [Arb97].

Nonlinear effects, such as XPM and SPM, play a central role in the operation of a fiber laser, especially in the achieving of mode-locking. Dispersion causes the broadening of the output pulse.

Fiber lasers can be configured for active or passive mode-locking, where the second option is normally simpler and cheaper. Two cavities designs are relevant: ring cavity and linear Fabry-Perot cavity. We will describe them in the next sections.

4.4.1 Ring Cavity Fiber Lasers

A simple ring fiber laser is shown in Figure 4.2, where the isolator works as the nonlinear medium. The repetition period is equal to the time needed to complete one round over the ring.

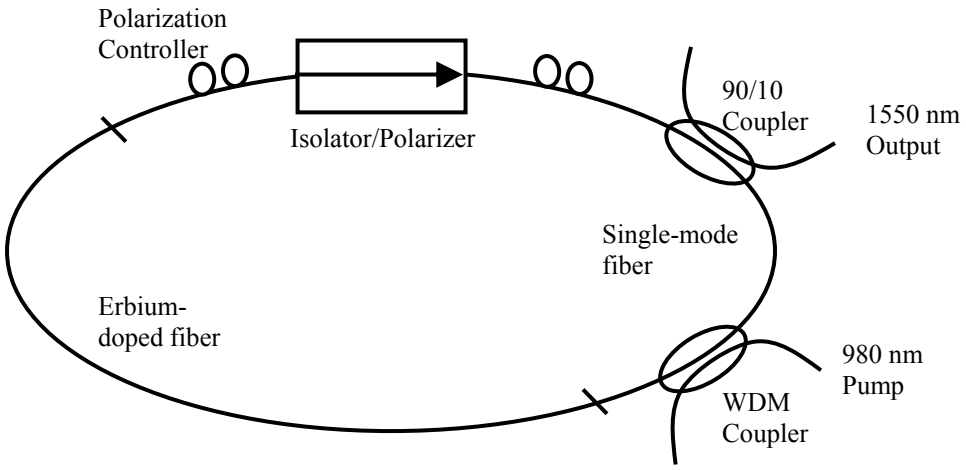

Figure 4.2 All-fiber ring-laser. An isolator works as a polarizer in the forward direction and blocks the light propagation in the reverse direction [Nel97].

In a passive mode locking configuration, the pulse shortening is performed by the coherent addition of self-phase modulated pulses, thus it is very fast. We explain this process in Figure 4.3; a pulse with arbitrary polarization is elliptically polarized by the use of a polarizer and a quarter-wave plate. The nonlinear medium will cause the pulse peak to rotate its polarization more than the pulse's edges. The last two elements (a half-wave plate and an output polarizer) filter the low intensity components, making the overall effect a stretch of the original pulse. The input and output polarizers are adjustable, and will be useful for the starting process.

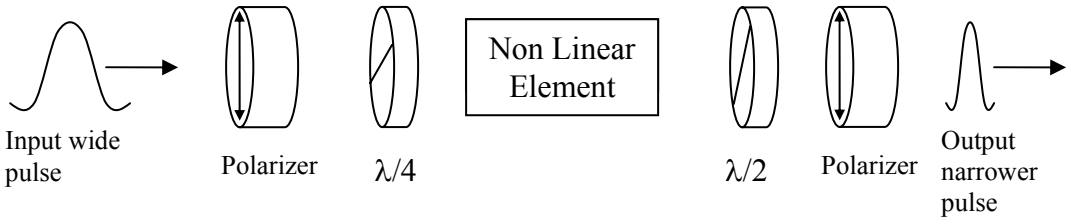

Figure 4.3 Pulses Shortening in a Ring Fiber Laser [Nel97].

Ideally, a passive mode-locked laser will evolve into a pulsed state on its own, without an external perturbation or trigger. This is called “self-starting”, where the pulses start up from the initial noise fluctuations. A mode-locked state can only be achieved if the gain experienced by the fluctuation is long enough to allow it to complete a round trip within its lifetime [Nel97]. Lasers in a unidirectional ring configuration have shown to self-start easily with relative low powers.

4.4.2 Fabry-Perot or Linear cavities

Another configuration for fiber lasers are linear cavities, where the gain medium is placed between two high-reflecting mirrors. Alignment of these cavities is not easy as cavity losses increases rapidly with a tilt of the fiber end or the mirror. This problem can be solved by depositing dielectric mirrors directly onto the fiber ends.

Dielectric coating can be damaged by the high power pump. Consequently, several alternatives exist including the use of WDM couplers, Bragg gratings or fiber-loop mirrors.

Figure 4.4 shows a schematic for a fiber laser with a saturable Bragg reflector used both as one edge of the cavity and as the non-linear element that allows the passive mode-locking.

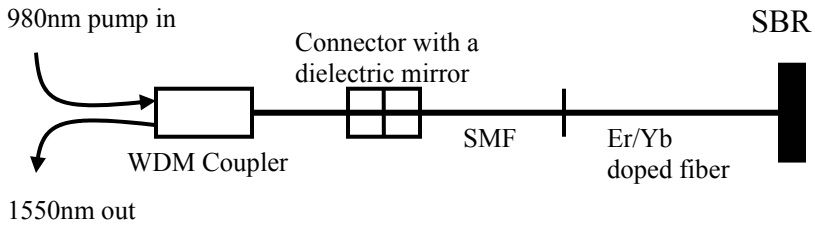

Figure 4.4: Schematic of a fiber laser where a Bragg reflector is used also for mode locking [Agra201].

Linear-cavity lasers will normally need between 10 to 100 times more powers than ring-lasers for self-starting.

4.5 High Power Pulsed Fiber Lasers

Single-mode fibers can not handle very high peak power signals due to their small fundamental mode area. In order to solve this problem, several techniques have been developed including cladding pumped lasers and cladding pumped holey fiber lasers.

Multimode fibers (MMF) are well known for its large area, and thus are a feasible medium for high power fiber lasers (MMF can handle up to 30 times larger power than SMF). However, when using MMF there are several problems derived from the interaction between modes: multimode dispersion, mode coupling, an increase in generated amplified spontaneous emission (ASE) power noise, etc.

Ideally, we would like to preserve single mode propagation in the MMF. This could be checked by splicing a MMF in between two single-mode fiber filters and measuring the insertion loss as a function of the MMF length. For a silica fiber with a cladding diameter of 250μm and a core diameter of 50μm, single-mode propagation can be preserved over lengths shorter than 20m. Also, in such fibers mode-coupling is relative insensitive to fiber bends [Fer00].

Figure 4.5 shows an experimental setup for a diffraction-limited passively locked (through a saturable absorber) MM fiber laser. In this case the pulse stretching is achieved by the use of two Faraday rotators and a fixed polarizer.

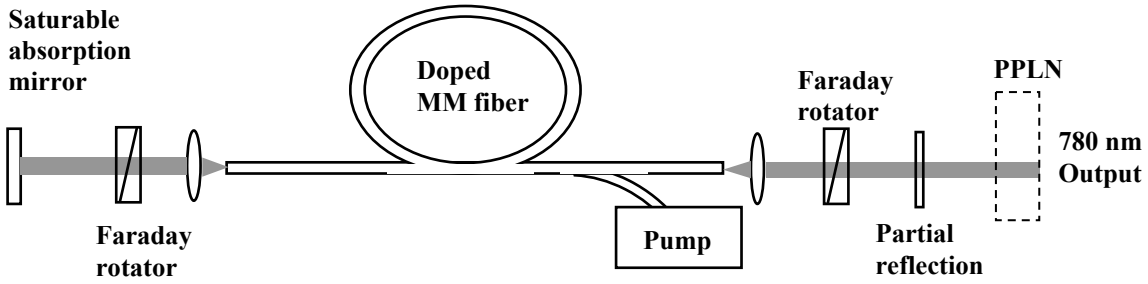

Figure 4.5: MM fiber oscillator side-pumped with a broad-area laser diode [Fer00]. A PPLN is introduced at the edge to frequency double the output signal.

Chapter 5: Photonic Crystal Fibers

5.1 Fundamentals of photonic crystal waveguiding

Photonic Crystal Fibers (PCF), also known as Microstructured Fibers (MF) or Microstructured Optical Fibers (MOF) [Bja03], represent one of the most active research areas in optics. Their main characteristic is the presence of a periodic or aperiodic structure (particularly air holes) in the core-cladding area of the fiber. Optical applications for periodic structures are well known in nature, a classical example are the colorful spots on several butterfly's wings; as the insect moves them, we can appreciate the spots changing color [Bja03].

One Dimensional (1D) periodic structures, or one dimensional photonic crystals (PC), are extensively used for important applications in optics, such as diffraction gratings, Bragg stacks, etc.

Fiber optics and waveguides propagation usually relies on internal reflection or index guiding. However, PCF, which are a 2D array, normally rely on the bandgap effect. This phenomenon, similar to the recombination of a electron-hole pair in a

semiconductor, inhibits the electromagnetic field to propagate with certain frequencies, forming a bandgap.

5.2 Classification of PCF

Different applications of PCF have different requirements in the fabrication process. When observing its profile we can vary the number, size, form and position of the holes. For some applications it is also important to dope the core in order to dominate the attenuation and dispersion. Figure 5.1 shows the most used terms and major classes of PCF.

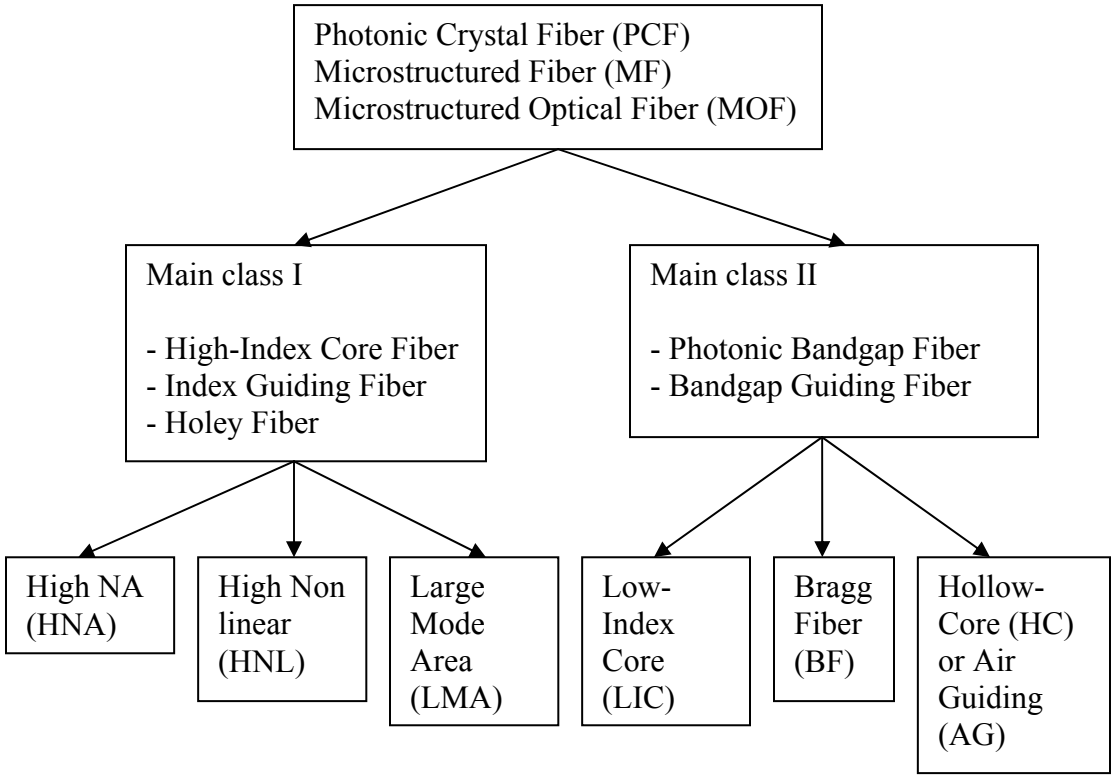

Figure 5.1: Classification of PCF [Bja03].

Only the fibers on the Main Class II propagate thanks to the bandgap effect, while the rest are index-guiding fibers.

HNL are especially relevant for this work. These fibers normally have few holes located in the cladding area and a very small (~2μm) core diameter.

5.3 Modeling of microstructured fibers

Two dimensional photonic crystals are the most studied case of periodical structures *[Bja03]*. Figure 5.2 shows an axial cut of a PCF where for simplicity a hexagonal representation is chosen. In this example we have a background material (normally SiO_2) and cylinders of diameter d arranged in a hexagonal lattice with a period Λ. Most fiber parameters will depend on the factor d/ Λ.

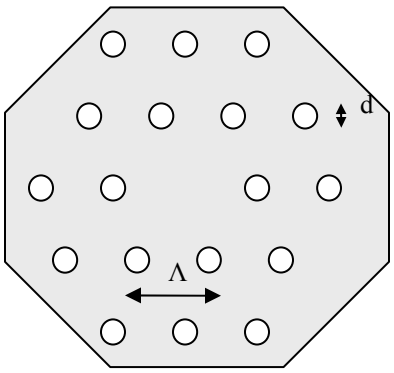

Figure 5.2: Geometrical characteristics of PCF.

Cylinders normally contain just air, but eventually they can be filled with gasses or other substances in order to build an optical sensor.

When modeling a Photonic Bandgap Fiber, the full vectorial nature of the electromagnetic waves has to be taken into account. A simulation software developed by MIT is widely used by the research community [MIT04].

On the other hand, when working with Index Guided Fibers, it is possible to apply the methodology developed for standard fibers by calculating an effective index for the cladding. The idea is to replace the PCF by an equivalent step-index fiber, where the core is pure silica and the cladding has a refraction index that considers the geometry of the PCF. The calculation of the core radius of the equivalent step-index fiber, as well as other numerical methods for modeling PCF can be found in the literature. [Bja03]

When considering HNL-PCF, its Raman gain coefficient will vary from a standard fiber. There are two factors that affect this coefficient, first the smaller effective area (less than $10\mu m^2$). Second, the existence of air holes where no Raman Effect can occur. The numerical calculations for both parameters from the geometrical characteristics of the fiber are shown in [Fuo03].

5.4 Fabrication of photonic crystal fibers

The idea of producing optical fibers with microscopy air holes goes back to the early days of optical fiber technologies.

As in the standard fiber, PCF fabrication consists of two main steps: the preform production and the drawing process using a high temperature furnace in a tower set-up.

It is not desired to build a preform by drilling every hole in the bulk silica. However, the product is obtained by directly staking silica tubes and rods with a circular outer shape. Employing circular elements introduces additional air gaps in the fiber preform. These could be avoided by using hexagonal elements, but in that case the manufacturing process would be more complex. For air core fibers, the center rod is replaced by capilar tubes that will break during the drawing process, forming an empty core structure. After stacking, the capilars and rods may be held together by thin wires and fused in an intermediate process, forming preform-canes.

One of the main disadvantages of the stack and pull technique is the contamination of the glass elements. In recent years, other fabrication methods such as extrusion of the core preform have been introduced.

The drawing of PCF is done in conventional towers. In order to avoid the collapse of air holes due to its low surface tension, low temperatures are used (around 1900^{o}C). The key element of this process is to keep the fiber regular structure from the preform up to the fiber dimension.

5.5 Applications

The most popular PCF are the High Nonlinear Fibers (HNL). They can achieve a high non-linear coefficient and a positive dispersion parameter in the visible region, allowing the formation of optical solitons. This effect is used to build highly wavelength-tunable fiber lasers, with short fiber lengths. HNL fibers are also used for supercontinuum (500 to 1700nm) generation, which has applications in metrology (frequency references), coherence tomography and spectroscopy. When the zero-dispersion wavelength is shifted at 1550nm, HNL fibers are very attractive for telecom applications such as 2R Regenerators, multiple clock recovery, pulse compression, wavelength conversion and supercontinuum WDM sources.

Double claddings PCF are of predominant interest in the context of high power devices. Normally the fiber is doped with rare-earth elements such as Yb^{3+} and Nd^{3+}. These fibers have a high numerical-aperture, permitting an effective coupling of the pump power.

Air guiding fibers can be used as the active medium for optical sensors, where the core can be filled with the target gas or biological species.

Chapter 6: Experimental and Numerical Analysis of Soliton Self-Frequency Shift

The goal for this Chapter is to build and simulate a wavelength shifter to be used in conjunction with a pulsed fiber laser as a pump for two photons microscopy. We will show the complete setup in Chapter 8. Similar systems were reported in [Nor99] and [Nor02]. However, there have been no reports of the use of these sources for two photon imaging.

We will first introduce the experimental setup and show the resulting spectrums. We will then generalize the NLS equation in order to include the Raman scattering. Through the numerical analysis we will show the pulse evolution while propagating along the optical fiber.

6.1 Experimental Results

The experimental setup is shown in Figure 6.1. The pump is a pulsed fiber laser (IMRA Femtolite Ultra) which transmits 100fsec pulses in the 780nm wavelength at a repetition rate of 50MHz and a maximum output average power of 20mW. The non-linear medium consisted of 7m HNL-PCF (Photonic Crystal Fiber NL-18-710). The fiber parameters are detailed in Appendix A. The fiber's zero-dispersion wavelength

is 710nm. For the selected pump, the fiber is working at the anomalous dispersion region as needed to generate bright solitons.

The power launched into the fiber was adjusted by mechanically misaligning the optical system. The signal at the output of the fiber was coupled into an optical spectrum analyzer (ANRO AQ6317B).

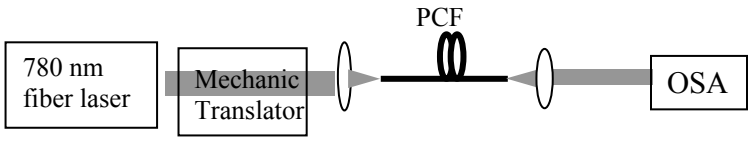

Figure 6.1: Experimental Setup for a Wavelength-Tunable Pulsed Laser Source.

When the incoming pulse has low average power, the chromatic dispersion is the predominant effect and the pulse is simply broadened when traveling trough the fiber. As we increase the input power, the SPM effect decreases the amount of total broadening of the original pulse. After exceeding the Raman threshold, the pulse will change its central frequency thanks to the SRS in a process known as pulse self-frequency shift (PSFS) [Zys87].

After an initial stage of narrowing and when the incoming pulse exceeds a certain threshold (in our case 200μW of average power), the pump pulse brakes into two pulses by a phenomenon described by Zysset et al [Zys87] [Bea87]. The generated pulse is formed at the longer-wavelength side of the pump (also called Stokes bands)

and forms a fundamental soliton. The center wavelength of this soliton is shifted as the soliton propagates along the optical fiber. The shifting process is called soliton self-frequency shift (SSFS) and is a result of the SRS. The amount of frequency shift will depend on the pump peak power and the fiber length. Figure 6.2 shows the experimental spectrum obtained for the setup in Figure 6.1 while varying the launching power.

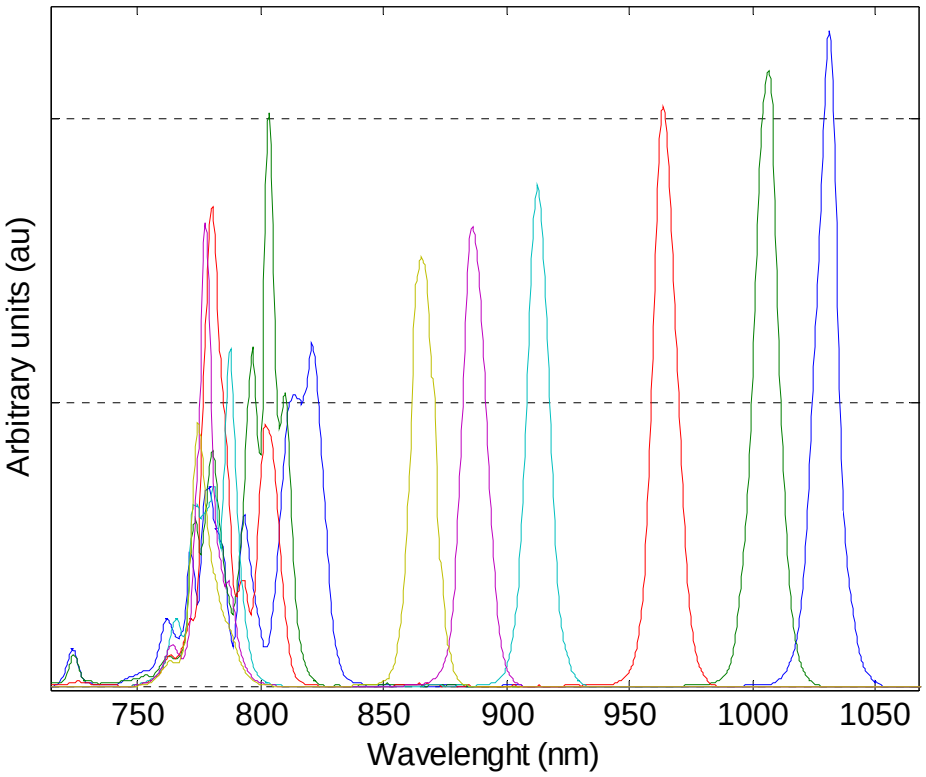

Figure 6.2: Experimental spectrums for a wavelength shifter where a mechanical translator is used to vary the input average power as shown in figure 6.1.Different colors correspond to different input powers.

We can observe in figure 6.2 that the fundamental soliton is shifted over 1μm, but a second order soliton is formed from the remaining power of the original pulse when the fundamental soliton is above 920nm.

6.2 Generalized Non-Linear Schrödinger Equation

In this section we will generalize the NLS equation in order to explain the experimental results of the previous section. Although equation (2.2.8) explains most of the common nonlinear effects in an optical fiber, it does not include the SRS which origins the SSFS.

Intra-pulse Stimulated Raman Scattering is related to the delayed nature of the vibrational response of the SiO_2 molecules. Thus, mathematically, we need to use the most general form for the nonlinear polarization given in equation (2.1.6) assuming the following functional form for the third-order susceptibility:

$$\chi^{(3)}(t-t_1,t-t_2,t-t_3)=\chi^{(3)}R(t-t_1)\delta(t-t_2)\delta(t-t_3) \tag{6.2.1}$$

Where R(t) is the normalized nonlinear response function. It includes both the electronic and the vibrational (Raman) contributions. Assuming that the electronic contribution is instantaneous, R(t) can be written as [Sto89] [Sto92]:

$$R(t)=(1-f_R)\delta(t)+f_R h_R(t) \tag{6.2.2}$$

Here f_R represents the fractional contribution of the delayed Raman response to the nonlinear polarization and $h_R(t)$ is the Raman response function which is responsible for the Raman gain whose spectrum is given by:

$$g_R(\Delta\omega) = \frac{\omega_0}{cn_0} f_R \chi^{(3)} \operatorname{Im}\left[\tilde{h}_R(\Delta\omega)\right] \tag{6.2.3}$$

The Raman gain can be found experimentally as shown in [Sto92]. The real part of $\tilde{h}_R(\Delta\omega)$ is found by using the Kramers-Kronig relations. Figure 6.3 shows the temporal variation of $h_R(t)$ and Figure 6.4 shows a typical Raman gain for a SiO_2 fiber. We should note that $h_R(t)$ becomes nearly zero for pulses wider than 5ps.

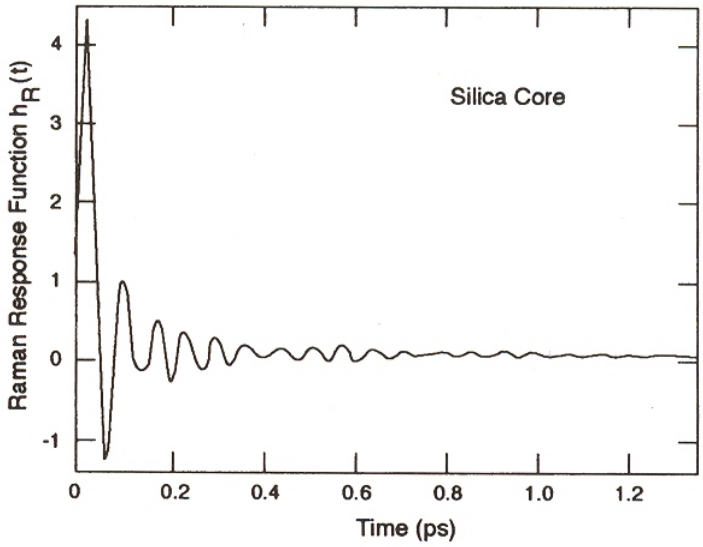

Figure 6.3: Raman Response Function [Agr01].

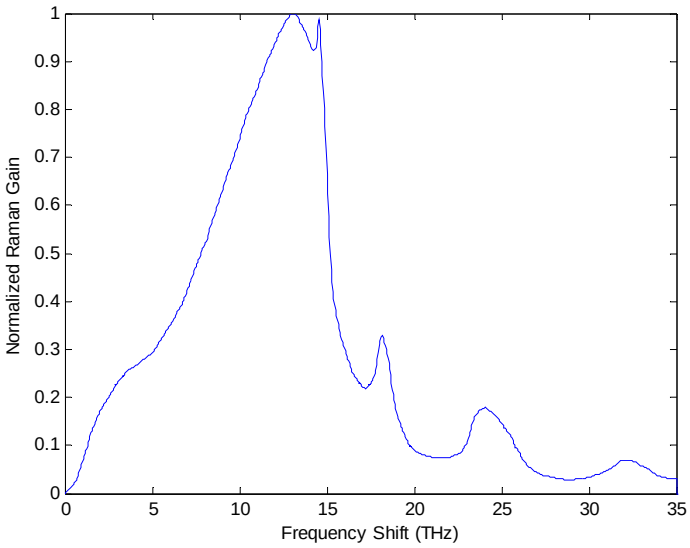

Figure 6.3: Normalized Raman Gain for a SiO2 fiber. The maximum value is at $\Delta\upsilon = 13.2THz$ ***(equivalent to*** $\Delta\lambda = 26.7nm$ ***) when the central frequency is 780nm [VPI05].***

A common analytical approximation for the Raman response function is:

$$h_R(t) = \frac{\tau_1^2 + \tau_2^2}{\tau_1 \tau_2^2} e^{(-t/\tau_2)} \sin(t/\tau_1) \tag{6.2.4}$$

The parameters τ_1 and τ_2 are adjustable for a good fit to the experimentally known gain spectrum. The generally accepted values are: τ_1=12.2fsec, τ_2=32fsec and f_R=0.18.

By considering equation (6.2.1), the new expression for the nonlinear Schrödinger equation is generalized to include the Raman scattering as:

$$\frac{\partial A}{\partial z} + \frac{\alpha(\omega)}{2} A + \beta_1 \frac{\partial A}{\partial t} + \frac{i}{2}\beta_2 \frac{\partial^2 A}{\partial t^2} - \frac{1}{6}\beta_3 \frac{\partial^3 A}{\partial t^3} = i\gamma(\omega)\left(1 + \frac{i}{\omega_0}\frac{\partial}{\partial t}\right)\left(A(z,t)\int_{-\infty}^{+\infty} R(t')\left|A(z,t'-t)\right|^2 dt'\right)$$

(6.2.5)

The accuracy of this equation is verified by showing that it preserves the number of photons during the pulse propagation if the fiber losses are set to zero (α=0). The pulse energy is not conserved as part of the pulse energy is absorbed by the silica molecules (Raman scattering is inelastic). These nonlinear losses are included in (6.2.5).

For pulses wide enough to contain many optical cycles (widths>>10fsec), we can use a Taylor-series expression for the pulse envelope:

$$\left|A(z,t-t')\right|^2 \approx \left|A(z,t)\right|^2 - t'\frac{\partial}{\partial t}\left|A(z,t)\right|^2 \tag{6.2.6}$$

Another simplification consists on defining the first moment of the nonlinear response function as:

$$T_R = \int_{-\infty}^{\infty} tR(t)dt = f_R \int_{-\infty}^{\infty} th_R(t)dt = f_R \left.\frac{d\left(\mathrm{Im}\,\tilde{h}_R\right)}{d(\Delta\omega)}\right|_{\Delta\omega=0} \tag{6.2.7}$$

The result in the Schrödinger equation is:

$$\frac{\partial A}{\partial z} + \frac{\alpha}{2}A + \frac{i}{2}\beta_2\frac{\partial^2 A}{\partial T^2} - \frac{1}{6}\beta_3\frac{\partial^3 A}{\partial T^3} = i\gamma\left(\left|A\right|^2 A + \frac{i}{\omega_0}\frac{\partial}{\partial T}\left(\left|A\right|^2 A\right) - T_R A\frac{\partial\left|A\right|^2}{\partial T}\right) \tag{6.2.8}$$

In this case the time frame moves with the pulse at the group velocity:

$$T = t - z/\upsilon_g \equiv t - \beta_1 z \tag{6.2.9}$$

Equation (6.2.5) is the most generic NLS formulation where the complete solution can only be found numerically using, for example, the Split-Step Fourier Method as explained in Chapter 2.

6.3 Numerical Analysis

In order to understand the experimental results obtained in section 6.1 we will numerically solve equation (6.2.5) for different input powers and fiber lengths.

The numerical calculations were done using the software VPItransmissionMaker [VPI05] where the numerical parameters are detailed in Appendix B. The fiber parameters are the same as in the experimental setup and are shown in Appendix A.

As it was already mentioned, when the input optical average power exceeds 200μW, the original power is breaking into two pulses creating an optical soliton. Figure 6.5 shows the numerical simulation of the formation of this soliton over the "wide" pump pulse in time domain.

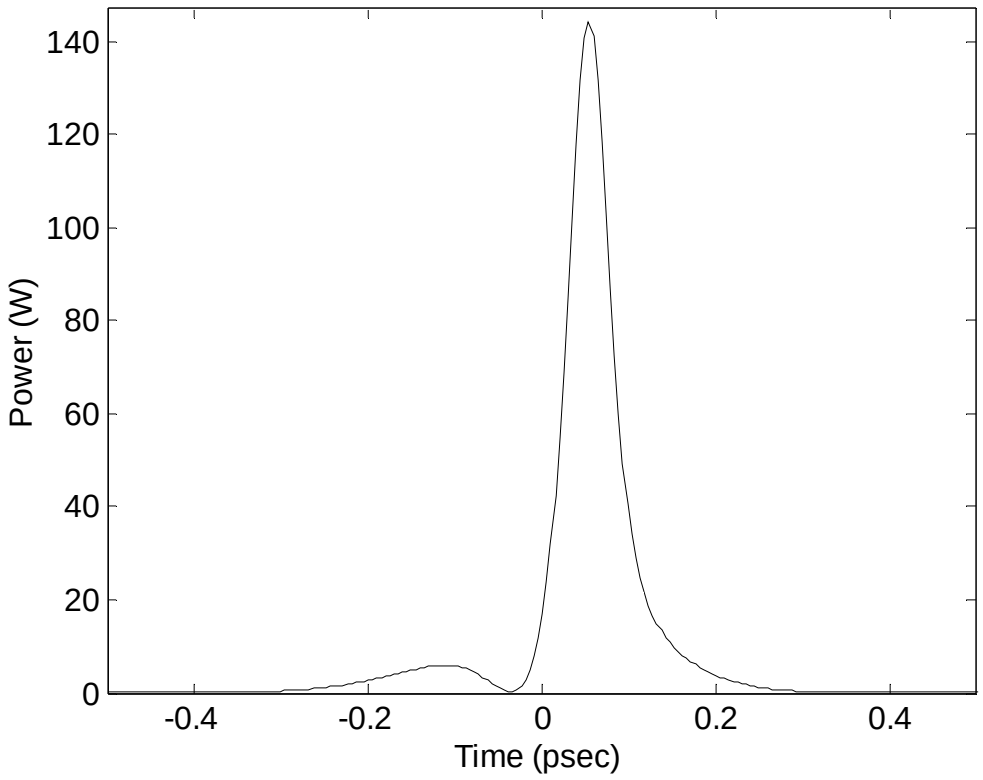

Figure 6.5: Soliton formation from the original pump pulse through pulse break-up. The input pulse was 300μW of average power and 0.5m of HNL-PCF.

While propagating along the fiber, the new pulse (a soliton) is shifted in frequency. The Soliton Self-Frequency Shift (SSFS) was first observed by L.F.Mollenauer, et al. [Mol85] and analytically described by Gordon [Gor86]; this will be detailed in Chapter 7. The magnitude of the wavelength shift is dependent upon the fiber length and the pump power. These two dependencies will be studied in this section.

The first analysis consists of studying the time (Figure 6.6) and spectrum (Figure 6.7) characteristics at the output of 7m of HNL-PCF when the average input power is modified.

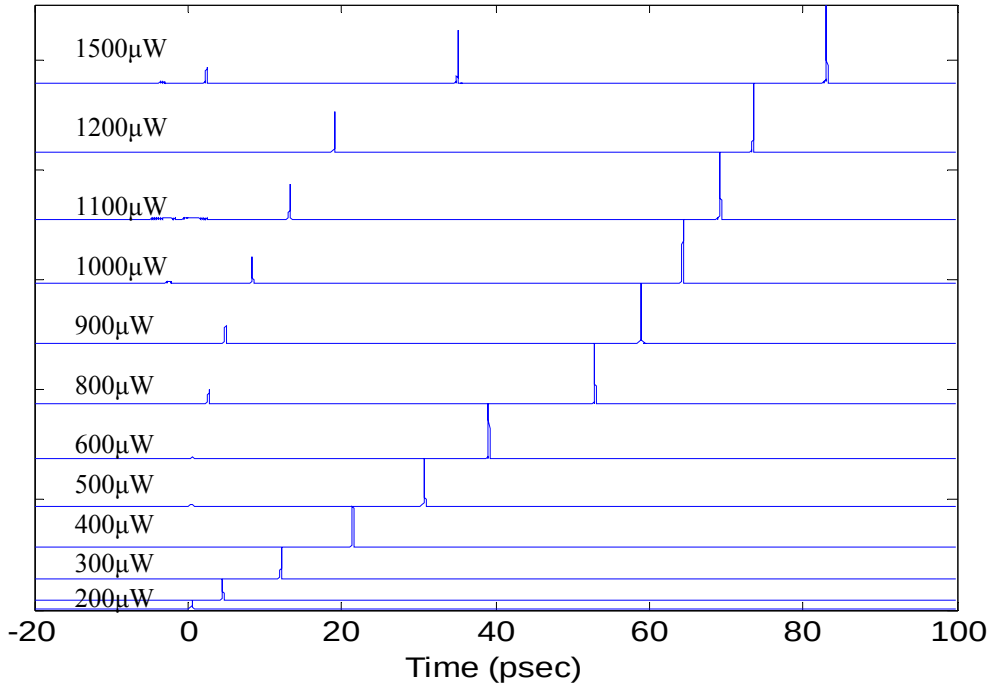

Figure 6.6: Time domain Characteristics of the output from a 7m HNL-PCF for different input average power.

Soliton formation in a HNL-PCF was first predicted by Reid et al in [Rei02]. In our simulation, the fundamental soliton is generated when the input average power is 200µW and the second order soliton when it is 800 µW, which agrees with equation (3.2.6). After the soliton is generated it rapidly shifts its central wavelength.

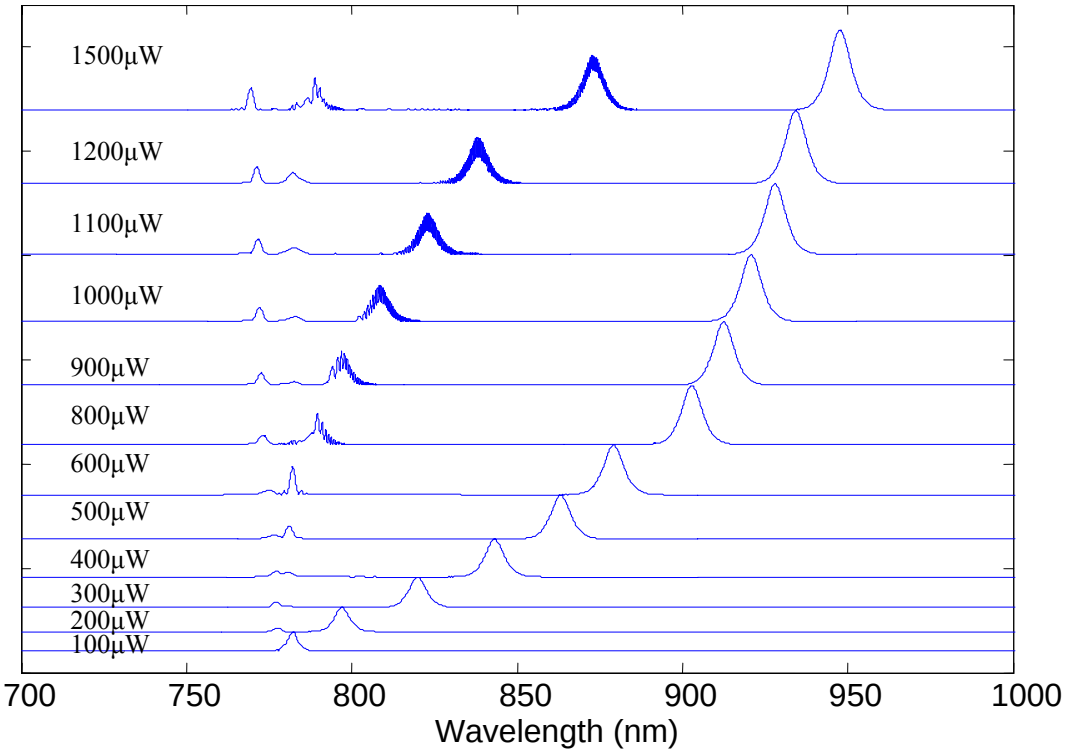

Figure 6.7: Wavelength Shift for different Input Average Power in a 7m HNL-PCF.

It can be observed in the time domain analysis (Figure 6.6) that the fundamental soliton is delayed with respect to the pump pulse. This delay has two components: the group delay dispersion and the delayed nature of the Stimulated Raman Scattering. If we suppose a dispersion parameter of D = 68 ps/nm/km and a bandwidth of 10nm, the delay due to the linear dispersion would be: $\Delta T = 68 \times 10 \times 0.007 = 5 ps$. Consequently, the delay shown in figure 6.6 is mainly due to the Raman Effect.

Figure 6.7 shows that it is possible to build a wavelength shifter without second order generation in the range of 780 to 920nm. Further shift is possible if we filter these lower wavelength components.

Figure 6.8 shows how the wavelength shift evolves when we vary the input average power for 3m and 7m of HNL-PCF. This study was done by [Nor99] for a polarization maintaining fiber. For low input power the group delay dispersion dominates and there is no soliton formation. As the power increases, the fundamental soliton is formed and shifts its central wavelength linearly until it reaches a saturation behavior. This is caused by both the fraction of power taken by the second order soliton and the wavelength dependency of the fiber parameters. The effect of the fiber parameters on the soliton self-frequency shift is analyzed in Chapter *7*.

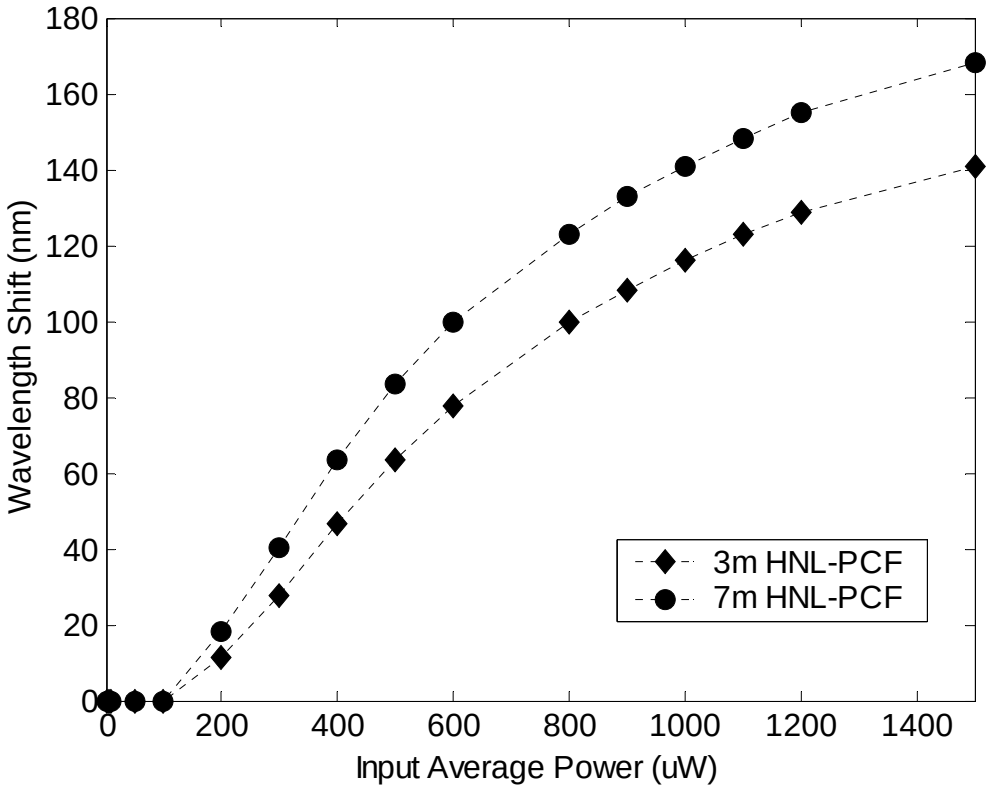

Figure 6.8: Wavelength Shift and Input Average Power for 3m and 7m HNL-PCF.

When the input power reaches certain limit, we can observe the formation of a supercontinuum (SC) [Ort02]. This phenomenon consists on the considerable spectral broadening of optical pulses and has applications in the fields of optical communications, metrology and coherence tomography [Ort02]. The origin to the SC generation in HNL-PCF is related to the split of higher-order solitons into several pulses with different red-shifted central frequencies. The non-solitonic pulses maintain a phase relationship that causes the SC radiation [Por03]. Figure 6.9 shows the numerical spectrum after applying a 5mW pulse to 7m of HNL-PCF, where a SC is generated.

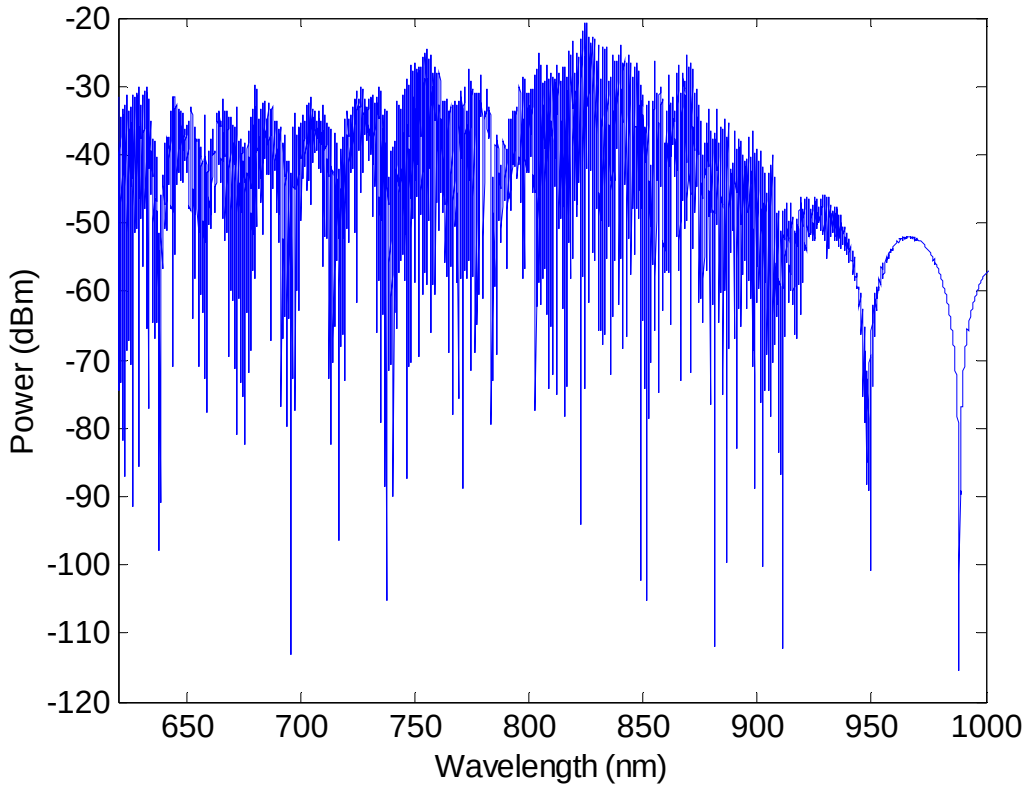

Figure 6.9: Supercontinuum generation after applying 5mW pulses to 7m of HNL-PCF.

In figure 6.8 we can also observe that the difference between the wavelength shifts for 3m and 7m of fiber is very small. By studying the dependency of the wavelength shift on the fiber length, we will also understand how the pulse evolves as it propagates through the fiber. We perform a numerical simulation for a HNL-PCF varying its length form 0.1m up to 7m. The results are shown in figures 6.11 to 6.14. In the first section of the fiber, the chromatic dispersion and the self phase modulation (SPM) compete between each other causing the narrowing of the original pulse. After the soliton is formed through the break-up process, it starts shifting its central wavelength. As it propagates, the soliton suffers the effects of fiber losses and changes on the

wavelength-dependent fiber parameters. The consequence of the presence of fiber losses can be summarized as follows: as the peak power decreases, the width of the soliton increases in order to maintain the fundamental soliton relationship. The overall effect is a decrease on the wavelength shift slope as the fiber length increases. Figure 6.10 shows the time characteristics as a function of the fiber length; we observe the pulse attenuation and the pulse broadening.

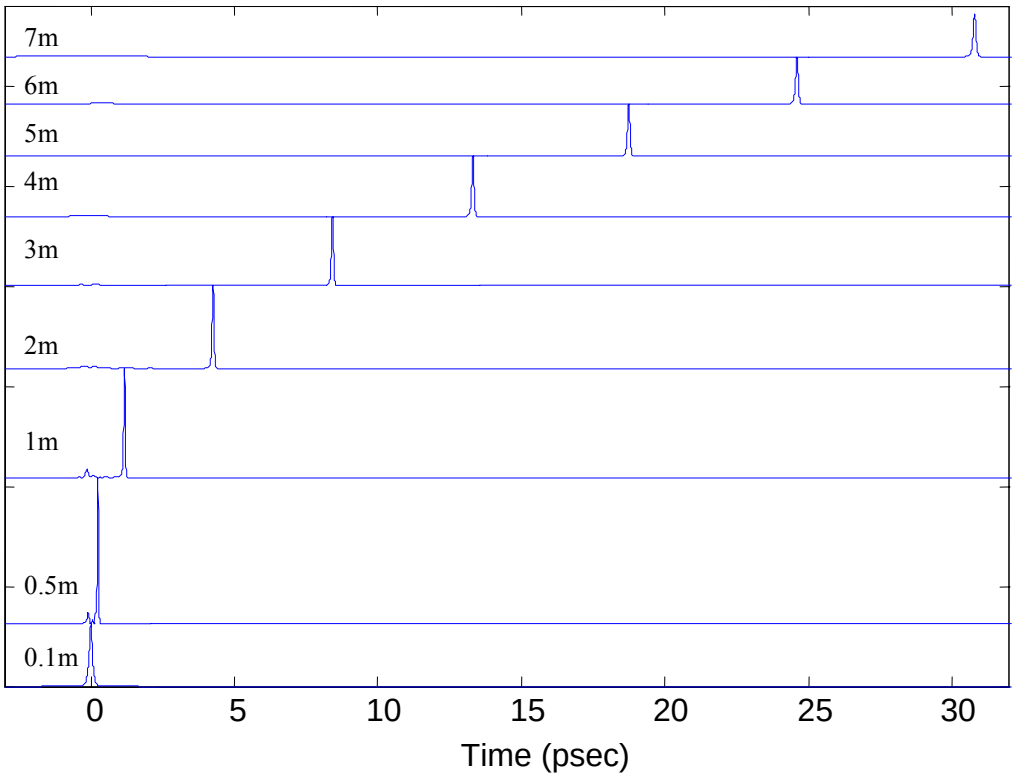

Figure 6.10: Time domain characteristics for different HNL-PCF lengths and an input average power of 500μW. The soliton is form after propagating along over 0.5m of fiber and then is attenuated and broadened.

In the next two figures we show the evolution of the wavelength shift and the soliton's pulse width as a function of the fiber length where both cases agree with the results of [Nor99] for a polarization maintaining fiber.

In Figure 6.11 we can verify the saturation behavior of the wavelength shift as we increase the fiber length. In the case of an input signal of 1mW average power, a second order soliton is formed soon after the fundamental soliton. The second order soliton has a lower peak power that gives a lower shift but it also has saturation behavior as a function of the fiber length.

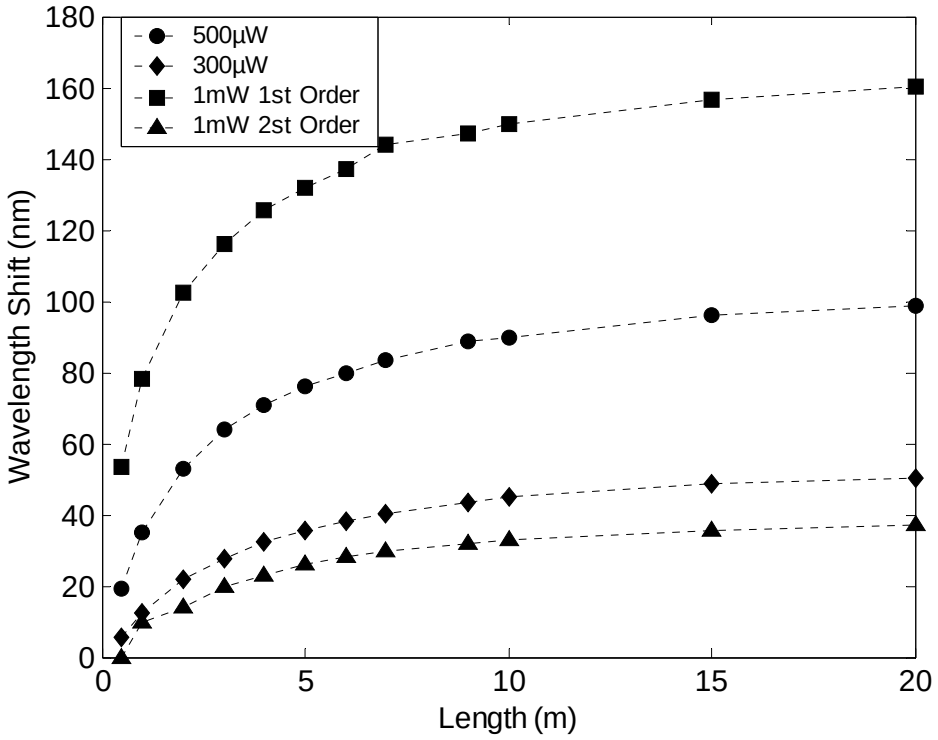

Figure 6.11: Wavelength Shift and Fiber length for a HNL-PCF and different input average powers. For 1mW, we show the 1st and 2nd order soliton shift.

From Figure 6.11 it can be seen that a higher power pump pulse will produced a narrower soliton. In the next chapter it will be demonstrated that a narrower pulse width will cause a longer wavelength shift. As the pulse propagates along the fiber, its

pulse width is increased in order to maintain the fundamental soliton condition. In figure 6.13 we show how the soliton order is maintain around N=1 as explained in [Sto92].

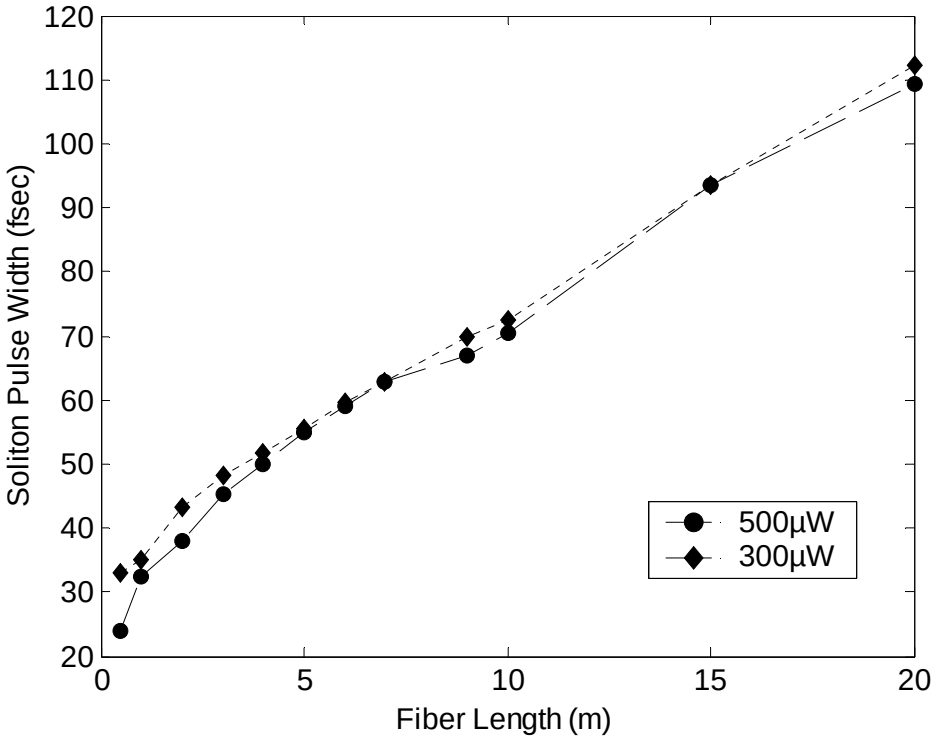

Figure 6.12: Soliton Pulse width and Fiber Length for a HNL-PCF.

We will finally compare the numerical spectrum and the experimental data for 7m of HNL-PCF detailed in section 6.1. The Input optical power is modified by optical misalignment as shown in figure 6.1. Figure 6.14 shows the good agreement between the wavelength shift observed in our experiments and the shift predicted by the numerical analysis

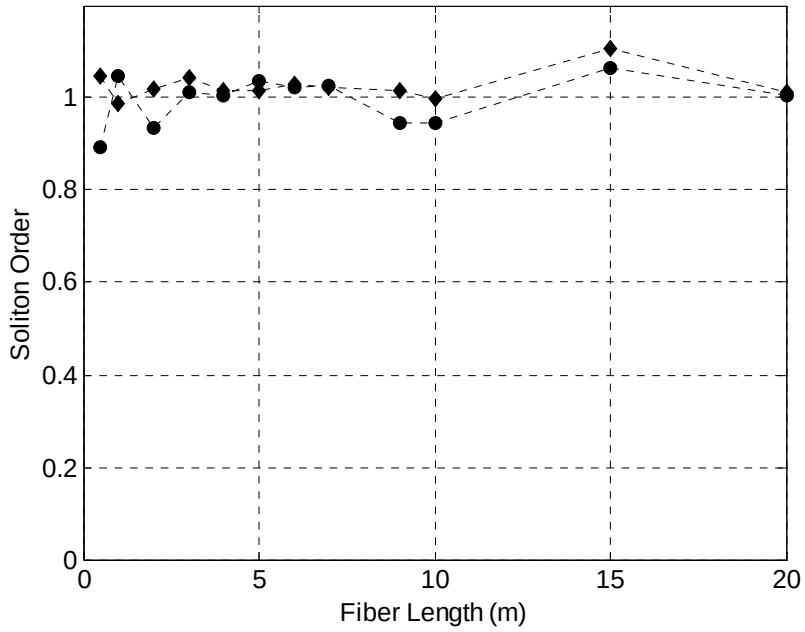

Figure 6.13: Soliton order N and fiber length. Circles represent the values for an input average power of 500μW and the diamonds for 300 μW.

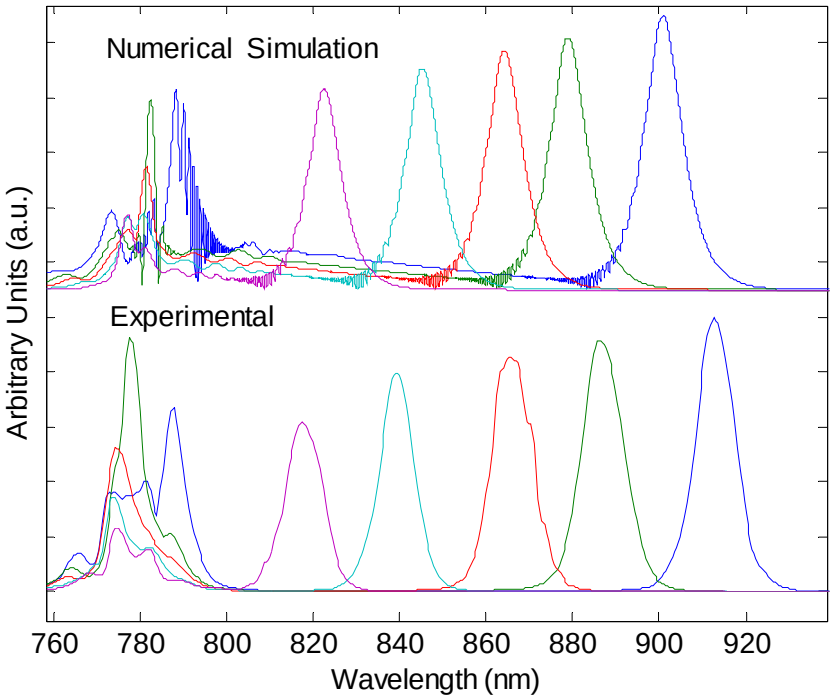

Figure 6.14: Numerical and Experimental Results Wavelength Shifts for the setup in figure 6.1.

Chapter 7: Analytical Analysis of Soliton Self-Frequency Shift

Solitons have been introduced in Chapter 3 as a solution for the NLS equation that preserves the pulse shape as it propagates. In this section we are only going to consider fundamental order solitons.

Stimulate Raman Scattering will cause a pulse mean frequency to shift toward lower values while propagating in an optical fiber. In the special case of an optical soliton, it is possible to formulate an analytical expression for this shift as a function of its pulse width. However, this expression is only valid while the fiber parameters stay constant while the pulse is shifting its central frequency.

In this chapter we take a close look at the analytical theory formulated by Gordon [Gor86] and experimentally confirmed by Mitschke and Mollenauer [Mit86]. We will then introduce a semi-analytical method for calculating the SSFS when the fiber parameters are not constant and we will contrast it with numerical calculations for different fibers.

7.1 Analytical Model

Shifts of the mean soliton frequency can only be caused by frequency-dependent losses or gain in the fiber. The Raman scattering will amplify the lower frequency components (acting as the signal) at the expense of the higher-frequency parts (acting as the pump).

Optical Solitons are the solutions of equation (3.2.4) that will not change its shape while propagating. That normalized equation needs to be generalized in order to consider the Raman scattering effect in a similar form as in equation (6.2.5):

$$-i\frac{\partial u(\tau)}{\partial Z} = -\frac{1}{2}\frac{\partial^2 u(\tau)}{\partial \tau^2} + u(\tau)\int ds\, f(s)\left|u(\tau - s)\right|^2 \qquad (7.1.1)$$

In this expression we are neglecting the electronic vibrational contributions and all other nonlinear dispersive terms, *f(s)* represent the normalized fractional Raman response function: $f(s) = f_R h_R(s)$, where *f(-s)=0* (due to causality) and $\int f(s)ds = 1$.

The Fourier Transform expression for a fundamental soliton as in equation (3.2.5) is:

$$\tilde{u}(\Omega) = \int d\tau\, u(\tau) e^{j\Omega\tau} = \frac{1}{2}\sec h\left(\frac{\pi\Omega}{2}\right) \qquad (7.1.2)$$

Where $\Omega = (\omega - \omega_0)T_0$ is the frequency deviation in soliton units and ω_0 the mean (or central) frequency of the pulse. We can now represent equation (7.1.1) in the frequency domain (FT):

$$-i\frac{\partial\tilde{u}(\Omega)}{\partial Z}=-\frac{1}{2}\Omega^2\tilde{u}(\Omega)+FT\left[u(\tau)\int ds\, f(s)\left|u(\tau-s)\right|^2\right] \tag{7.1.3}$$

$$FT\left[u(\tau)\int ds\, f(s)\left|u(t-s)\right|^2\right]=\tilde{u}(\Omega)*FT\left[f(\tau)*\left|u(\tau)\right|^2\right] \tag{7.1.4}$$

We introduce the function $\chi(\Omega)=FT[f(\tau)]=\int ds\, f(s)e^{i\Omega s}$ that has the nature of a susceptibility due to the conditions on *f*. Returning to our analysis for the NLS equation in frequency domain and using the Fourier transform properties for the convolution and the complex conjugate:

$$-j\frac{\partial\tilde{u}(\Omega)}{\partial Z}=-\frac{1}{2}\Omega^2\tilde{u}(\Omega)+\int d\Omega''\tilde{u}(\Omega-\Omega'')\chi(\Omega'')\int d\Omega'\tilde{u}^*(\Omega')\tilde{u}(\Omega'+\Omega'') \tag{7.1.5}$$

The complex function $\chi(\Omega)=\chi'(\Omega)+j\chi''(\Omega)$ verifies the Kramers-Kronig relations. Its imaginary part can be related to a loss coefficient that we will call the Raman attenuation coefficient (α_R). To find this relationship, we split the spectrum of our pulse in two components: the pump (u_p) and the signal (u_s). The first one is considered as a single frequency, constant amplitude signal and the second one is only a small perturbation:

$$u(t)=u_p e^{-i\Omega_p t}+u_s(t) \tag{7.1.6}$$

$$\tilde{u}(\Omega)=u_p\delta(\Omega-\Omega_p)+\tilde{u}_s(\Omega) \tag{7.1.7}$$

Substituting (7.1.7) in (7.15), where we only consider the terms proportional to the pump power and the imaginary part on the right-side terms, we get:

$$\frac{\partial|\tilde{u}_s(\Omega)|^2}{\partial Z}=-2\chi''(\Omega-\Omega_p)|u_p|^2|\tilde{u}_s(\Omega)|^2 \tag{7.1.8}$$

We finally obtain an expression for the nonlinear Raman attenuation coefficient:

$$\alpha_R(\Omega) = -2\chi''(\Omega - \Omega_p) = 2\,\mathrm{Im}\left[\int ds\, f(s) e^{j\Omega s}\right] \tag{7.1.9}$$

After finding a frequency-dependent attenuation, we would like to obtain its relationship with the central frequency shift. In order to proceed, we will first define the mean frequency deviation of the soliton as:

$$<\Omega>= \pi \int d\Omega \Omega |\tilde{u}|^2 \tag{7.1.10}$$

This magnitude is normally zero, when considering a fundamental soliton. We would like to evaluate its derivative with respect of the Z position:

$$\frac{d<\Omega>}{dZ} = \frac{d\left(\pi \int d\Omega\Omega|\tilde{u}|^2\right)}{dZ} = \pi \int d\Omega\Omega \frac{d|\tilde{u}|^2}{dZ} \tag{7.1.11}$$

Considering the module relationship: $\frac{d|\tilde{u}|^2}{dZ} = \tilde{u}\frac{d}{dZ}(\tilde{u}^*) + \tilde{u}^*\frac{d}{dZ}(\tilde{u})$ and equations (7.1.5) and (7.1.9), we find the expression:

$$\frac{d<\Omega>}{dZ} = -\pi \int d\Omega'' \alpha_R(\Omega'') \int d\Omega\Omega \tilde{u}^*(\Omega)\tilde{u}(\Omega'') \int d\Omega' \tilde{u}^*(\Omega')\tilde{u}(\Omega' + \Omega'') \tag{7.1.12}$$

When we are in the presence of a fundamental soliton, its Fourier Transform satisfies equation (7.1.2). We also need to consider the following integral relationship:

$$\int dx \sec h(x + a/2)\sec h(x - a/2) = 2a/\sinh(a) \tag{7.1.13}$$

We should recognize by their definitions that a change in $<\Omega>$ corresponds to a change in the central frequency ω_0. We finally arrive to the expression:

$$\frac{d\omega_0}{dZ} = -\frac{\pi}{8}\int \frac{d\Omega\Omega^3 \alpha_R(\Omega)}{\sinh^2\left(\frac{\pi\Omega}{2}\right)} \tag{7.1.14}$$

Where we relabeled Ω'' as Ω.

We now need to get an expression for the Raman loss from its definition in equation (7.1.9). The time varying Raman response function is related to the Raman Gain by equation (6.1.3), which has been experimentally measured by Stolen et al [Sto89] [Sto92]. The resulting relationship is:

$$\alpha_R(\Omega) = \frac{\lambda}{2\pi n_2} g_R(-\Omega/2\pi T_0) = R(\Omega/2\pi T_0) \tag{7.1.15}$$

Where R is the Raman loss spectrum normalized to the peak value, g_R in cm/W, n_2 in cm^2/W and λ in cm. If we express the pulse width in picoseconds, $\upsilon = -\Omega/2\pi T_0$ represents the frequency displacement in terahertz.

If we would like to convert equation (7.1.14) into an expression for υ, we need to convert soliton's variables back to real variables. Considering equations (3.2.1) and (3.2.2):

$$dZ = dz \frac{\lambda^2 |D|}{T_0^2 2\pi c} \tag{7.1.16}$$

$$d\tau = \frac{1}{T_0} dt \tag{7.1.17}$$

This leads us to a units converting coefficient: $D\lambda^2/2\pi c T_0^3$. The most general expression for the frequency shift is:

$$\frac{d\upsilon_0}{dz}[THz/cm] = -\frac{\lambda^2 |D|}{16\pi c T_0^3} \int \frac{d\Omega \Omega^3 R(\Omega/2\pi T_0)}{\sinh^2\left(\frac{\pi\Omega}{2}\right)} \tag{7.1.18}$$

Where λ, D, c and T_0 are in units of centimeters and picoseconds.

In a particular case, we can approximate the R(υ) function by a linear function:

$$R(\upsilon) = C\upsilon \Rightarrow R(\Omega/2\pi T_0) = C\frac{\Omega}{2\pi T_0} \tag{7.1.19}$$

Where the constant C (in 1/THz) is a fiber-dependent constant that can be calculated from its Raman gain. This approximation has been verified as accurate by Stolen et al [Sto89] [Sto92].

To evaluate the integral in equation (7.1.19) we consider the following formula:

$$\int_0^\infty \frac{d\Omega\Omega^4}{\sinh^2(\pi\Omega/2)} = \frac{16}{15\pi} \tag{7.1.20}$$

Thus obtaining the expression:

$$\frac{\partial \upsilon_0}{\partial z}[THz/km] = -K\frac{|D|\lambda^2}{T_o^{\,4}} \tag{7.1.21}$$

Again, the constant K is a fiber-dependent parameter.

If we consider the following example: $\lambda=1.5\text{x}10^{-7}$cm, D=1500 psec/cm^2 and $R(\upsilon) = (0.492/13.2)\upsilon$, we get the expression:

$$\frac{\partial \upsilon_0}{\partial z}[THz/km] = -\frac{0.0045}{T_o^{\,4}} \tag{7.1.22}$$

The dependency on the fourth power of the pulse width can be understood as follows. First a factor of -2 represents the dependency on the soliton's peak power, which is expressed in equation (3.2.6). Second, a factor of -1 due to the relationship between the frequency displacement and the soliton's spectral width and finally, a factor of -1 due to the linearization of the Raman loss as detailed in (7.1.19).

7.2 Limitations of the previous analytical model.

The theory detailed in the previous section published by Gordon [Gor86] has been experimentally corroborated by Mitschke and Mollenauer [Mit86], when using single-mode polarization preserving fiber. The pulses widths varied from 420 fsec to 45 psec. In those experiments, the maximum frequency shift was 2THz which is equivalent to 16nm.

We should make it clear under what hypothesis equation (7.1.21) is valid. First, while working with soliton units, we are assuming that the fiber dispersion and nonlinear parameter have no wavelength dependency; this is reasonable for a single mode fiber with small wavelength shifts as in [Mit86]. Second, the fiber was considered to have no loss (α_s=0), which is also reasonable for a single mode fiber (α_s=0.25 dB/km). The effect of fiber losses over a soliton was studied in section 3.6. The final hypothesis was that the nonlinear loss α_R was linearized in (7.1.19).

In recent years, the use of new and powerful pulsed lasers as well as highly nonlinear fibers, such as the HNL-PCF presented in Chapter 5, make it possible to have wavelength shifts larger than 100nm. Several wavelength tunable pulsed lasers have been reported in both 1550 – 2000nm and 780 – 1000nm regions [Nor02] [Nor99].

For these amounts of wavelength shifts, we should no longer consider constant fiber parameters such as dispersion and nonlinear coefficient. Moreover, in fibers such as HNL-PCF, the attenuation coefficient could be as high as 200 dB/km and should not be neglected. Consequently, the fourth power rule does not stand.

7.3 A semi-analytical method for soliton self frequency shift in an optical fiber.

When considering a generic lossy fiber, with wavelength variable dispersion and nonlinear coefficient, the analytical analysis goes back to the generalized NLS equation (6.2.5). The only possible action is to numerically evaluate this equation with tools like VPI Transmission Maker [VPI05]. However, because femtosecond level pulse widths are usually used, very wide bandwidth is required in the numerical simulation and the process is generally very time-consuming. Another drawback of numerical simulation is that it does not directly show the effects of various physical mechanisms behind the results.

We propose a semi-analytical method to investigate the characteristics of soliton self-frequency shift (SSFS) in optical fibers. This method is useful to significantly increase the speed of calculation compared to numerical simulations, while maintaining excellent accuracy. SSFS in two different types of fibers were evaluated and the results agree very well with those of numerical simulations. We show that when the frequency shift is small enough, it is inversely proportional to the fourth power of the initial soliton pulse width. However, with large frequency shift, this fourth power rule needs to be modified.

7.3.1 Semi-Analytic Method Formulation

We consider a generic formulation where all fiber parameters can be wavelength dependent: $D(\lambda)$ and $\gamma(\lambda)$ and $\alpha_s(\lambda)$. In order to obtain a semi-analytical solution, we truncate the fiber into short sections as shown in Figure 7.1. Within each section, a fixed signal wavelength can be assumed and fiber parameters at this specific wavelength can be used.

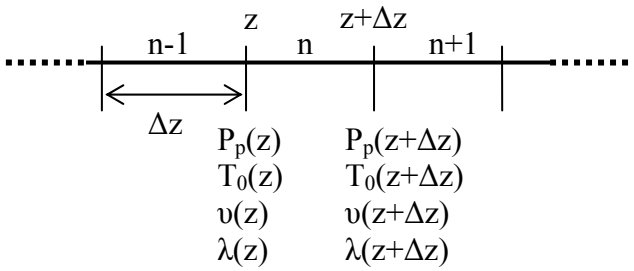

Figure 7.1: Semi-analytical method for SSFS in an optical fiber. Pp is the peak power of the pulse.

The optical frequency of a soliton passing through a short fiber section from z to z+Δz can be expressed using equation (7.1.21) as:

$$\upsilon(z+\Delta z)=\upsilon(z)-K\frac{|D(\lambda(z))|\lambda^2(z)}{T_o(z)^4}\Delta z \tag{7.3.1}$$

As SSFS is a non-elastic effect, in addition to the frequency shift, the peak power (P_p) of the pulse also changes after passing through the short section. This peak power change is caused by three major effects, namely, fiber attenuation, pulse width change and energy loss of each photon due to the red-shift of the wavelength. The nonlinear Raman attenuation was studied in section 7.1. However we could do a simpler analysis if we consider the average effect over the central frequency.

We can calculate the fundamental order soliton energy as:

$$E=\int_{-\infty}^{+\infty}\left|\sqrt{P_p}\,\sec h(T/T_0)e^{j\frac{z|\beta_2|}{T_0^2}}\right|^2 dT=P_p\int_{-\infty}^{+\infty}\left|\sec h(T/T_0)\right|^2 dT=2P_pT_0 \tag{7.3.2}$$

When the pulse travels along the fiber, it changes its energy as a consequence of the quantum loss:

$$\frac{E(z+\Delta z)}{E(z)}=\frac{2P_p(z+\Delta z)T_0(z+\Delta z)}{2P_p(z)T_0(z)}=\frac{Nh\upsilon(z+\Delta z)}{Nh\upsilon(z)} \tag{7.3.3}$$

Where N is the total number of photons and *h* the Plank's constant. We find then a simplified expression for the nonlinear Raman attenuation:

$$P_p(z+\Delta z)=\frac{P_p(z)T_0(z)}{T_0(z+\Delta z)}\frac{\upsilon(z+\Delta z)}{\upsilon(z)} \tag{7.3.4}$$

If we also consider the fiber losses, the pulse peak power at the output of the short fiber section is:

$$P_p(z+\Delta z) = P_p(z)e^{-\alpha(\lambda(z))\Delta z}\frac{\upsilon(z+\Delta z)}{\upsilon(z)}\frac{T_0(z)}{T_0(z+\Delta z)} \tag{7.3.5}$$

Assuming a fundamental soliton is maintained when pulses propagate along the fiber; the soliton's peak power is also related to its width by equation (3.2.6) that can be rewritten as:

$$P_p(z)T_0^2(z) = \frac{cD(\lambda(z))}{2\pi\upsilon^2(\lambda(z))\gamma(\lambda(z))} \tag{7.3.6}$$

Combining the last three equations, an expression of pulse width at z + Δz can be obtained as:

$$T_0(z+\Delta z) = \frac{\lambda^3(z+\Delta z)D(\lambda(z+\Delta z))}{2\pi c\gamma(\lambda(z+\Delta z))\lambda(z)P_p(z)e^{-\alpha(\lambda(z+\Delta z))\Delta z}T_0(z)} \tag{7.3.7}$$

Where $\lambda(z+\Delta z) = c/\upsilon(z+\Delta z)$ is the wavelength of the pulse at the output of the fiber section which can be obtained by equation (7.3.1); $D(\lambda(z+\Delta z))$, $\gamma(\lambda(z+\Delta z))$ and $\alpha(\lambda(z+\Delta z))$ are the dispersion nonlinearity parameter and fiber attenuation, respectively, evaluated at this new wavelength.

Figure 7.3 shows the block diagram for the semi-analytical method. With the parameters of a soliton pulse known at the input, equations (7.3.5) and (7.3.7) can be used together to calculate the central frequency and the pulse width of the wavelength shifted soliton at the output of a short fiber section. These parameters can in turn be

used as the input to the next fiber section. SSFS characteristics of a long fiber can be obtained by dividing the fiber into short sections and repeating this calculation section by section, along the fiber. Because the transfer function of each fiber section described by equations (7.3.5) and (7.3.7) is analytical, the calculation is straightforward and fast. In addition, since the wavelength of the optical pulse at different fiber sections may be very different due to SSFS, precise fiber parameters at each section can be used corresponds to the exact signal wavelength at that section. This assures the accuracy of the calculation.

The Matlab code of the implementation for the method is attached in Appendix C.

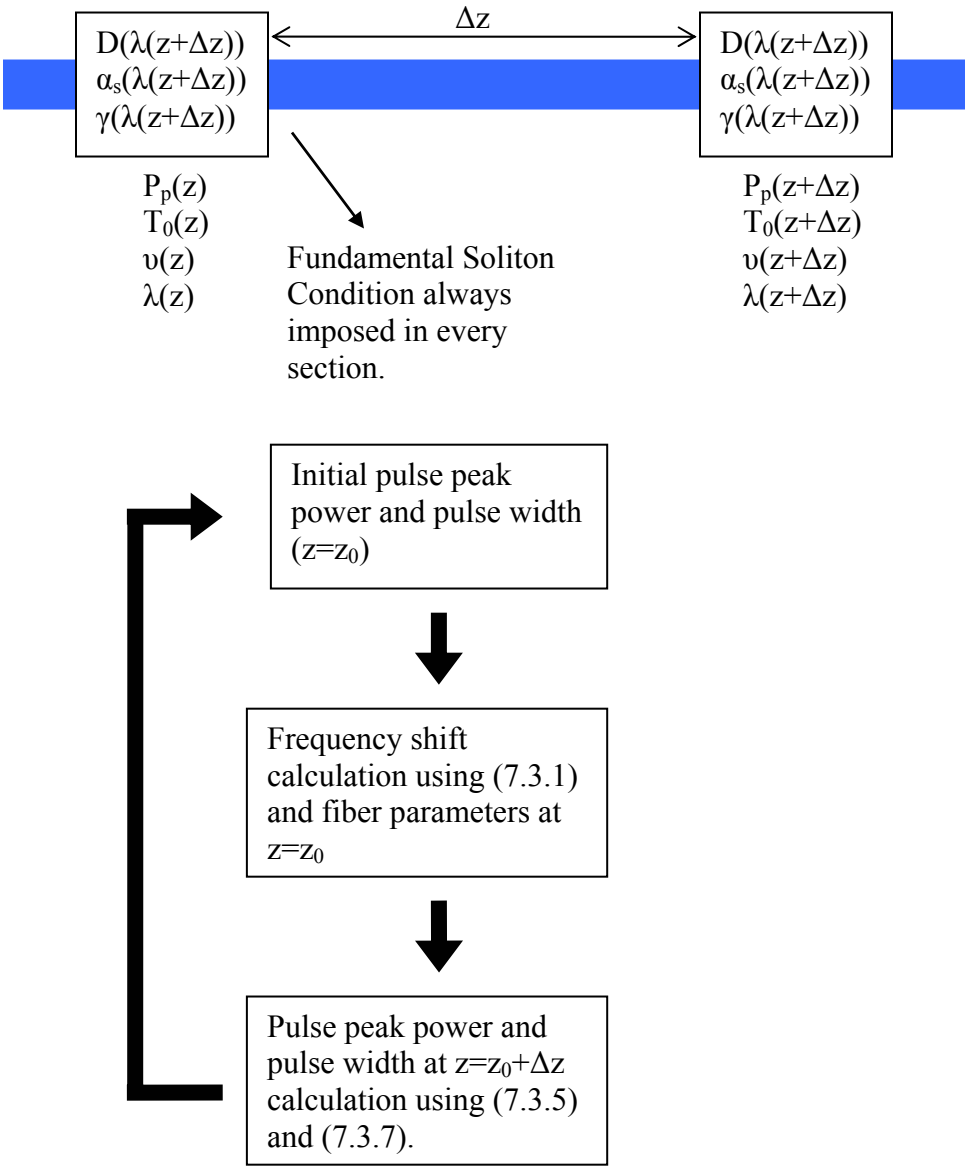

Figure 7.2: Block diagram for the semi-analytical method. Each segment is considered to have constant fiber parameters; at the edge of each span the pulse peak power and pulse width is calculated and used as the input for the next span.

7.3.2 Results and Discussion.

In order to evaluate the accuracy of our semi-analytical model, the results were compared with those of numerical simulations using VPI Transmission Maker [VPI05]

where the split-step Fourier method was used. Two fibers were used, a polarization maintaining fiber (PMF) and a HNL-PCF. All the fiber parameters are shown in Appendix A and the numerical parameters in Appendix B.

In the first case, we consider 100m of PMF (3M FS-PM-7811) as used in [Nor99]. The wavelength of the input soliton pulse is set at 1550nm. Soliton frequency shift versus input optical pulse width is shown in Fig.7.3, in which, results of semi-analytical calculation represented by triangles agree well with those obtained by numerical simulations represented by open circles. The figure also shows the evolution of the exponent x that relates the SSFS and the pulse width as:

$$\Delta\upsilon \propto T_0^{-x} \tag{7.3.8}$$

In equation (7.1.21) x was 4, representing the fourth power rule. This is verified for pulses wider than 100fsec, which agrees with the experimental work of [Mit86] where pulses wider than 420fsec were used.

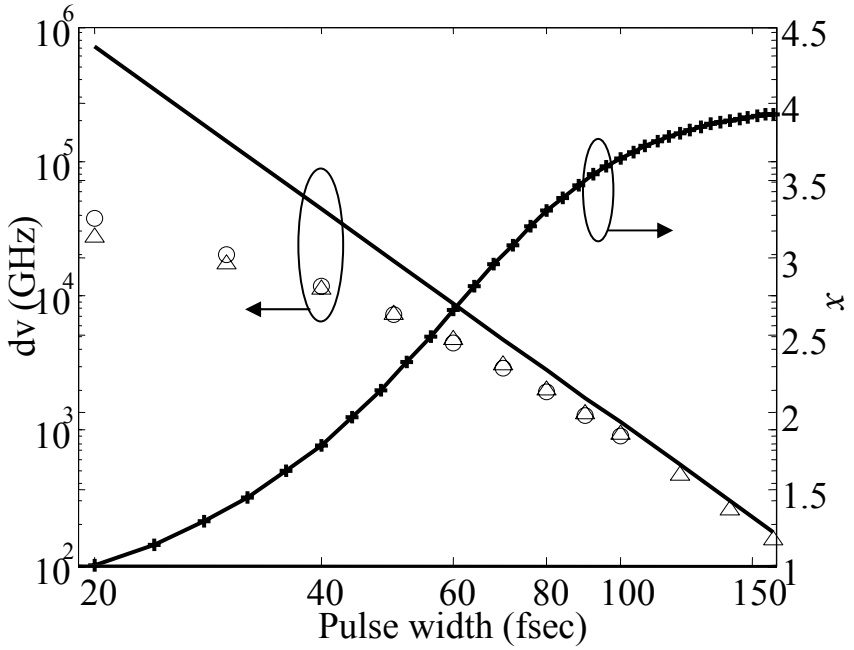

Figure 7.3: Frequency shift versus pulse width for a 100m PMF in log scale (left). The stray line represents the analytical result in (7.1.21), triangles represent the complete semi-analytical solution and circles represent the numerical results. The figure also shows the difference on the exponent x from the analytical value of 4(right).

When the pulse is shifted to a longer wavelength, it is broadened due to the higher dispersion. This behavior explains the saturation in the frequency shift for narrow pulses. It needs to be mentioned that when the pulse width is narrower than 20fs, the nonlinear Schrödinger equation (6.1.5) is no longer accurate because the narrowband approximation fails [Agr01] which is beyond the scope of this work.

The fiber loss in this case is only 0.26dB, and thus has not an important impact in the overall behavior.

The second fiber tested was a HNL-PCF (Photonic Crystal Fiber NL-18-710) which parameters are shown in Appendix A.

In Figure 7.4 we show the numerical results of the SSFS as a function of the pulse width for different fiber lengths. In every case we verify the saturation behavior for narrow pulses.

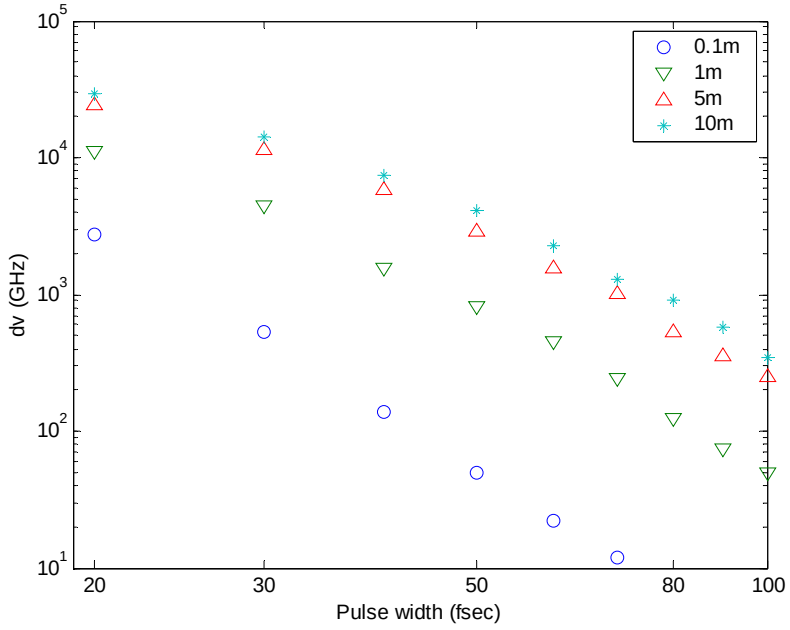

Figure 7.4: SSFS for a HNL-PCF with different fiber lengths in log scale. For very short fibers (0.1m) the shift is small enough to maintain the linear characteristic; however, for longer fibers we can see the saturation effect.

In this case, while the pulse propagates through the fiber, we should not only consider the increase of the chromatic dispersion, but also the decrease of its nonlinear parameter and the high attenuation. The overall effect is a decrease of the peak power of the pulse; as the soliton tries to maintain its fundamental relationship as in equation (7.3.6), the pulse will also be broadened.

Figure 7.5 shows the frequency shift versus soliton pulse width in 10m of HNL-PCF calculated by semi-analytical model (triangles) and numerical simulations (open circles). The impact of fiber losses in PCF can not be neglected as it can take values up 200 dB/km. To illustrate this effect, soliton frequency shift calculated without fiber loss is also plotted in figure 7.5 (squares) for comparison. Similar to what happened in the polarization maintaining fiber, the exponent x is equal to 4 at a relatively wide pulse width and is reduced significantly when the pulse width is narrower than 100fs.

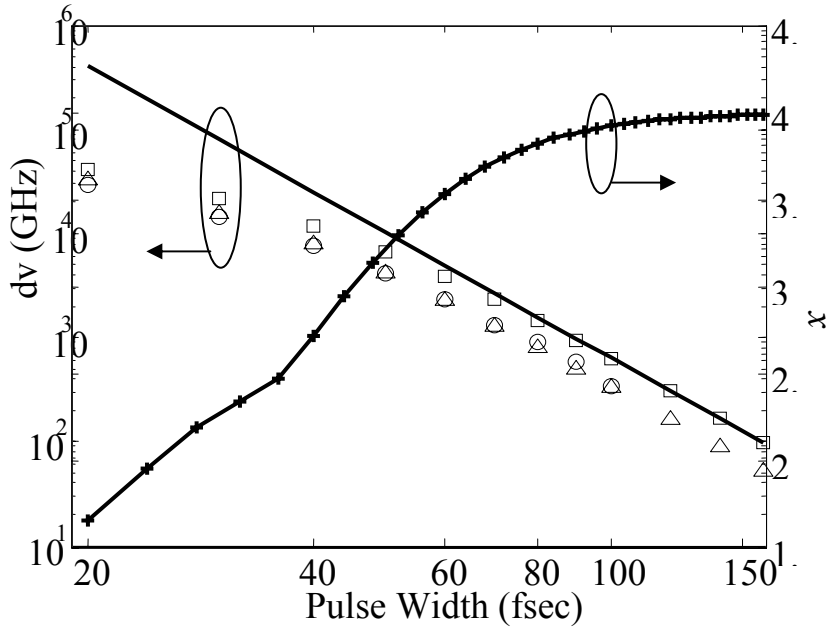

Figure 7.5: Frequency shift and pulse width for a 10m HNL-PCF in log scale (left). The strait line represents the analytical result (7.1.21), squares the semi-analytical solution with no losses, triangles the complete semi-analytical solution and circles the numerical result. The figure also shows the difference on the exponent x from the analytical value of 4 (right).

If we consider figure 7.4 for a fixed initial pulse width and different fiber lengths (vertical direction), we can also observed a saturation behavior. Figure 7.6 shows an

example of the wavelength shift as a function of the fiber length, for the same HNL-PCF, for different pulse widths calculated with semi-analytical model (continuous) and numerical simulations (circles). The results clearly show the saturation in the frequency shift at long fiber lengths as has been demonstrated experimentally [Nor99]. The discrepancy between the semi-analytical model and the numerical simulation when the pulse width is narrower than 40fs is attributed to the effect of higher order dispersion, which is not included in the semi-analytical model. This discrepancy was not evident in the previous plots as we were using log scale.

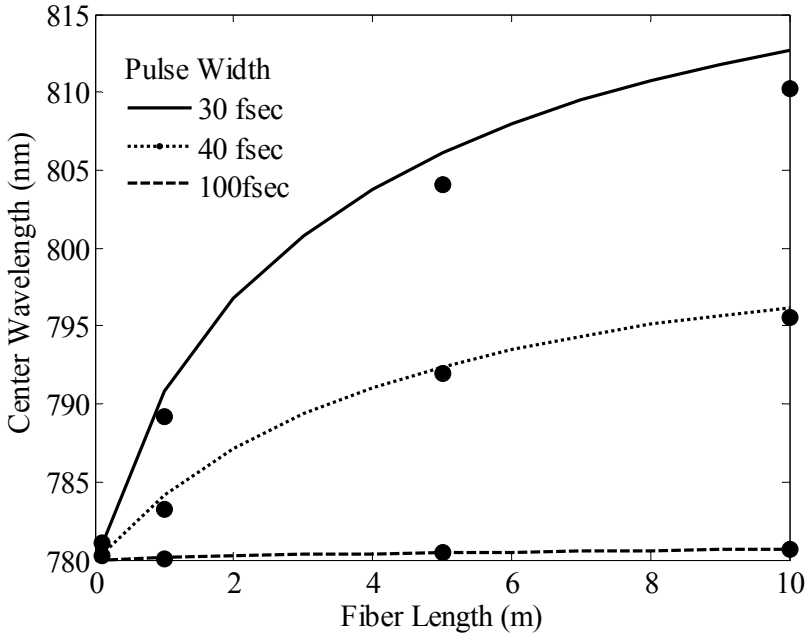

Figure 7.6: Wavelength shift and fiber length for a PCF for different soliton pulse widths. Circles represent the numerical data.

In all the cases, there is also agreement between the semi-analytical solution and the numerical solution in both the output peak power and the output pulse width. The output fundamental order of the soliton from the numerical solution was verified.

As a conclusion for this chapter, the analysis introduced in [Gor86] needs to be modified when considering large frequency shifts and fiber with no-constant parameters. The semi-analytical method introduced agrees with the analytical formulation for relatively wide pulses and with the numerical solution in every case. This method does not include the effect of the higher order dispersion.

Chapter 8: Short Pulsed Lasers Applications for Two Photons Microscopy

Femtosecond pulses lasers serve as a source for fluorescence microscopy. In this technique, fluorescent dyes are attached to the target molecule (normally a protein) by covalent labeling strategies. Once attached, the dyes will absorb the incident light at a particular wavelength and emit photons at a known longer wavelength. Fluorescence could be used to determinate presence or absence of the specific species, to determinate concentration, to perform imaging, to study dynamic characteristics, etc. [Sch01]

A common implementation consists of a one-photon confocal microscope, using a Ti:Sa pulsed laser as the pulse source. In recent years two-photon microscopy has emerged as the selected method for fluorescence microscopy in thick tissues and live animals. The main difficulty in building a two-photon instrument is the cost of the laser source as well as the expertise needed to maintain a solid-state laser. The introduction of a high-power fiber laser allows overcoming both limitations.

In this chapter we will first give a short overview to one and two-photon microscopy, detailing the differences between both methods. Then, we will introduce our experimental setup and finally show different two-photon images.

8.1 One-Photon Confocal Microscopy

In a one-photon confocal microscopy system the excitation from the pulsed laser is directed into a microscope objective and focused on the sample. This technique gives a diffraction-limited spot of approximately 0.5 μm in diameter. [Sch01]

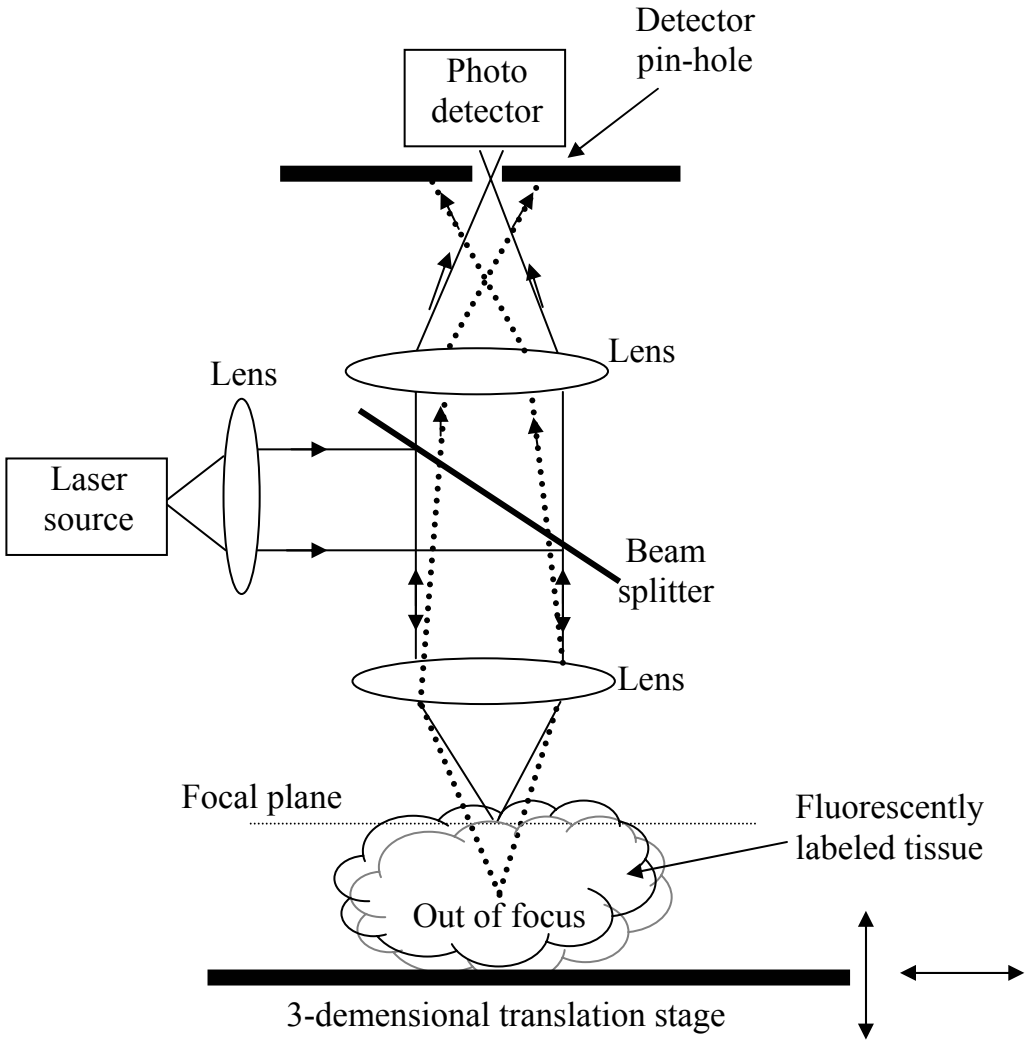

Figure 8.1: A Scanning Laser Confocal Microscope Setup. The sample is moving in the three dimensions in order to obtain a 3D image. A pin-hole is introduced in front of the detector for improving the system's resolution.

Figure 8.1 shows a typical setup where the energy from one absorbed photon gives rise to the generation of one fluorescent photon.

We can identify several problems with confocal microscopy. First, the receiving signal will include light from structures above and below the focus plane, limiting the system's resolution. A common solution to overcome this background is to introduce a pin-hole near the detector; in this case we have a loss of signal at the receiver and thus it may be needed to increase the pump power. Nevertheless, the pin-hole will not help to reject the scattered excitation light from the target volume. In this case very narrow bandpass filters may be needed as fluorescence and pump signals are close in frequency domain.

The second problem that we can identify is related to the wavelength range where this instruments works. Normally used fluorescence dyes (or fluorophores) will absorb in the UV-Visible region and will emit at longer wavelength. An example of emission and absorption spectrum for a family of such dyes is shown in Figure 8.2.

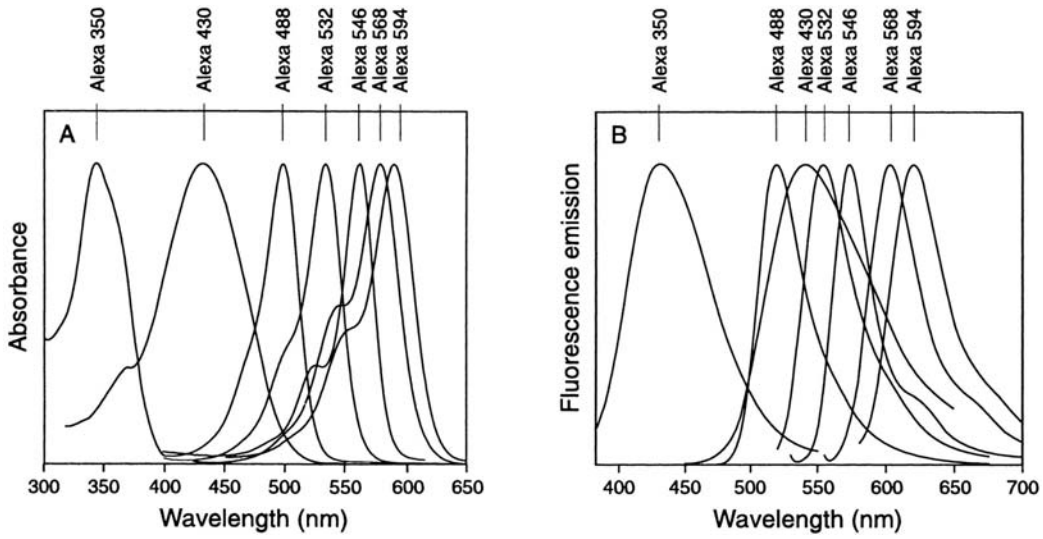

Figure 8.2: Absorption and emission spectrum of the Alexa-series one-photon fluorescence dyes.

Working in the UV-Visible region has three major problems: first, tissue cells have very high absorption coefficient at these wavelengths, thus the penetration depth is reduced and the possibility of photo-damage living cells increases. Second, fluorophores are easily bleached when excited by a visible light. Finally, it is difficult to build appropriate optical elements such as lenses and beam splitters [Den90].

8.2 Two Photons Microscopy

The simultaneous absorption of two photons by an atom or molecule in a single event was first predicted in 1931 [Xu95] and was called Two-Photon Excitation (TPE). However, it was only recently that two-photon laser scanning fluorescence microscopy was demonstrated. In this method, the sample is illuminated with light of a wavelength approximately twice the peak absorption wavelength of the fluorophore

in use. For example a dye absorbing at 400nm will be excited by two photons at 800nm.

As TPE is a second-order process, the number of photons absorbed per molecule per unit of time (N_{abs}) by means of TPE depends on the square of the incident optical power (I(t)) [Xu95]:

$$N_{abs}(t) = \int_V dV \delta C(\vec{r},t) I^2(\vec{r},t) \tag{8.1}$$

Where $C(\vec{r},t)$ represents the dye concentration and δ the two-photon absorption cross section. Measuring the two-photon absorption cross section is usually difficult and it will vary from the one-photon cross section. Consequently, if for example we take the dyes in Figure 8.2, their two-photon absorption spectrum will not be the same as in the figure.

When working in TPE, we can neglect the effects of photo-bleaching because the target volume is very small and only a small number of dyes would be affected. Taking a large time scale, we can assume that the dye concentration is constant. Consequently, we can consider that the time and space components of the pump intensity can be separated as: $I(\vec{r},t) = I_0(t) S(\vec{r})$, where $S(\vec{r})$ is unitless. Equation 8.1 can be rewritten as:

$$N_{abs}(t) = C\delta {I_0}^2(t) \int_V dV S^2(\vec{r}) \tag{8.2}$$

This result can be used to find the time-averaged number of fluorescence photons [Xu95]:

$$< F(t) >= \frac{1}{2}\left[\frac{< I_0^2(t) >}{< I_0(t) >^2}\right]\phi\eta_2 C\delta < I_0(t) >^2 \int_V dV S(\vec{r})^2 \qquad (8.3)$$

Where the factor 1/2 reflects that two absorbed photons are needed to generate one fluorescence photon, the term $\frac{< I_0^2(t) >}{< I_0(t) >^2}$ is a measure of the second order temporal coherence of the pump and should be a constant (normally named g), ϕ is the fluorescence quantum efficiency of the dye and η_2 the efficiency of the measurement system at the collecting wavelength. The square dependency of the two-photon absorption on the pump power means that this phenomenon can only occur over a very small volume around the focus point. Thus, the resolution of the instrument is improved over the one-photon excitation and there is no need to use a pin-hole at the receiver.

Another advantage of two-photon based imaging is that biological tissue has considerable less scattering and absorption in the NIR wavelength. Consequently, the penetration depth is increased and the probability of photo-damage reduced [Den90].

8.3 Experimental Acquisition of Two-Photon Images

A classical setup for obtaining a two-photon image will still utilize a pulsed Ti:Sa laser source. As we mention in this thesis, there are several advantages when using a fiber based pulsed laser instead.

Working in collaboration with Dr. Carey Johnson's lab, we performed two experiments. First we obtained two-photon images using a pulsed fiber-laser emitting at 780nm as the input pump. Then, we obtained a two-photon image shifting the pump's central wavelength to 920nm using a Photonic Crystal Fiber as demonstrated in Chapter 6. In this second experiment, we do not need any filter at the output of the wavelength shifter as there was not second order soliton generation and the pumping pulse (after being dispersed by the fiber) was too broad to generate TPE.

The experimental setup is shown in Figure 8.3; when working at 780nm, the 7m PCF was removed from the optical table. We utilized a Nikon TE2000 microscope with a 100X objective lens and equipped with a 2D piezo-electric scanning stage; the z-dimension translation was achieved by manually moving the objective lens.

The sample was composed of fluospheres with 24nm of diameter that were doped with a fluorescence material. The spheres were immobilized in a 3% agarose solution at a concentration of 5nM. With these small samples, we were able to measure the diffraction limit of our instrument when we identify a signal of 310nm of $1/e^2$ diameter.

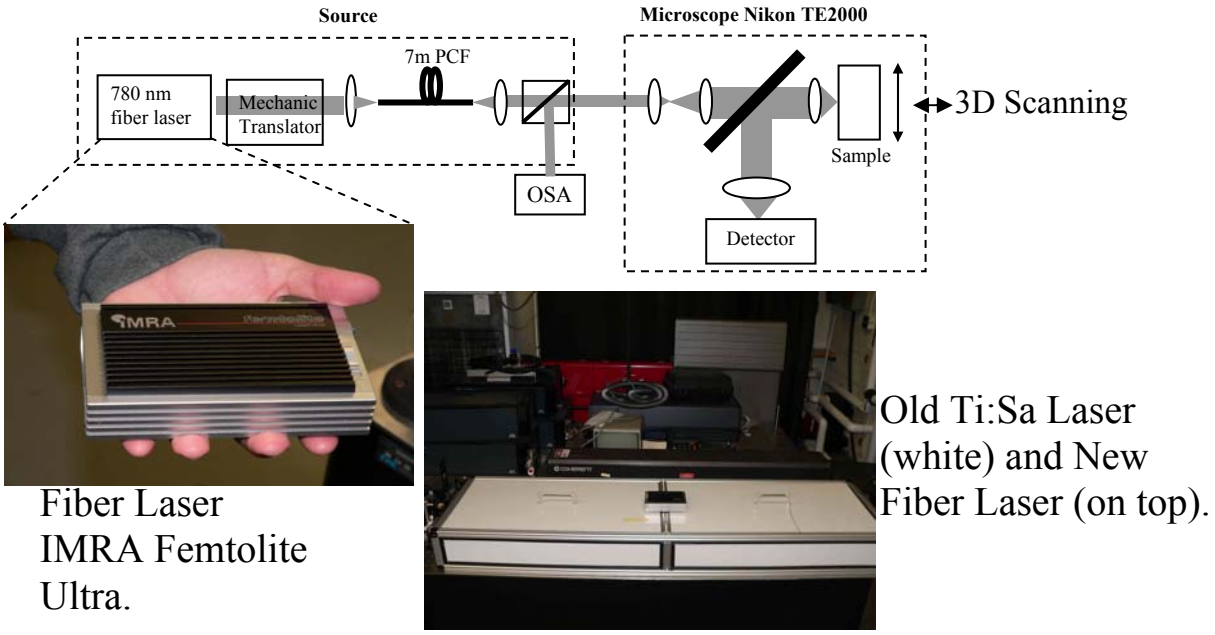

Figure 8.3: Experimental setup for acquiring a two-photon image. The PCF was removed when working of the 780nm region. The pictures shows the fiber-laser used for the experiment (IMRA Femtolite Ultra) and compares it size with a classical Ti:Sa laser.

In Figure 8.4 we show a two-photon 2D image of a fluosphere taken in the radial dimension when using the original pump laser at 780nm. Figure 8.5 shows the radial intensity profile for the same sample. These were the first two-photon images recorded at the University of Kansas.

Figure 8.6 and 8.7 show the same results but when the pump laser is shifted to a longer wavelength using the HNL-PCF. There is no previous record available in the literature of a two-photon image in this wavelength using a fiber laser.

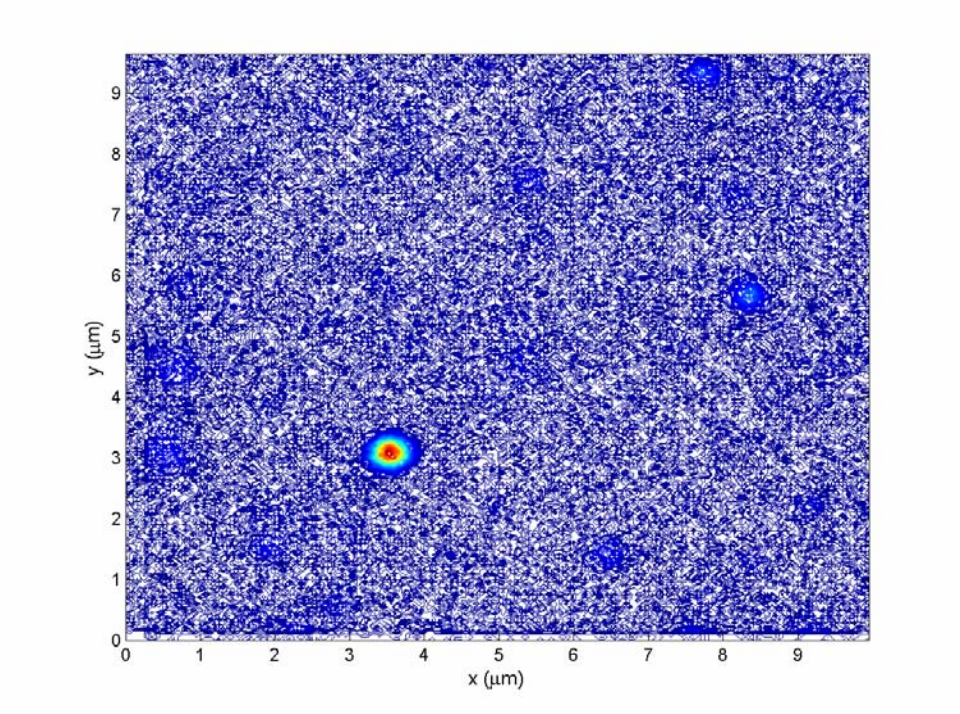

Figure 8.4: Two-photon image of a fluosphere using a 780nm pump laser.

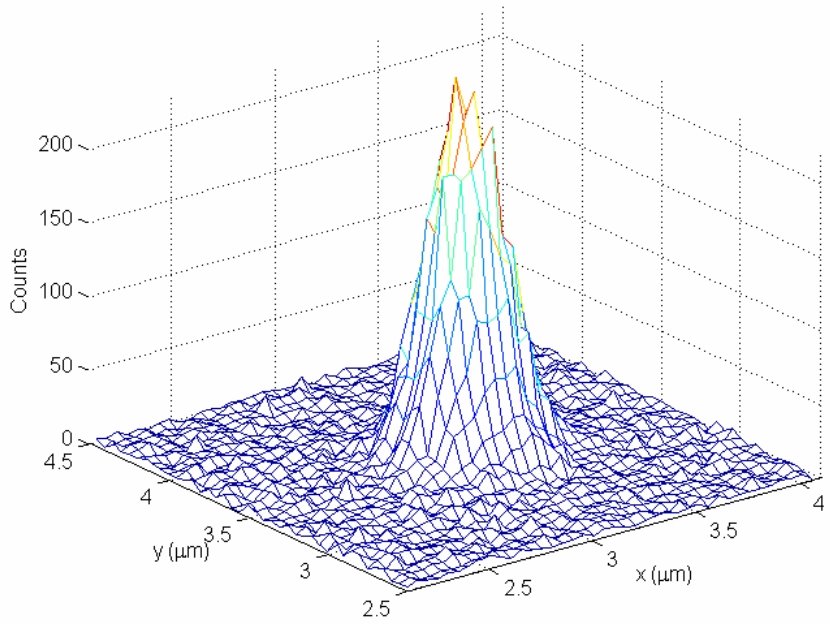

Figure 8.5: Radial intensity profile for a fluosphere using a pump laser at 780nm.

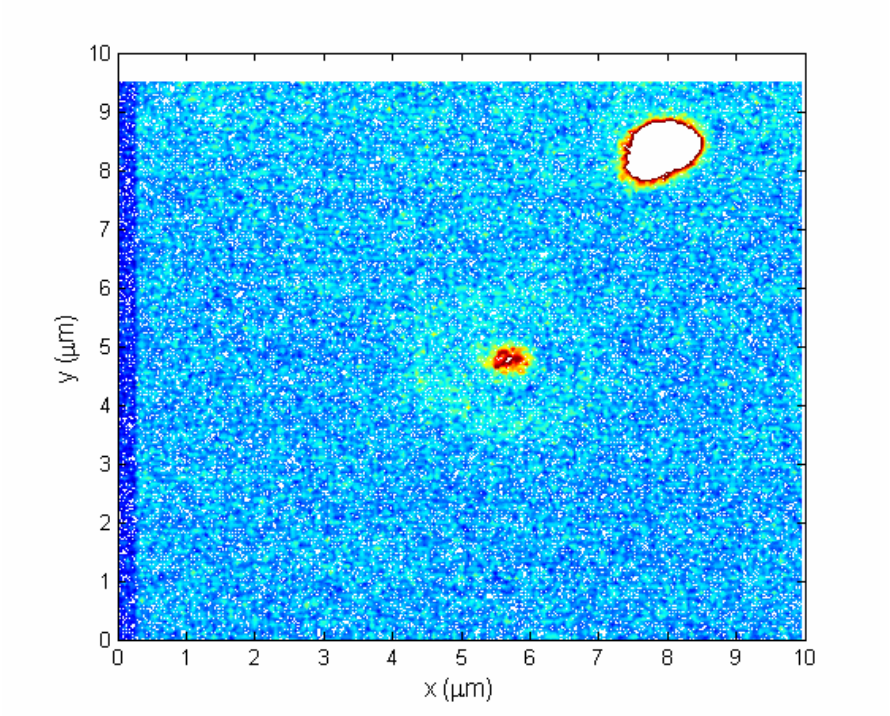

Figure 8.6: Two-photon image of a fluosphere using a shifted pump laser to 920nm. We can observe one sphere in the middle of the image and an aggregate in the upper right.

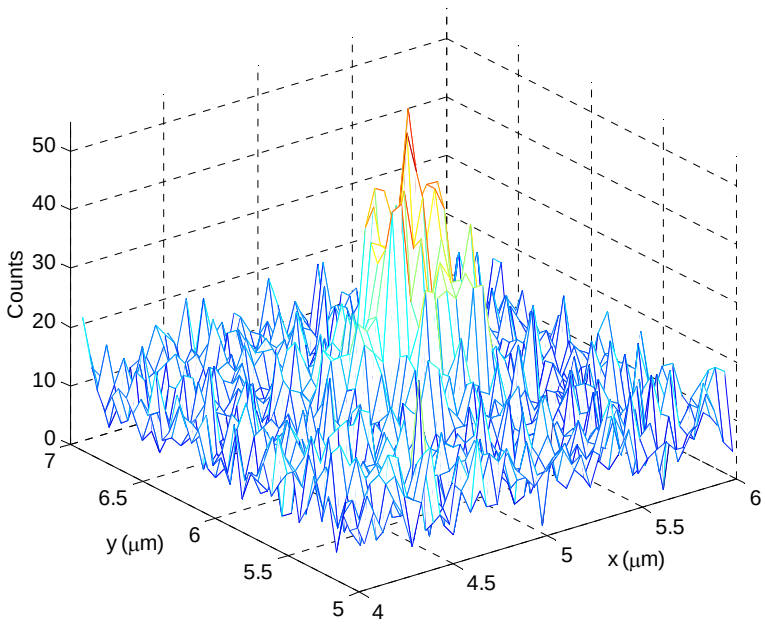

Figure 8.7: Radial intensity profile for the fluosphere at the center of figure 8.6.

8.4 Other applications

The optical setup shown in figure 8.3 can be adapted to perform a variety of fluorescence based experiments that are out of the scope of this work.

First, we consider the two-photon fluorescence correlation spectroscopy (TPFCS). In this technique, fluorescence fluctuations caused by the diffusion of molecules through the focal area are detected and analyzed by autocorrelation or cross-correlation functions. Applications include concentration assays, measurements of mobility, reaction kinetics, detection of co-localization of proteins and high throughput screening [Sch01].

Coherent anti-Stokes Raman scattering (CARS) is a nonlinear Raman process in which two pump beams (at frequencies ω_p and ω_s respectively) are mixed in a sample to generate a signal at the anti-Stoke frequency of $\omega_{as}=2\omega_p-\omega_s$. By using CARS we can obtain high-quality three-dimensional images. A normal setup will include two different (and expensive) pulsed lasers. However, a small change in our setup would allow performing the experiment with a single pump. This objective represents several challenges such as the stretch of the pulse spectrum and the synchronization of the two beams.

CONCLUSIONS

In this work we studied the propagation of short optical pulses along a high nonlinear photonic crystal fiber. We observed and simulated the formation of Raman solitons and their frequency shift as a function of the fiber length and the input average power. A wavelength-shifter was built and its experimental spectrum compared with the numerical simulation results.

A semi-analytical method for the dependency of the soliton self-frequency shift on its initial pulse width was introduced as a generalization of the fourth power rule introduced in [Gor86]. The method agrees well with numerical results and behaviors predicted in the literature. It also agrees with the analytical result in [Gor86] for small frequency shifts and no fiber losses. This work was submitted for publication and the resulting paper is shown in Appendix D.

The wavelength-shifter was introduced in a two-photon microscopy setup to obtain the first two-photon images at the University of Kansas. The central frequency of the pump laser was then shifted to obtain an image in a different pump wavelength. There is no evidence in the literature of any previous successful implementation of this last experiment.

As a consequence of the work detailed in this thesis, a NSF proposal was submitted for the acquisition of a new laser source and microscope to build a permanent two-photon instrument.

FUTURE WORK

Future work related to this master thesis can be focused in two areas. First, the analytical formulation of the relationship between the pulse-breakup process and the formed Raman soliton's peak power. This analysis, in combination with the soliton self-frequency shift, will allow obtaining an analytical relationship between the frequency shift and the input pump average power.

In an experimental phase, a new laser source and a permanent setup will allow to perform two-photon images, even simultaneously acquiring different colors. It will also permit the realization of TPFCS and CARS analysis. This last technique represents some technology challenges as pulse spectrum stretching and pulse synchronization [Che93].

The availability of a width-varying and power-varying laser source would allow the experimental verification of the semi-analytical method introduced in this work.

GLOSSARY

ASE – Amplified Spontaneous Emission

CARS – Coherent anti-Stokes Raman Scattering

CW – Continuous Wave

DNA – Deoxyribose Nucleic Acid

DDF – Dispersion-Decreasing Fiber

EDFA – Erbium Doped Fiber Amplifier

FT – Fourier Transform

FWHW – Full Width Half Width

FWM – Four Wave Mixing

GVD – Group Velocity Dispersion

HNL – High Nonlinear

MDF – Modal Diameter Field

MF – Microstructured Fiber

MM – Multimode

MMF – Multimode Fiber

MOF – Microstructured Optical Fiber

NIR – Near Infrared

NLS – Nonlinear Schrödinger equation.

PC – Photonic Crystal

PCF – Photonic Crystal Fiber

PMD – Polarization Mode Dispersion

PMF – Polarization Maintaining Fiber

PPLN – Periodically Poled Lithium-Niobate

PSFS – Pulse Self-Frequency Shift

SBS – Stimulated Brillouin Scattering

SC – Supercontinuum

SMF – Single Mode Fiber

SPM – Self Phase Modulation

SRS – Stimulated Raman Scattering

SSFS – Soliton Self Frequency Shift

TPE – Two-photon Excitation

TPFCS – Two-Photon Fluorescence Spectroscopy

TPLSM – Two-Photon Laser Scanning Microscopy

UV – Ultra-Violet

WDM – Wavelength Division Multiplexing

XPM – Cross-Phase Modulation

REFERENCES

[Agr01] Govind P. Agrawal, *Nonlinear Fiber Optics, 3rd edition,* Academic Press, 2001.

[Agr201] Govind P. Agrawal, *Applications of Nonlinear Fiber Optics,* Academic Press, 2001.

[Agr03] Govind P. Agrawal, Yuri S. Krivshar, *Optical Solitons, Elsevier Science*, 2003.

[Akh92] Sergei A. Akhmanov, *Optics of Femtosecond Laser Pulses,* AIP, 1992.

[Arb97] M. A. Arbore, M. M. Fejer, M. E. Fermann, A. Hariharan, A. Galvanauskas and D. Harter, "*Frequency Doubling of femtosecond erbium-fiber soliton lasers in periodically poled lithium niobate*", Opt. Lett. 22 (1997), 13-15.

[Arb97] M.A. Arbore, M.M. Fejer, M.E. Fermann, A. Hariharan, A. Galvanauskas, D. Harter, "*Frequency doubling of femtosecond erbium-fiber soliton lasers in periodically poled lithium niobate*", Opt. Lett. 22 (1997),13-15.

[Bea87] P. Beaud, W. Hodel, B. Zysset and H. P. Weber, "*Ultrashort pulse propagation, pulse breakup, and fundamental soliton formulation in a single-mode optical fiber*", IEEE J. Quantum Electron. 23 (1987), 1938-1946.

[Bja03] Anders Bjarklev, Jes Broeng, Araceli Sanchez Bjarklev, *Photonic Crystal Fibres,* Kluwer AP, 2003.

[Bus04] K. Busch, S. Lolkes, R B Wehrspohn, H Foll, *Photonic Crystals*, Wiley VCH, 2004.

[Che93] S.V.Chernikov, E.M.Dianov, D.J. Richardson and D. N. Payne, "*Soliton pulse compression in dispersion-decreasing fiber*", Opt. Lett. 18 (1993), 476-478

[Che02] Ju-xin Cheng, Andreas Volkmer, Lewis D. Book and X. Sunney Xie, "*Multiplex Coherent Ant-Stokes Raman Scattering Microspectroscopy and Study of Lipid Vesicle*", J. Phys. Chem. B 106 (2002), 8493-8498.

[Den90] Winfried Denk, James H. Strickler and Watt W. Webb, "*Two-Photon Laser Scanning Fluorescence Microscopy*", Science. 248 (1990),73-76.

[Egg03] Slusher Eggleton, *Nonlinear Photonic Crystals,* Springer, 2003

[Fer00] M.E.Fermann, A. Galvanauskas, M. Hofer, "*Ultrafast pulse sources based on multi-mode optical fibers*", Appl. Phys. B 70 (2000), S13-S23.

[Fuo03] M. Fuochi, F. Poli, S. Selleri, A. Cucinotta, and L, Vincetti, "*Study of Raman amplification properties in triangular photonic crystal fibers*", J. Lightware Technol 21 (2003) 2247-2254.

[Gor86] J.P. Gordon, "*Theory of the soliton self-frequency shift",* Opt. Lett. 11 (1986) 659-661.

[Gri00] V. S. Grigoryan, R. M. Mu, G. M. Carter and C. R. Menyuk, "*Experimental Demostration of Long-Distance Dispersion-Managed Soliton Propagation at Zero Average Dispersion*", Photonic Technology Lett. 12 (2000) 45-46.

[Mit86] F.M.Mitschke and L.F.Mollenauer, "*Discovery of the soliton self-frequency shift*", Opt. Lett 11 (1986), 659-661.

[MIT04] MIT Photonic-Bands (MPB), http://ab-initio.mit.edu/mpb.

[Mol85] L.F.Mollenauer, R.H. Stolen and M.N. Islam, "*Experimental demonstration of soliton propagation in long fibers: loss compensated by Raman gain*", Opt. Lett. 10 (1985) 229-231.

[Nel97] L.E. Nelson, D.J. Jones, K. Tamura, H.A. Haus, E.P.Ippen, "*Ultrashort-pulse fiber ring lasers*", Appl. Phys. B 65 (1997), 277-294.

[Nor99] Norihito Nishizawa, Ryuyi Okamura, Toshio Goto, "*Analysis of Widely Tunable Femtosecond Soliton Pulse Generation Using Optical Fibers",* J. Appl. Phys. 38 (1999) 4768.

[Nor02] Norihiko Nishizawa, Youta Ito and Toshio Goto, "*0.78-0.90-μm Wavelength-Tunable Femtosecond Soliton Pulse Generation Using Photonic Crystal Fiber*", Photonic Technology lett. 14 (2002) 986-988.

[Ort02] A. Ortigosa-Blanch, J. C. Knight and P. St. J. Russell, "*Pulse breaking and supercontinuum generation with 200 fs pump pulses in photonic crystal fibers*", JOSA B 19 (2002), 2567-2572.

[Pau03] H.N. Paulsen, K.M. Hilligsoe, J. Thogersen, S.R. Keiding, J.J. Larsen, "*Coherent anti-Stokes Raman Scaterring microscopy with a photonic crystal fiber based light source*", Opt Lett. 28 (2003), 1123-1125.

[Por03] K. Porsezian, V.C. Kuriakose (Editors), *Optical Solitons, Theoretical and Experimental Challenges*, Springer, 2003.

[Rei02] D.T. Reid, I.G. Cormack, W.J. Wadsworth,J.C. Knight and P.St.J. Russell, "*Soliton Selft-frequency Shift Effect in Photonic Crystal Fibre*", CLEO 2002.

[Rul03] Claude Rulliere, *Femtosecond Laser Pulses, 2nd edition,* Springer, 2003.

[Sch01] P. Schwille and E. Haustein, *Fluorescence Correlation Spectroscopy*, available online.

[Sto89] R.H.Stolen, J.P.Gordon, W.J. Tomlinson and H.A. Haus, *"Raman response function of silica-core fibers*", JOSA B 6 (1989) 1159-1166.

[Sto92] R.H. Stolen and W.J.Tomlinson, "*Effect of the Raman part of the nonlinear refractive index on the propagation of ultrashort optical pulses in fibers*", JOSA B 9 (1992), 565-573.

[VPI05] VPI Transmission Maker Users Manual, VPI Photonics (http://www.vpiphotonics.com), 2005.

[Xu95] Chris Xu and Watt W. Webb, "*Measurement of two-photon excitation cross sections of molecular fluorophores with data from 690 to 1050nm*", JOSA B 13 (1996), 481-491.

[Zys87] B. Zysset, P. Beaud and W. Hodel, "*Generation of optical solitons in the wavelength region 1.37-1.49 μm*", Appl. Phys. Lett. 50 (1987), 1027-1029.

APPENDIX A: Optical Fibers Characteristics

- Crystal Fibre NL-18-710

This nonlinear photonic crystal fiber has a zero dispersion wavelength at 710nm. Figure A.1 shows an axial profile and Table A.1 its main parameters as given by the manufacturer.

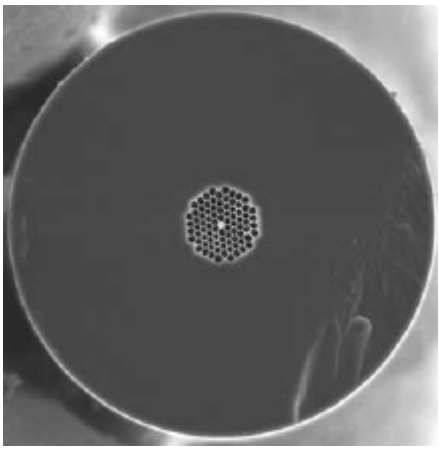

Figure A.1: Crystal Fibre NL-18-710 axial profile (http://www.crystal-fibre.com)

λ (nm)	D (ps/nm/km)	D slope (ps/nm^2/km)	γ (W^{-1} km^{-1})	α (dB/km)
710	0	0.58	139	190
600	-142	1.70	171	210
800	68	0.59	122	170
1000	148	0.25	92	130
1550	185	-0.08	49	80

Table A.1: Crystal Fibre NL-18-710 Parameters (http://www.crystal-fibre.com)

Other fiber parameters:

• Core diameter (average): 1.8±0.1μm.

• Pitch (distance between cladding holes): 2.1±0.1 μm

• Air Filling Fraction in the holey region: >90%

• Width of struts holding the core: 70±10 nm

• Diameter of holey region: 21±0.5 μm

• Diameter of outer silica cladding (OD): 125±1 μm

• Coating diameter (single layer acrylate): 230±5 μm

In Figures A.2 through A.4 we plot the wavelength dependency of the fiber´s parameters.

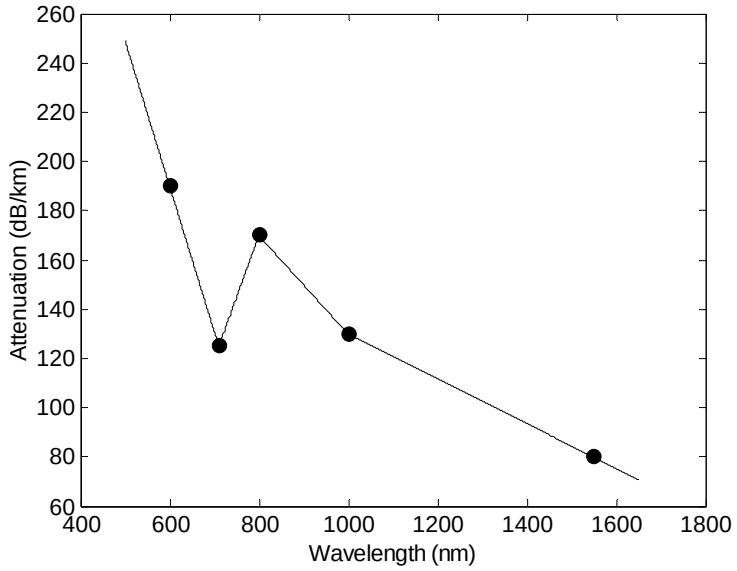

Figure A.2: Attenuation Parameter (α) for Crystal Fibre NL-18-710. The circles represent the values on Table A.1, the rest of the values were calculated by linear interpolation.

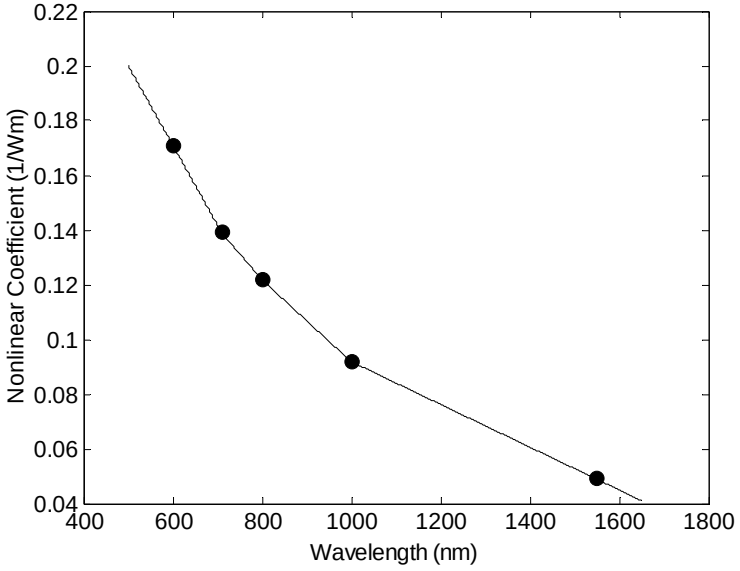

Figure A.3: Nonlinear Coefficient (γ) for a Crystal Fibre NL-18-710. The circles represent the values on Table A.1, the rest of the values were calculated by linear interpolation.

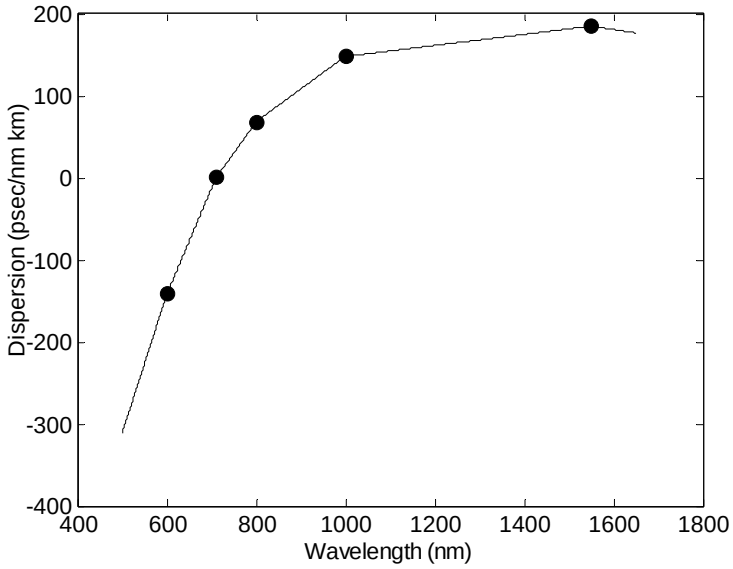

Figure A.4: Dispersion Coefficient (D) for a Crystal Fibre NL-18-710. The circles represent the values on Table A.1, the rest of the values were calculated by linear interpolation.

- 3M FS-PM-7811

This is a polarization-maintaining fiber with a small core area in order to achieve a large nonlinear index.

The fiber parameters are:

• Operating Wavelength: 1550nm.

• Mode Field Diameter: 5.5 μm.

• Dispersion parameter: 1.177 s/m^2.

• Dispersion slope at 1550nm: 80 s/m^3.

• Dispersion Law: $D = 11.77 + 8 \times 10^{-5}\left(\lambda - 1.55 \times 10^{-7}\right)$ in [ps/nm^2], where λ is in [cm].

• Nonlinear Parameter: $\gamma = 0.0044\left(W^{-1} \cdot m^{-1}\right)$.

• Attenuation Typical at 1550nm: $\alpha = 2.6\, dB / km$.

• Birefringence: 7×10^{-4} .

APPENDIX B: VPI Models and Numerical Parameters

The numerical simulations in this Thesis were performed using the software VPI Transmission Maker [VPI05]. It is a graphical programming software that includes an important library of optical components. In our study we just needed to model different pulses propagation through different fibers, so the simulation model was very simple. The simulation model is shown in Figure B.1 and the principal numerical parameters in Table B.1.

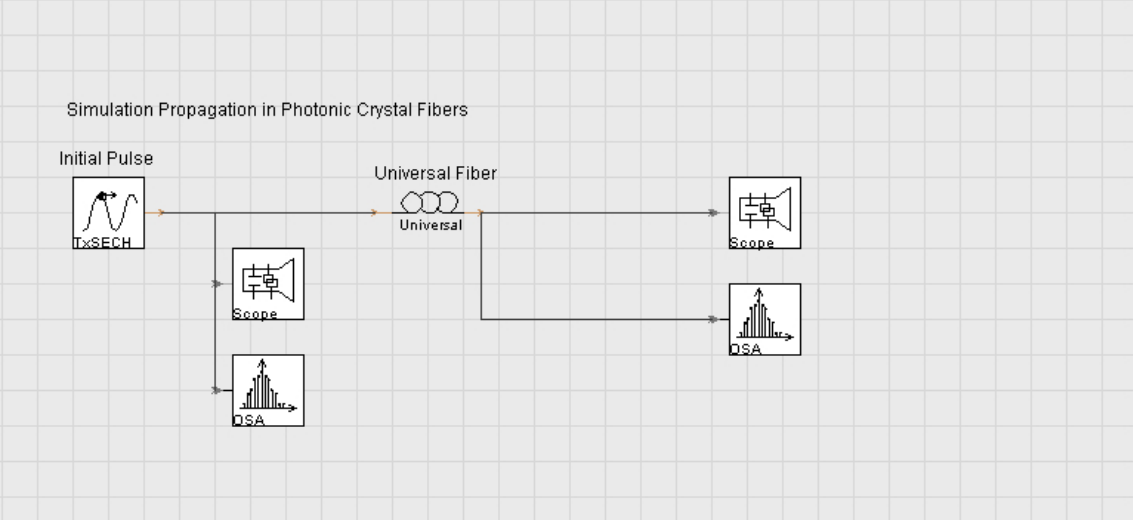

Figure B.1: VPI Model used for simulations.

Parameter	Value
Time Windows	40ps (*)
Frequency Bandwidth	204.8 THz
Bit Rate Default	$1/40 \times 10^{12}$ bps

Table B.1: Numerical Parameters.

(*) for very small frequency shifts, this value was increased to 80ps or 160ps.

The parameters' values in an xml format are shown next for each type of fiber.

1) Photonic Crystal Fiber Simulation Parameters:

i. Global Parameters:

```
<?xml version='1.0' encoding='UTF-8' ?>
<!DOCTYPE SAVEDSTATES>
<SAVEDSTATES master="PhotonicCrystalFiberThesis.vtmu">
<STATEVALUE unit="s" category="Global" label="TimeWindow" value="4e-
11" __key="value" type="float"></STATEVALUE>
<STATEVALUE unit="" category="Global" label="InBandNoiseBins"
value="OFF" __key="value" type="enumeration"></STATEVALUE>
<STATEVALUE unit="" category="Global" label="BoundaryConditions"
value="Periodic" __key="value" type="enumeration"></STATEVALUE>
<STATEVALUE unit="" category="Global" label="LogicalInformation"
value="ON" __key="value" type="enumeration"></STATEVALUE>
<STATEVALUE unit="Hz" category="Global" label="SampleModeBandwidth"
value="204.8e12" __key="value" type="float"></STATEVALUE>
<STATEVALUE unit="Hz" category="Global"
label="SampleModeCenterFrequency" value="384.615e12" __key="value"
type="float"></STATEVALUE>
<STATEVALUE unit="Hz" category="Global" label="SampleRateDefault"
value="204.8e12" __key="value" type="float"></STATEVALUE>
<STATEVALUE unit="bit/s" category="Global" label="BitRateDefault"
value="1/4e-11" __key="value" type="float"></STATEVALUE>
<STATEVALUE unit="Hz" category="PulsedLaser"
label="PulseCenterFrequency" value="384.615e12" __key="value"
type="float"></STATEVALUE>
<STATEVALUE unit="W" category="PulsedLaser" label="AveragePower"
value="5e-3" __key="value" type="float"></STATEVALUE>
<STATEVALUE unit="Hz" category="PulsedLaser" label="RepeatitionRate"
value="50e6" __key="value" type="float"></STATEVALUE>
```

```
<STATEVALUE unit="s" category="PulsedLaser" label="To" value="100e-
15" __key="value" type="float"></STATEVALUE>
</SAVEDSTATES>
```

ii. Fiber Parameters:

```
<?xml version='1.0' encoding='UTF-8' ?>
<!DOCTYPE SAVEDSTATES>
<SAVEDSTATES master="UniversalFiberFwd.vtmg">
<STATEVALUE unit="" category="Physical" label="NumberOfFiberSpans"
value="1" __key="value" type="int"></STATEVALUE>
<STATEVALUE unit="m" category="Physical" label="Length" value="0.1"
__key="value" type="floatarray"></STATEVALUE>
<STATEVALUE unit="" category="Physical"
label="AttenuationDescription" value="AttenuationFile" __key="value"
type="enumeration"></STATEVALUE>
<STATEVALUE unit="dB/m" category="Physical" label="Attenuation"
value="0.2e-3" __key="value" type="floatarray"></STATEVALUE>
<STATEVALUE unit="" category="Physical" label="AttFilename"
value="Attenuation710.txt" __key="value"
type="inputfilearray"></STATEVALUE>
<STATEVALUE unit="Hz" category="Physical" label="ReferenceFrequency"
value="PulseCenterFrequency" __key="value" type="float"></STATEVALUE>
<STATEVALUE unit="" category="Physical" label="DispersionDescription"
value="DispersionFile" __key="value" type="enumeration"></STATEVALUE>
<STATEVALUE unit="s/m^2" category="Physical" label="Dispersion"
value="16e-6" __key="value" type="floatarray"></STATEVALUE>
<STATEVALUE unit="s/m^3" category="Physical" label="DispersionSlope"
value="0.08e3" __key="value" type="floatarray"></STATEVALUE>
<STATEVALUE unit="" category="Physical" label="DispersionFilename"
value="Dispersion710.txt" __key="value"
type="inputfilearray"></STATEVALUE>
<STATEVALUE unit="" category="Physical" label="RamanScattering"
value="Yes" __key="value" type="enumeration"></STATEVALUE>
<STATEVALUE unit="" category="Physical" label="RamanFilename"
value="RamanNew.txt" __key="value"
type="inputfilearray"></STATEVALUE>
<STATEVALUE unit="" category="Physical"
label="RamanAdjustmentFactors" value="0.5" __key="value"
type="floatarray"></STATEVALUE>
<STATEVALUE unit="" category="Physical"
label="SpontaneousRamanScattering" value="No" __key="value"
type="enumeration"></STATEVALUE>
<STATEVALUE unit="" category="Physical" label="RamanFraction"
value="0.17" __key="value" type="floatarray"></STATEVALUE>
<STATEVALUE unit="K" category="Physical" label="Temperature"
value="300.0" __key="value" type="floatarray"></STATEVALUE>
<STATEVALUE unit="s/(m^1/2)" category="Physical"
label="PMDCoefficient" value="0.1e-12/31.62" __key="value"
type="float"></STATEVALUE>
<STATEVALUE unit="m" category="Physical" label="CorrelationLength"
```

```
value="50.0" __key="value" type="float"></STATEVALUE>
<STATEVALUE unit="" category="Physical" label="NonlinearDescription"
value="NonlinearFile" __key="value" type="enumeration"></STATEVALUE>
<STATEVALUE unit="m^2/W" category="Physical" label="NonLinearIndex"
value="8.2e-19" __key="value" type="floatarray"></STATEVALUE>
<STATEVALUE unit="" category="Physical" label="NonLinearFilename"
value="NonLinear710.txt" __key="value"
type="inputfilearray"></STATEVALUE>
<STATEVALUE unit="" category="Physical" label="CoreAreaDescription"
value="CoreAreaParameter" __key="value"
type="enumeration"></STATEVALUE>
<STATEVALUE unit="m^2" category="Physical" label="CoreArea"
value="1.77e-12" __key="value" type="floatarray"></STATEVALUE>
<STATEVALUE unit="" category="Physical" label="CoreAreaFilename"
value="" __key="value" type="inputfilearray"></STATEVALUE>
<STATEVALUE unit="" category="Physical"
label="OverlapIntegralFilename" value="" __key="value"
type="inputfilearray"></STATEVALUE>
<STATEVALUE unit="" category="Physical" label="EventLossDescription"
value="EventLossParameter" __key="value"
type="enumeration"></STATEVALUE>
<STATEVALUE unit="dB" category="Physical" label="EventLoss"
value="0.0" __key="value" type="floatarray"></STATEVALUE>
<STATEVALUE unit="" category="Physical" label="EventLossFilename"
value="" __key="value" type="inputfilearray"></STATEVALUE>
<STATEVALUE unit="Hz" category="Numerical" label="FreqResolutionNB"
value="25e9" __key="value" type="float"></STATEVALUE>
<STATEVALUE unit="Hz" category="Numerical" label="FreqResolutionSFB"
value="25e9" __key="value" type="float"></STATEVALUE>
<STATEVALUE unit="Hz" category="Numerical"
label="GridReferenceFrequency" value="PulseCenterFrequency"
__key="value" type="float"></STATEVALUE>
<STATEVALUE unit="" category="Numerical"
label="SpectralDiscretizerDescription" value="FixedFrequencies"
__key="value" type="enumeration"></STATEVALUE>
<STATEVALUE unit="Hz" category="Numerical"
label="NoiseCenterFrequency" value="PulseCenterFrequency"
__key="value" type="float"></STATEVALUE>
<STATEVALUE unit="Hz" category="Numerical" label="NoiseBandwidth"
value="10e12" __key="value" type="float"></STATEVALUE>
<STATEVALUE unit="dB" category="Numerical" label="AccuracyGoal"
value="0.01" __key="value" type="float"></STATEVALUE>
<STATEVALUE unit="" category="Numerical"
label="IterationAccuracyFactor" value="10.0" __key="value"
type="float"></STATEVALUE>
<STATEVALUE unit="m" category="Numerical" label="InitialStepSize"
value="0.01" __key="value" type="floatarray"></STATEVALUE>
<STATEVALUE unit="m" category="Numerical" label="MinimumStepSize"
value="0.005" __key="value" type="float"></STATEVALUE>
<STATEVALUE unit="" category="Numerical" label="SplitStepType"
value="Symmetric" __key="value" type="enumeration"></STATEVALUE>
<STATEVALUE unit="m" category="Numerical" label="MaxStepWidth"
value=".1" __key="value" type="float"></STATEVALUE>
<STATEVALUE unit="deg" category="Numerical" label="MaxPhaseChange"
```

value="0.5" __key="value" type="float"></STATEVALUE>
<STATEVALUE unit="m" category="Numerical" label="MeanStepWidth"
value="1.0e3" __key="value" type="float"></STATEVALUE>
<STATEVALUE unit="m" category="Numerical" label="WidthDeviation"
value="100.0" __key="value" type="float"></STATEVALUE>
<STATEVALUE unit="" category="Enhanced" label="PolarizationAnalysis"
value="Scalar" __key="value" type="enumeration"></STATEVALUE>
<STATEVALUE unit="" category="Enhanced" label="NoisePolarization"
value="Unpolarized" __key="value" type="enumeration"></STATEVALUE>
<STATEVALUE unit="" category="Enhanced"
label="DistortionPolarization" value="Unpolarized" __key="value"
type="enumeration"></STATEVALUE>
<STATEVALUE unit="" category="Enhanced"
label="NonlinearAdjustmentFactors" value="1.0 1.0 1.0 1.0 0.5"
__key="value" type="floatarray"></STATEVALUE>
<STATEVALUE unit="" category="Enhanced" label="WidthRandomNumberSeed"
value="0" __key="value" type="int"></STATEVALUE>
<STATEVALUE unit="" category="Enhanced"
label="ScatteringRandomNumberSeed" value="0" __key="value"
type="int"></STATEVALUE>
<STATEVALUE unit="" category="Enhanced" label="FreezeWidth" value="0"
__key="value" type="int"></STATEVALUE>
<STATEVALUE unit="" category="Enhanced" label="FreezeScattering"
value="0" __key="value" type="int"></STATEVALUE>
<STATEVALUE unit="" category="Enhanced"
label="CorrelationScatteringFactor" value="0.0" __key="value"
type="float"></STATEVALUE>
<STATEVALUE unit="" category="Enhanced" label="BirefringenceProfile"
value="None" __key="value" type="enumeration"></STATEVALUE>
<STATEVALUE unit="" category="Enhanced"
label="BirefringenceFileDataType" value="RotationMatrices"
__key="value" type="enumeration"></STATEVALUE>
<STATEVALUE unit="" category="Enhanced"
label="BirefringenceInputFilename" value="" __key="value"
type="inputfile"></STATEVALUE>
<STATEVALUE unit="" category="Enhanced"
label="BirefringenceOutputFilename" value="" __key="value"
type="outputfile"></STATEVALUE>
<STATEVALUE unit="" category="Enhanced"
label="LikelihoodRatiosFilename" value="" __key="value"
type="outputfile"></STATEVALUE>
<STATEVALUE unit="" category="Enhanced" label="FieldAnalysis"
value="Yes" __key="value" type="enumeration"></STATEVALUE>
<STATEVALUE unit="" category="Enhanced" label="SkipFieldAnalysis"
value="0" __key="value" type="int"></STATEVALUE>
<STATEVALUE unit="" category="Enhanced" label="SPM_EC" value="Yes"
__key="value" type="enumeration"></STATEVALUE>
<STATEVALUE unit="" category="Enhanced" label="XPM_EC" value="Yes"
__key="value" type="enumeration"></STATEVALUE>
<STATEVALUE unit="" category="Enhanced" label="XPM_MC" value="Yes"
__key="value" type="enumeration"></STATEVALUE>
<STATEVALUE unit="" category="Enhanced" label="IntraBandRaman"
value="Yes" __key="value" type="enumeration"></STATEVALUE>
<STATEVALUE unit="" category="Enhanced" label="InterBandRaman"

```
value="Yes" __key="value" type="enumeration"></STATEVALUE>
<STATEVALUE unit="" category="Enhanced" label="HigherOrderNLEffects"
value="Yes" __key="value" type="enumeration"></STATEVALUE>
<STATEVALUE unit="" category="Enhanced" label="NoiseBinInteractions"
value="Yes" __key="value" type="enumeration"></STATEVALUE>
<STATEVALUE unit="" category="Enhanced"
label="DistortionInteractions" value="Yes" __key="value"
type="enumeration"></STATEVALUE>
<STATEVALUE unit="" category="Enhanced" label="Options" value=""
__key="value" type="string"></STATEVALUE>
<STATEVALUE unit="" category="Enhanced" label="PowerPlotPoints"
value="101" __key="value" type="int"></STATEVALUE>
<STATEVALUE unit="" category="Enhanced" label="LogFilename" value=""
__key="value" type="outputfile"></STATEVALUE>
<STATEVALUE unit="" category="Enhanced" label="ConserveMemory"
value="No" __key="value" type="enumeration"></STATEVALUE>
<STATEVALUE unit="" category="Enhanced" label="NoiseRandomNumberSeed"
value="0" __key="value" type="int"></STATEVALUE>
<STATEVALUE unit="" category="Enhanced" label="Active" value="On"
__key="value" type="enumeration"></STATEVALUE>
</SAVEDSTATES>
```

iii. Pulse Parameter:

```
<?xml version='1.0' encoding='UTF-8' ?>
<!DOCTYPE SAVEDSTATES>
<SAVEDSTATES master="TxPulseSechOpt.vtmg">
<STATEVALUE unit="Hz" category="Physical" label="SampleRate"
value="SampleRateDefault" __key="value" type="float"></STATEVALUE>
<STATEVALUE unit="bit/s" category="Physical" label="BitRate"
value="BitRateDefault" __key="value" type="float"></STATEVALUE>
<STATEVALUE unit="Hz" category="Physical" label="EmissionFrequency"
value="PulseCenterFrequency" __key="value" type="float"></STATEVALUE>
<STATEVALUE unit="W" category="Physical" label="PeakPower" value="!
&amp;quot; expr {AveragePower} / ({RepeatitionRate} * {To})&amp;quot;"
__key="value" type="float"></STATEVALUE>
<STATEVALUE unit="s" category="Physical" label="FWHM" value="!&amp;quot;
expr {To}*2* sqrt( log(2) )&amp;quot;" __key="value"
type="float"></STATEVALUE>
<STATEVALUE unit="" category="Physical" label="CenterPosition"
value="0.5" __key="value" type="float"></STATEVALUE>
<STATEVALUE unit="deg" category="Physical" label="InitialPhase"
value="0.0" __key="value" type="float"></STATEVALUE>
<STATEVALUE unit="deg" category="Physical" label="Azimuth" value="0"
__key="value" type="float"></STATEVALUE>
<STATEVALUE unit="deg" category="Physical" label="Ellipticity"
value="0" __key="value" type="float"></STATEVALUE>
<STATEVALUE unit="" category="Physical" label="PreSpaces" value="0"
```

```
__key="value" type="int"></STATEVALUE>
<STATEVALUE unit="" category="Physical" label="PostSpaces" value="0"
__key="value" type="int"></STATEVALUE>
<STATEVALUE unit="" category="Physical" label="PRBS_Type"
value="PRBS" __key="value" type="enumeration"></STATEVALUE>
<STATEVALUE unit="" category="Physical" label="MarkProbability"
value="0.5" __key="value" type="float"></STATEVALUE>
<STATEVALUE unit="" category="Physical" label="PRBS_Order" value="7"
__key="value" type="int"></STATEVALUE>
<STATEVALUE unit="" category="Physical" label="MarkNumber" value="7"
__key="value" type="int"></STATEVALUE>
<STATEVALUE unit="" category="Physical" label="CodeWord" value=""
__key="value" type="intarray"></STATEVALUE>
<STATEVALUE unit="" category="Physical" label="InputFilename"
value="" __key="value" type="inputfile"></STATEVALUE>
<STATEVALUE unit="" category="Numerical" label="ExcessPulseSlots"
value="3" __key="value" type="int"></STATEVALUE>
<STATEVALUE unit="" category="Enhanced" label="RandomNumberSeed"
value="0" __key="value" type="int"></STATEVALUE>
<STATEVALUE unit="" category="Enhanced" label="OutputFilename"
value="" __key="value" type="outputfile"></STATEVALUE>
<STATEVALUE unit="" category="Enhanced" label="ControlFlagReset"
value="Continue" __key="value" type="enumeration"></STATEVALUE>
<STATEVALUE unit="" category="Enhanced" label="ControlFlagWrite"
value="Overwrite" __key="value" type="enumeration"></STATEVALUE>
<STATEVALUE unit="" category="Enhanced" label="OutputDataType"
value="Blocks" __key="value" type="enumeration"></STATEVALUE>
<STATEVALUE unit="" category="Enhanced" label="ChannelLabel" value=""
__key="value" type="string"></STATEVALUE>
</SAVEDSTATES>
```

2) Polarization maintaining fiber parameters:

i. Global Parameters:

```
<?xml version='1.0' encoding='UTF-8' ?>
<!DOCTYPE SAVEDSTATES>
<SAVEDSTATES master="PhotonicCrystalFiber31.vtmu">
<STATEVALUE unit="s" category="Global" label="TimeWindow" value="80e-
12" __key="value" type="float"></STATEVALUE>
<STATEVALUE unit="" category="Global" label="InBandNoiseBins"
value="OFF" __key="value" type="enumeration"></STATEVALUE>
<STATEVALUE unit="" category="Global" label="BoundaryConditions"
value="Periodic" __key="value" type="enumeration"></STATEVALUE>
<STATEVALUE unit="" category="Global" label="LogicalInformation"
value="ON" __key="value" type="enumeration"></STATEVALUE>
<STATEVALUE unit="Hz" category="Global" label="SampleModeBandwidth"
```

```
value="204.8e12" __key="value" type="float"></STATEVALUE>
<STATEVALUE unit="Hz" category="Global"
label="SampleModeCenterFrequency" value="193.1e12" __key="value"
type="float"></STATEVALUE>
<STATEVALUE unit="Hz" category="Global" label="SampleRateDefault"
value="204.8e12" __key="value" type="float"></STATEVALUE>
<STATEVALUE unit="bit/s" category="Global" label="BitRateDefault"
value="1/80e-12" __key="value" type="float"></STATEVALUE>
<STATEVALUE unit="Hz" category="PulsedLaser"
label="PulseCenterFrequency" value="193.1e12" __key="value"
type="float"></STATEVALUE>
<STATEVALUE unit="W" category="PulsedLaser" label="AveragePower"
value="5.5e-3" __key="value" type="float"></STATEVALUE>
<STATEVALUE unit="Hz" category="PulsedLaser" label="RepeatitionRate"
value="48e6" __key="value" type="float"></STATEVALUE>
<STATEVALUE unit="s" category="PulsedLaser" label="To" value="100e-
15" __key="value" type="float"></STATEVALUE>
</SAVEDSTATES>
```

ii. Fiber Parameters:

```
<?xml version='1.0' encoding='UTF-8' ?>
<!DOCTYPE SAVEDSTATES>
<SAVEDSTATES master="UniversalFiberFwd.vtmg">
<STATEVALUE unit="" category="Physical" label="NumberOfFiberSpans"
value="1" __key="value" type="int"></STATEVALUE>
<STATEVALUE unit="m" category="Physical" label="Length" value="0.1"
__key="value" type="floatarray"></STATEVALUE>
<STATEVALUE unit="" category="Physical"
label="AttenuationDescription" value="AttenuationParameter"
__key="value" type="enumeration"></STATEVALUE>
<STATEVALUE unit="dB/m" category="Physical" label="Attenuation"
value="2.6e-3" __key="value" type="floatarray"></STATEVALUE>
<STATEVALUE unit="" category="Physical" label="AttFilename"
value="AttenuationL01.txt" __key="value"
type="inputfilearray"></STATEVALUE>
<STATEVALUE unit="Hz" category="Physical" label="ReferenceFrequency"
value="PulseCenterFrequency" __key="value" type="float"></STATEVALUE>
<STATEVALUE unit="" category="Physical" label="DispersionDescription"
value="DispersionParameters" __key="value"
type="enumeration"></STATEVALUE>
<STATEVALUE unit="s/m^2" category="Physical" label="Dispersion"
value="1.177e-5" __key="value" type="floatarray"></STATEVALUE>
<STATEVALUE unit="s/m^3" category="Physical" label="DispersionSlope"
value="0.08e3" __key="value" type="floatarray"></STATEVALUE>
<STATEVALUE unit="" category="Physical" label="DispersionFilename"
value="DispersionL01.txt" __key="value"
type="inputfilearray"></STATEVALUE>
<STATEVALUE unit="" category="Physical" label="RamanScattering"
value="Yes" __key="value" type="enumeration"></STATEVALUE>
<STATEVALUE unit="" category="Physical" label="RamanFilename"
```

value=""$BNROOT/data/UFM/RamanGain.dat"" __key="value"
type="inputfilearray"></STATEVALUE>
<STATEVALUE unit="" category="Physical"
label="RamanAdjustmentFactors" value="0.5" __key="value"
type="floatarray"></STATEVALUE>
<STATEVALUE unit="" category="Physical"
label="SpontaneousRamanScattering" value="No" __key="value"
type="enumeration"></STATEVALUE>
<STATEVALUE unit="" category="Physical" label="RamanFraction"
value="0.17" __key="value" type="floatarray"></STATEVALUE>
<STATEVALUE unit="K" category="Physical" label="Temperature"
value="300.0" __key="value" type="floatarray"></STATEVALUE>
<STATEVALUE unit="s/(m^1/2)" category="Physical"
label="PMDCoefficient" value="0.1e-12/31.62" __key="value"
type="float"></STATEVALUE>
<STATEVALUE unit="m" category="Physical" label="CorrelationLength"
value="50.0" __key="value" type="float"></STATEVALUE>
<STATEVALUE unit="" category="Physical" label="NonlinearDescription"
value="NonlinearIndexParameter" __key="value"
type="enumeration"></STATEVALUE>
<STATEVALUE unit="m^2/W" category="Physical" label="NonLinearIndex"
value="2.6e-20" __key="value" type="floatarray"></STATEVALUE>
<STATEVALUE unit="" category="Physical" label="NonLinearFilename"
value="NonLinearL01.txt" __key="value"
type="inputfilearray"></STATEVALUE>
<STATEVALUE unit="" category="Physical" label="CoreAreaDescription"
value="CoreAreaParameter" __key="value"
type="enumeration"></STATEVALUE>
<STATEVALUE unit="m^2" category="Physical" label="CoreArea"
value="23.76e-12" __key="value" type="floatarray"></STATEVALUE>
<STATEVALUE unit="" category="Physical" label="CoreAreaFilename"
value="Area710.txt" __key="value" type="inputfilearray"></STATEVALUE>
<STATEVALUE unit="" category="Physical"
label="OverlapIntegralFilename" value="" __key="value"
type="inputfilearray"></STATEVALUE>
<STATEVALUE unit="" category="Physical" label="EventLossDescription"
value="EventLossParameter" __key="value"
type="enumeration"></STATEVALUE>
<STATEVALUE unit="dB" category="Physical" label="EventLoss"
value="0.0" __key="value" type="floatarray"></STATEVALUE>
<STATEVALUE unit="" category="Physical" label="EventLossFilename"
value="" __key="value" type="inputfilearray"></STATEVALUE>
<STATEVALUE unit="Hz" category="Numerical" label="FreqResolutionNB"
value="100e9" __key="value" type="float"></STATEVALUE>
<STATEVALUE unit="Hz" category="Numerical" label="FreqResolutionSFB"
value="100e9" __key="value" type="float"></STATEVALUE>
<STATEVALUE unit="Hz" category="Numerical"
label="GridReferenceFrequency" value="PulseCenterFrequency"
__key="value" type="float"></STATEVALUE>
<STATEVALUE unit="" category="Numerical"
label="SpectralDiscretizerDescription" value="FixedFrequencies"
__key="value" type="enumeration"></STATEVALUE>
<STATEVALUE unit="Hz" category="Numerical"
label="NoiseCenterFrequency" value="193.1e12" __key="value"

```
type="float"></STATEVALUE>
<STATEVALUE unit="Hz" category="Numerical" label="NoiseBandwidth"
value="10e12" __key="value" type="float"></STATEVALUE>
<STATEVALUE unit="dB" category="Numerical" label="AccuracyGoal"
value="0.01" __key="value" type="float"></STATEVALUE>
<STATEVALUE unit="" category="Numerical"
label="IterationAccuracyFactor" value="10.0" __key="value"
type="float"></STATEVALUE>
<STATEVALUE unit="m" category="Numerical" label="InitialStepSize"
value="1000.0" __key="value" type="floatarray"></STATEVALUE>
<STATEVALUE unit="m" category="Numerical" label="MinimumStepSize"
value="1.0" __key="value" type="float"></STATEVALUE>
<STATEVALUE unit="" category="Numerical" label="SplitStepType"
value="Symmetric" __key="value" type="enumeration"></STATEVALUE>
<STATEVALUE unit="m" category="Numerical" label="MaxStepWidth"
value="1.0e3" __key="value" type="float"></STATEVALUE>
<STATEVALUE unit="deg" category="Numerical" label="MaxPhaseChange"
value="0.05" __key="value" type="float"></STATEVALUE>
<STATEVALUE unit="m" category="Numerical" label="MeanStepWidth"
value="1.0e3" __key="value" type="float"></STATEVALUE>
<STATEVALUE unit="m" category="Numerical" label="WidthDeviation"
value="100.0" __key="value" type="float"></STATEVALUE>
<STATEVALUE unit="" category="Enhanced" label="PolarizationAnalysis"
value="Scalar" __key="value" type="enumeration"></STATEVALUE>
<STATEVALUE unit="" category="Enhanced" label="NoisePolarization"
value="Unpolarized" __key="value" type="enumeration"></STATEVALUE>
<STATEVALUE unit="" category="Enhanced"
label="DistortionPolarization" value="Unpolarized" __key="value"
type="enumeration"></STATEVALUE>
<STATEVALUE unit="" category="Enhanced"
label="NonlinearAdjustmentFactors" value="1.0 1.0 1.0 1.0 0.5"
__key="value" type="floatarray"></STATEVALUE>
<STATEVALUE unit="" category="Enhanced" label="WidthRandomNumberSeed"
value="0" __key="value" type="int"></STATEVALUE>
<STATEVALUE unit="" category="Enhanced"
label="ScatteringRandomNumberSeed" value="0" __key="value"
type="int"></STATEVALUE>
<STATEVALUE unit="" category="Enhanced" label="FreezeWidth" value="0"
__key="value" type="int"></STATEVALUE>
<STATEVALUE unit="" category="Enhanced" label="FreezeScattering"
value="0" __key="value" type="int"></STATEVALUE>
<STATEVALUE unit="" category="Enhanced"
label="CorrelationScatteringFactor" value="0.0" __key="value"
type="float"></STATEVALUE>
<STATEVALUE unit="" category="Enhanced" label="BirefringenceProfile"
value="None" __key="value" type="enumeration"></STATEVALUE>
<STATEVALUE unit="" category="Enhanced"
label="BirefringenceFileDataType" value="RotationMatrices"
__key="value" type="enumeration"></STATEVALUE>
<STATEVALUE unit="" category="Enhanced"
label="BirefringenceInputFilename" value="" __key="value"
type="inputfile"></STATEVALUE>
<STATEVALUE unit="" category="Enhanced"
label="BirefringenceOutputFilename" value="" __key="value"
```

```
type="outputfile"></STATEVALUE>
<STATEVALUE unit="" category="Enhanced"
label="LikelihoodRatiosFilename" value="" __key="value"
type="outputfile"></STATEVALUE>
<STATEVALUE unit="" category="Enhanced" label="FieldAnalysis"
value="Yes" __key="value" type="enumeration"></STATEVALUE>
<STATEVALUE unit="" category="Enhanced" label="SkipFieldAnalysis"
value="0" __key="value" type="int"></STATEVALUE>
<STATEVALUE unit="" category="Enhanced" label="SPM_EC" value="Yes"
__key="value" type="enumeration"></STATEVALUE>
<STATEVALUE unit="" category="Enhanced" label="XPM_EC" value="Yes"
__key="value" type="enumeration"></STATEVALUE>
<STATEVALUE unit="" category="Enhanced" label="XPM_MC" value="Yes"
__key="value" type="enumeration"></STATEVALUE>
<STATEVALUE unit="" category="Enhanced" label="IntraBandRaman"
value="Yes" __key="value" type="enumeration"></STATEVALUE>
<STATEVALUE unit="" category="Enhanced" label="InterBandRaman"
value="Yes" __key="value" type="enumeration"></STATEVALUE>
<STATEVALUE unit="" category="Enhanced" label="HigherOrderNLEffects"
value="No" __key="value" type="enumeration"></STATEVALUE>
<STATEVALUE unit="" category="Enhanced" label="NoiseBinInteractions"
value="Yes" __key="value" type="enumeration"></STATEVALUE>
<STATEVALUE unit="" category="Enhanced"
label="DistortionInteractions" value="Yes" __key="value"
type="enumeration"></STATEVALUE>
<STATEVALUE unit="" category="Enhanced" label="Options" value=""
__key="value" type="string"></STATEVALUE>
<STATEVALUE unit="" category="Enhanced" label="PowerPlotPoints"
value="101" __key="value" type="int"></STATEVALUE>
<STATEVALUE unit="" category="Enhanced" label="LogFilename" value=""
__key="value" type="outputfile"></STATEVALUE>
<STATEVALUE unit="" category="Enhanced" label="ConserveMemory"
value="No" __key="value" type="enumeration"></STATEVALUE>
<STATEVALUE unit="" category="Enhanced" label="NoiseRandomNumberSeed"
value="0" __key="value" type="int"></STATEVALUE>
<STATEVALUE unit="" category="Enhanced" label="Active" value="On"
__key="value" type="enumeration"></STATEVALUE>
</SAVEDSTATES>
```

iii. Pulse Parameters:

```
<?xml version='1.0' encoding='UTF-8' ?>
<!DOCTYPE SAVEDSTATES>
<SAVEDSTATES master="TxPulseSechOpt.vtmg">
<STATEVALUE unit="Hz" category="Physical" label="SampleRate"
value="SampleRateDefault" __key="value" type="float"></STATEVALUE>
<STATEVALUE unit="bit/s" category="Physical" label="BitRate"
value="BitRateDefault" __key="value" type="float"></STATEVALUE>
<STATEVALUE unit="Hz" category="Physical" label="EmissionFrequency"
value="PulseCenterFrequency" __key="value" type="float"></STATEVALUE>
<STATEVALUE unit="W" category="Physical" label="PeakPower"
```

```
value="!&amp;quot; expr {AveragePower}/({RepeatitionRate}*{To})&amp;quot;"
__key="value" type="float"></STATEVALUE>
<STATEVALUE unit="s" category="Physical" label="FWHM" value="!&amp;quot;
expr {To}*2* sqrt( log(2) )&amp;quot;" __key="value"
type="float"></STATEVALUE>
<STATEVALUE unit="" category="Physical" label="CenterPosition"
value="0.5" __key="value" type="float"></STATEVALUE>
<STATEVALUE unit="deg" category="Physical" label="InitialPhase"
value="0.0" __key="value" type="float"></STATEVALUE>
<STATEVALUE unit="deg" category="Physical" label="Azimuth" value="0"
__key="value" type="float"></STATEVALUE>
<STATEVALUE unit="deg" category="Physical" label="Ellipticity"
value="0" __key="value" type="float"></STATEVALUE>
<STATEVALUE unit="" category="Physical" label="PreSpaces" value="0"
__key="value" type="int"></STATEVALUE>
<STATEVALUE unit="" category="Physical" label="PostSpaces" value="0"
__key="value" type="int"></STATEVALUE>
<STATEVALUE unit="" category="Physical" label="PRBS_Type"
value="PRBS" __key="value" type="enumeration"></STATEVALUE>
<STATEVALUE unit="" category="Physical" label="MarkProbability"
value="0.5" __key="value" type="float"></STATEVALUE>
<STATEVALUE unit="" category="Physical" label="PRBS_Order" value="7"
__key="value" type="int"></STATEVALUE>
<STATEVALUE unit="" category="Physical" label="MarkNumber" value="7"
__key="value" type="int"></STATEVALUE>
<STATEVALUE unit="" category="Physical" label="CodeWord" value=""
__key="value" type="intarray"></STATEVALUE>
<STATEVALUE unit="" category="Physical" label="InputFilename"
value="" __key="value" type="inputfile"></STATEVALUE>
<STATEVALUE unit="" category="Numerical" label="ExcessPulseSlots"
value="3" __key="value" type="int"></STATEVALUE>
<STATEVALUE unit="" category="Enhanced" label="RandomNumberSeed"
value="0" __key="value" type="int"></STATEVALUE>
<STATEVALUE unit="" category="Enhanced" label="OutputFilename"
value="" __key="value" type="outputfile"></STATEVALUE>
<STATEVALUE unit="" category="Enhanced" label="ControlFlagReset"
value="Continue" __key="value" type="enumeration"></STATEVALUE>
<STATEVALUE unit="" category="Enhanced" label="ControlFlagWrite"
value="Overwrite" __key="value" type="enumeration"></STATEVALUE>
<STATEVALUE unit="" category="Enhanced" label="OutputDataType"
value="Blocks" __key="value" type="enumeration"></STATEVALUE>
<STATEVALUE unit="" category="Enhanced" label="ChannelLabel" value=""
__key="value" type="string"></STATEVALUE>
</SAVEDSTATES>
```

APPENDIX C: MATLAB CODE

In this appendix we include the Matlab code for the semi-analytical method for the SSFS described in Chapter 7.

```
%-------------------------------------------------
% Roque Gagliano
% Semi-analytic method for soliton propagation in an optical-fiber

%-------------------------------------------------
%------- Fiber Parameters
lambdao=780e-9; %  Initial Cetral Wavelength in m

% loading files with arbitrary parameters:

load DispersionL01.txt
load AttenuationL01.txt
load NonLinearL01.txt

lambdax=DispersionL01(:,1)*1e-9*1e2; % Wavelength in cm
Dy=DispersionL01(:,2); % Dispersion profile in psec/nm/km
Do=interp1(lambdax,Dy,lambdao*1e2,'linear'); % Initial dispersion in psec/nm km

alfao=AttenuationL01(:,2)./(10*log10(exp(1))); % loss parameter in 1/km
lalfao=AttenuationL01(:,1)*1e-9*1e2; % Wavelength in cm

gamma0=NonLinearL01(:,2); % nonlinear coef in 1/(Wm)
lgamma=NonLinearL01(:,1)*1e-9*1e2;

Gammao=interp1(lgamma,gamma0,lambdao*1e2,'linear'); % Nonlinear Parameter in
1/(Wm)
Length=10; % Length in m

Corr=1.5; % Fiber dependent Parameter Set to 1.5

%-------------------------------------------------
%-------  Initial Soliton Parameter
```

```
c=3e8; % m/s
To=[20:4:300]*1e-15 ; % Initial Soliton width (sec)
vo=c/lambdao; % Initial Frequency (Hz)
Po=(lambdao.^2).*(Do*1e-6)./(Gammao*2*pi*c*(To.^2)); %Initial Peak Power for
Soliton

%-----------------------------------------------


Spams=1000; % Number of spans that the fiber is choped

for j=1:length(To)

% Initialization
T(j,1)=To(j)*1e12; % To in psec
l=Length/Spams*1e-3; % Spam Legnth in km
lambda(j,1)=lambdao*1e2; % Units is cm
v(j,1)=vo*1e-12; % Initial frequency in Thz
D(j,1)=Do*1e2; % Initial dispersion in psec/cm2
P(j,1)=Po(j);

for i=1:Spams,
   dv(j,i)=-((lambda(j,i).^2).*D(j,i)*133.58*Corr./(T(j,i).^4))*l; % Frequency Shift in
THz
   v(j,i+1)=v(j,i)+dv(j,i);
   lambda(j,i+1)=(c./(v(j,i+1)*1e12))*1e2; % New lambda in cm
   D(j,i+1)=interp1(lambdax,Dy,lambda(j,i+1),'linear')*1e2; % Dispersion in
psec/cm2
   alfa(j,i+1)=interp1(lalfao,alfao,lambda(j,i+1),'linear'); % Attenuation in 1/km
   Gamma(j,i+1)=interp1(lgamma,gamma0,lambda(j,i+1),'linear');
   T(j,i+1)=((lambda(j,i+1)^3).*D(j,i+1))./(Gamma(j,i+1)*2*pi.*c.*P(j,i).*exp(-
alfa(j,i+1)*l).*lambda(j,i).*T(j,i))*1e12; % T in psec
   P(j,i+1)=(lambda(j,i+1)^2).*D(j,i+1)./(Gamma(j,i+1)*2*pi*c.*T(j,i+1)^2)*1e12;
end
end

% Resuls display

disp(T(:,1))
disp(P(:,1))
disp(T(:,Spams)*1e3)
disp(P(:,Spams))
disp(-(v(:,Spams)-v(:,1))*1e3)
```

APPENDIX D: Submitted Publication

Some of the results of the work done for this Master Thesis were included in the following article submitted for publication at OSA Optics Letters in April 2005.

Semi-analytical model of soliton self-frequency shift in an optical fiber

Roque Gagliano Molla, *Student Member, IEEE* and Rongqing Hui, *Senior Member, IEEE*

Department of Electrical Engineering and Computer Science
The University of Kansas, Lawrence, KS 66045

Abstract:
A semi-analytical model is proposed to investigate the characteristics of soliton self-frequency shift (SSFS) in optical fibers. SSFS in two different types of fibers were evaluated and the results agree very well with those of numerical simulations. We show that when the frequency shift is small enough, it is inversely proportional to the fourth power of the initial soliton pulse width. However, with large frequency shift, this fourth power rule needs to be modified.

***Index Terms*—** Optical propagation in nonlinear media, optical soliton, Raman scattering.

I. Introduction

Soliton self frequency shift (SSFS) in optical fiber is due to the Stimulated Raman Scattering (SRS). Once the pulse optical power level, the chromatic dispersion and the fiber nonlinearity satisfy a well-known soliton condition, the Raman-shifted optical pulses will be transformed into wavelength-shifted solitons and the amount of SSFS can generally be adjusted by changing the power level of the optical pulses [1].

In recent years, new advances in high-power femtosecond fiber lasers and highly nonlinear optical fibers have made SSFS more practical to obtain wavelength tunable optical pulses. Because of its potential applications in optical communications and biomedical imaging where wavelength tunability is desired, SSFS has been investigated extensively. Experiments of SSFS in both 1550 – 2000nm and 780 – 1000nm wavelength regions have been reported [2, 3] and the results have been analyzed both analytically and numerically.

The analytical formulation of Gordon [4] predicted that, the amount of SSFS $(\Delta\upsilon)$ is inversely proportional to the forth power of the FWHW optical pulse width (τ) at the fiber input, that is, $\Delta\upsilon \propto \tau^{-x}, x = 4$. This result successfully explained the experimental results reported in [1] where pulse width in the range of 420fs - 45ps had been used. Although reference [4] provides a nice simple formula which predicts the general behavior of SSFS, several effects were neglected such as fiber attenuation and wavelength dependency of dispersion and nonlinearity. In fact, due to fiber attenuation, the pulse peak power will be reduced and pulse width will be increased while propagating along the fiber. As a result, the frequency shift tents to saturate as demonstrated in [3]. In addition, as the central wavelength of an optical pulse shifts while propagating along the fiber due to SSFS, its behavior will be determined by the fiber parameters and the pulse energy at that specific wavelength. Because the amount of SSFS is typically larger than 100nm, the wavelength dependent nature of chromatic dispersion and nonlinearity may play important roles and they have to be taken into account in theoretical calculations. On the other hand, numerical simulation using split-step Fourier method has been proven to be effective and accurate to model

the effect of SSFS. It has been used to predict the amount of wavelength shift versus pulse optical power and pulse width. However, because femtosecond level pulse widths are usually used, very wide bandwidth is required in the numerical simulation and the process is generally very time-consuming. Another drawback of numerical simulation is that it does not directly show the effects of various physical mechanisms behind the results.

In this letter, we demonstrate a simple semi-analytic method to model SSFS in optical fibers. By taking into account fiber attenuation and wavelength dependent dispersion and nonlinearity, we show that the SSFS becomes less sensitive to the input pulse width when this width is narrow enough and the fourth power rule predicted in [4] may need to be modified for many practical applications. The results of semi-analytic calculations are found to be in good agreement with numerical simulations using split-step Fourier method. Our results also indicate that the fourth-power rule predicted in [1] is accurate when the wavelength shift is small and the fiber loss is negligible.

II. SEMI-ANALYTIC FORMULATION

Nonlinear optical pulse propagation in optical fibers can be modeled by an extended nonlinear Schrödinger equation (NLS) in which the effect of Raman scattering is included [5]:

$$\frac{\partial A}{\partial z}+\frac{\alpha(\omega)}{2}A+\beta_1\frac{\partial A}{\partial t}+\frac{i}{2}\beta_2\frac{\partial^2 A}{\partial t^2}-\frac{1}{6}\beta_3\frac{\partial^3 A}{\partial t^3}= i\gamma(\omega)\left(1+\frac{i}{\omega_0}\frac{\partial}{\partial t}\right)\left(A(z,t)\int_{-\infty}^{+\infty}R(t')\left|A(z,t'-t)\right|^2 dt'\right) \quad (1)$$

Where $A(z, t)$ is the pulse envelope. The left-hand side represents the linear effects, α is the fiber loss, β_1 the group velocity, β_2 and β_3 the 1st order and the 2nd order dispersions, respectively. The right-hand side represents the non-linear effects, where γ is the nonlinear coefficient and R(t) is the response function that includes both the electronic and the vibration (Raman) contribution [6,7]:

$$R(t) = (1 - f_R)\delta(t) + f_R h_R(t) \tag{2}$$

Where $h_R(t)$ is the Raman response function obtained from the Raman gain spectrum of the fiber, f_R represents the fractional contribution of the delayed Raman response to nonlinear polarization.

When we neglect the fiber attenuation and consider that all fiber parameters are independent of the wavelength, a closed-form analytical relationship between the soliton central frequency shift and its initial pulse width can be found [4]:

$$\frac{\partial \upsilon_0}{\partial z}(THz/km) = -K\frac{|D|\lambda^2}{T_o^4} \tag{3}$$

Where $D(\lambda) = -2\pi c\beta_2/\lambda^2$ is the dispersion parameter in [ps/cm^2], λ is the wavelength in [cm] and $T_0 = \tau/1.763$ is the pulse width in [ps]. The proportionality constant K is a fiber type- dependent parameter that is related to the value of the Raman Gain. Although this analytical solution is simple, its derivation was based on a single wavelength of the optical signal and therefore the wavelength dependency of fiber parameters was not considered. Equation (3) is accurate when the amount of pulse wavelength shift is small. In recently reported SSFS experiments, the pulse wavelength shift can be as high as several hundred nanometers [3]. In this case, fixed-wavelength approximation is no longer valid and eq.(3) needs to be modified. Because different type of fibers may have very different wavelength dependency of their key parameters, $D(\lambda)$ and $\gamma(\lambda)$ and $\alpha(\lambda)$, therefore, a closed-form analytical solution may not be feasible. However, a semi-analytical formulation would be very useful to significantly increase the speed of calculation compared to numerical simulations, while maintaining excellent accuracy.

In order to obtain a semi-analytical solution, we truncate fiber into short sections, within each section, a fixed signal wavelength can be assumed and fiber parameters at this specific wavelength can be used. The optical frequency of a soliton passing through a short fiber section from z to z + Δz can be expressed as

$$\upsilon(z + \Delta z) = \upsilon(z) - K\frac{|D(\lambda(z))|\lambda^2(z)}{T_o(z)^4}\Delta z \tag{4}$$

Where $\upsilon(z)$ is the pulse optical frequency and T_0(z) is the pulse width at the input. $D(\lambda(z))$ is the fiber dispersion parameter at the wavelength λ(z). As SSFS is a non-elastic effect, in addition to frequency shift, the peak power of the pulse also changes after passing through the short section. This peak power change is caused by three major effects, namely, fiber attenuation, pulse width change and energy loss of each photon due to the red-shift of the wavelength. Therefore, the pulse peak power at the output of the short fiber section is:

$$P_p(z+\Delta z) = P_p(z) e^{-\alpha(\lambda(z))\Delta z} \frac{\upsilon(z+\Delta z)}{\upsilon(z)} \frac{T_0(z)}{T_0(z+\Delta z)} \tag{5}$$

Where $P_p(z)$ is the peak power at the input of the fiber section. Assuming a fundamental soliton is maintained when pulses propagate along the fiber, the soliton peak power is also related to its width by:

$$P_p(z) T_0^2(z) = \frac{cD(\lambda(z))}{2\pi\upsilon^2(\lambda(z))\gamma(\lambda(z))} \tag{6}$$

Combining equations (4 - 6), an expression of pulse width at $z + \Delta z$ can be obtained as:

$$T_0(z+\Delta z) = \frac{\lambda^3(z+\Delta z) D(\lambda(z+\Delta z))}{2\pi c\gamma(\lambda(z+\Delta z))\lambda(z) P_p(z) e^{-\alpha(\lambda(z+\Delta z))\Delta z} T_0(z)} \tag{7}$$

Where $\lambda(z+\Delta z) = c/\upsilon(z+\Delta z)$ is the wavelength of the pulse at the output of the fiber section which can be obtained by equation (5); $D(\lambda(z+\Delta z))$, $\gamma(\lambda(z+\Delta z))$ and $\alpha(\lambda(z+\Delta z))$ are the dispersion nonlinearity parameter and fiber attenuation, respectively, evaluated at this new wavelength. With the parameters of a soliton pulse know at the input, equations (5) and (7) can be used together to calculate the central frequency and the pulse width of the wavelength shifted soliton at the output of a short fiber section, these parameters can, in turn, be used as the input to the next fiber section. SSFS characteristics of a long fiber can be obtained by dividing the fiber into short sections and repeating this calculation section by section, along the fiber. Because the transfer function of each fiber section described by equations (5) and (7)

is analytical, the calculation is straightforward and fast. In addition, since the wavelength of the optical pulse at different fiber sections may be very different due to SSFS, precise fiber parameters at each section can be used corresponds to the exact signal wavelength at that section. This assures the accuracy of the calculation.

III. RESULTS AND DISCUSSION

In order to evaluate the accuracy of our semi-analytical model, the results were compared with those of numerical simulations using VPI Transmission Marker [8] where split-step Fourier method was used.

First we evaluated SSFS in a 100m polarization maintaining fiber (3M FS-PM-7811) with wavelength dependent dispersion $D = 11.77 + 8 \times 10^{-5}\left(\lambda - 1.55 \times 10^{-7}\right)$ in [ps/nm^2], where λ is in [cm], and wavelength-independent loss and nonlinearity $\alpha = 2.6\, dB/km$ and $\gamma = 0.0044\left(W^{-1} \cdot m^{-1}\right)$. The wavelength of the input soliton pulse is set at 1550nm. Soliton frequency shift versus input optical pulse width is shown in Fig.1, in which, results of semi-analytical calculation represented by triangles agree well with those obtained by numerical simulations represented by open circles. The vertical axis at the right indicates the exponent x. This parameter x is equal to 4 when the pulse width is wide and the amount of frequency shift is small as predicted by Gordon [4]. However, with pulse width narrower than 100fs, the frequency shift becomes less sensitive to the pulse width and this slope can be reduced significantly depending on fiber parameters. In this calculation, since the fiber loss is only 0.26dB, for a 100m fiber-length, the impact in the results is negligible. It needs to be mentioned that when the pulse width is narrower than 20fs, the nonlinear Schrödinger equation (1) is no longer accurate because the narrowband approximation fails [3] and that is beyond the scope of this work.

In order to show the effectiveness of this method, we also investigated SSFS in a 10m long photonic crystal fiber (PCF) with zero-dispersion wavelength at 710nm [9,10]. The wavelength dependent fiber parameters are linearly interpolated from the data listed in table 1. The wavelength of the input soliton pulses used in the

calculation is 780nm.

λ (nm)	D (ps/nm/km)	D slope (ps/nm^2/km)	γ (W^{-1} km^{-1})	α (dB/km)
710	0	0.58	139	190
600	-142	1.70	171	210
800	68	0.59	122	170
1000	148	0.25	92	130
1550	185	-0.08	49	80

Table 1: Photonic Crystal Fiber NL-18-710 characteristics.

Fig. 2, shows the frequency shift versus soliton pulse width in the PCF calculated by semi-analytical model (triangles) and numerical simulations (open cycles). Because of the high loss in PCF, its impact cannot be neglected. To illustrate this effect, soliton frequency shift calculated without fiber loss is also plotted in Fig.2 (squares) for comparison. Similar to what happened in the polarization maintaining fiber, the exponent x is equal to 4 at relatively wide pulse width and is reduced significantly when the pulse width is narrower than 100fs.

In all the cases, there is also agreement between the semi-analytical solution and the numerical solution in both the output peak power and the output pulse width. The output fundamental order of the soliton from the numerical solution was verified.

Fig.3 shows an example of the wavelength shift as a function of the fiber length for different pulse widths calculated with semi-analytical model (continuous) and numerical simulations. The results clearly show saturation in the frequency shift at long fiber lengths as has been demonstrated experimentally [3]. The discrepancy between semi-analytical model and numerical simulation when the pulse width is narrower than 40fs is attributed to the effect of higher order dispersion, which is not included in the semi-analytical model

IV. CONCLUSION

In this letter, we have introduced a semi-analytical method for the modeling of SSFS in optical fibers. Calculation using this model is fast and is provides a better understanding of the physical process involved. By comparing the calculated results with numerical simulations in two different fiber types, the accuracy of semi-analytical modeling is verified. When frequency shift is small enough, exponent x is equal to 4, which agrees with previous works.

References

[1] F.M.Mitschke and L.F.Mollenauer, “Discovery of the soliton self-frequency shift”, Opt. Lett 11 (1986), 659-661.

[2] Norihiko Nishizawa, Youta Ito and Toshio Goto, “0.78-0.90-μm Wavelength-Tunable Femtosecond Soliton Pulse Generation Using Photonic Crystal Fiber”, Photonic Technology lett. 14 (2002) 986-988.

[3] Norihiko Nishizawa, Ryuji Okamura and Toshio Goto, “Analysis of Widely Wavelength Tunable Femtosecond Soliton Pulse Generation Using Optical Fibers” J. Appl. Phys. 38 (1999), 4768-4771.

[4] J.P. Gordon, “Theory of the soliton self-frequency shift”, Opt Lett. 11 (1986) 662-664.

[5] G. P. Agrawal, Nonlinear Fiber Optics, 3rd ed. New York: Academic, 2001.

[6] R.H. Stolen and W.J.Tomlinson, “Effect of the Raman part of the nonlinear refractive index on the propagation of ultrashort optical pulses infibers”, JOSA B 9 (1992), 565-573.

[7] R.H.Stolen, J.P.Gordon, W.J. Tomlinson and H.A. Haus, “Raman response function of silica-core fibers”, *JOSA B* 6 (1989) 1159-1166.

[8] VPI Photonics, VPI Transmission Maker, www.vpiphotonics.com.

[9] D.T. Reid, I.G. Cormack, W.J. Wadsworth,J.C. Knight and P.St.J. Russell, “Soliton Selft-frequency Shift Effect in Photonic Crystal Fibre”, CLEO 2002.

[10] M. Fuochi, F. Poli, S. Selleri, A. Cucinotta, and L, Vincetti, “Study of Raman amplification properties in triangular photonic crystal fibers”, J. Lightware Technol 21 (2003) 2247-2254.

Figure captions:

Fig. 1. Frequency shift versus pulse width for a 100m PMF in log scale. The straight line represent the analytical result in [4], triangles the complete semi-analytical solution and circles the numerical results. The figure also shows the difference on the exponent x from the analytical value of 4

Fig. 2. Frequency shift and pulse width for a 10m PCF in log scale. The straight line represent the analytical result in [4], squares the semi-analytical solution with no losses, triangles the complete semi-analytical solution and circles the numerical result. The figure also shows the difference on the exponent x from the analytical value of 4.

Fig. 3. Wavelength shift and fiber length for a PCF for different soliton pulse widths. Circles represent the numerical data.

Figure 1

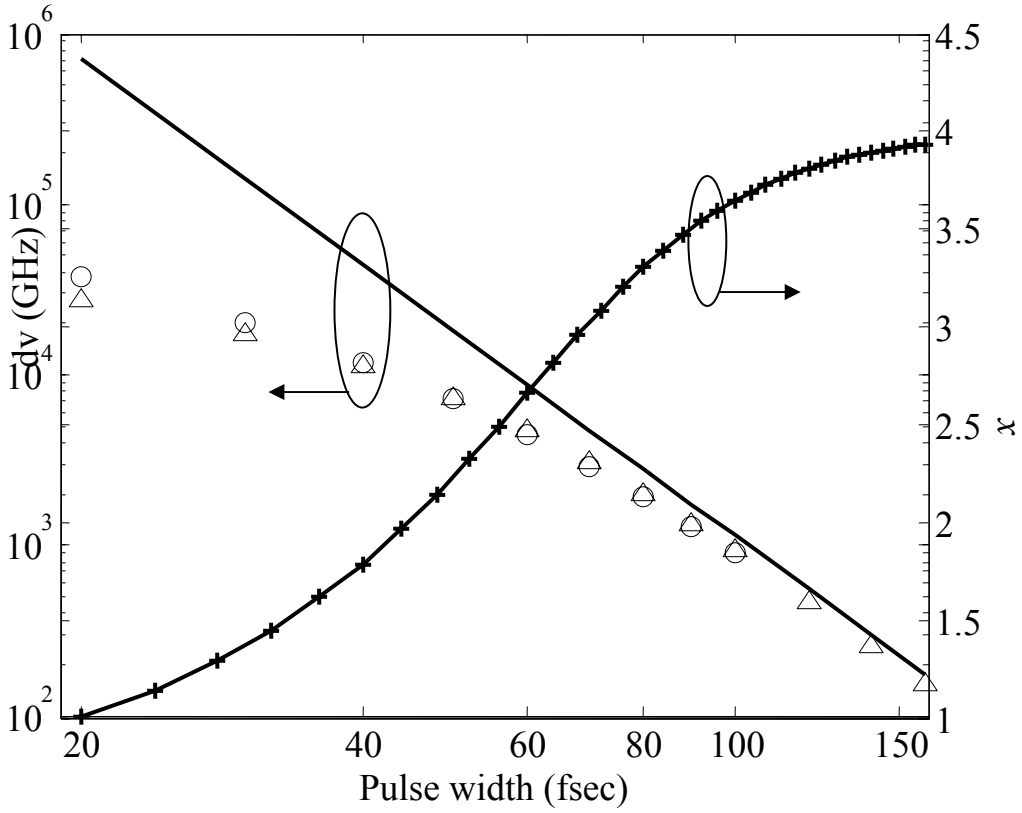
10^6
10^5
10^4
10^3
10^2
dv (GHz)
4.5
4
3.5
3
2.5
2
1.5
1
x
20
40
60
80
100
150
Pulse width (fsec)

Figure 2

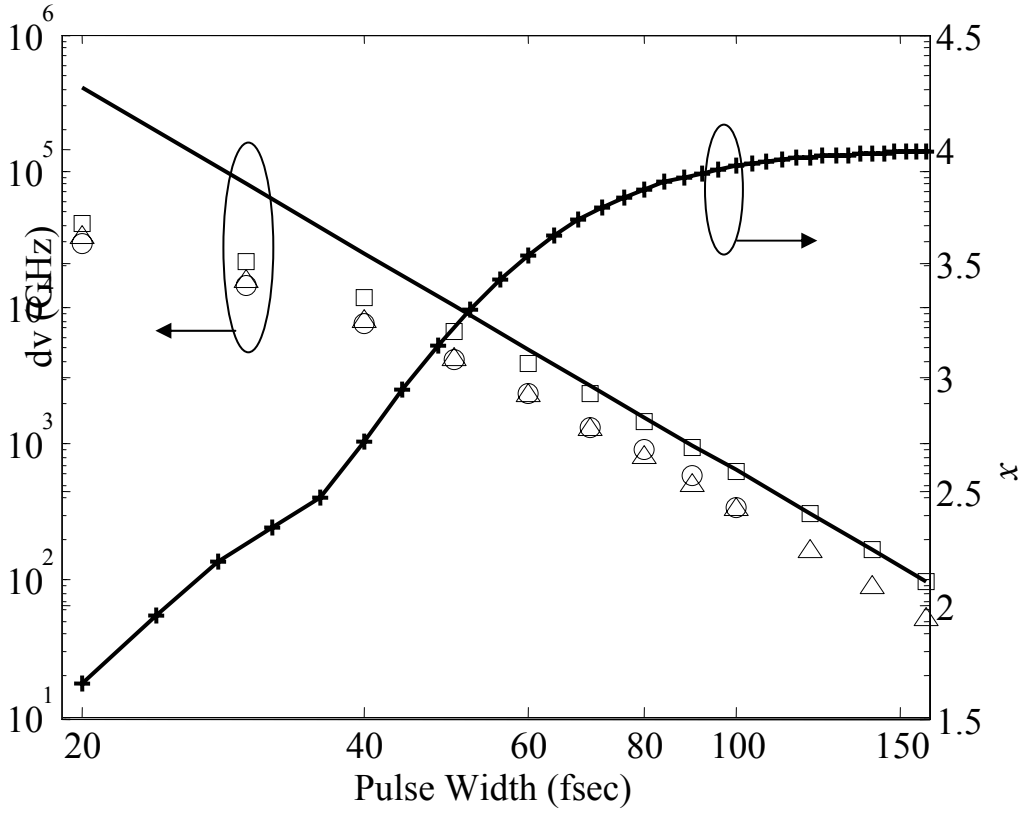
10^6
10^5
10^3
10^2
10^1
dv (GHz)
4.5
4
3.5
3
2.5
2
1.5
x
20
40
60
80
100
150
Pulse Width (fsec)

Figure 3

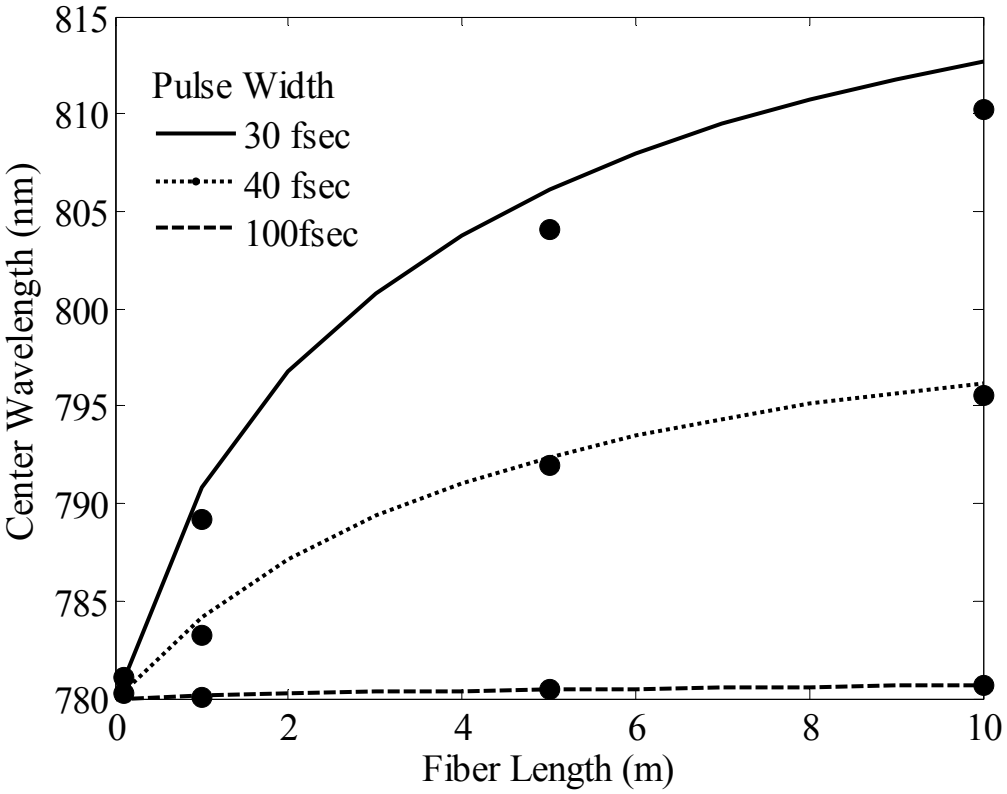
Pulse Width
30 fsec
40 fsec
100fsec
Center Wavelength (nm)
Fiber Length (m)
815
810
805
800
795
790
785
780
0
2
4
6
8
10